4 DYNAMIC ANALYSIS

4.1 Overview

Dynamic analysis in *UDEC* permits two-dimensional, plane-strain or plane-stress, fully dynamic analysis. The calculation is based on the explicit finite difference scheme (as discussed in Section 1 in **Theory and Background**) to solve the full equations of motion, using real rigid-block masses, or lumped gridpoint masses derived from the real density of surrounding zones (rather than scaled masses used for static solution). Background information on the dynamic formulation of the fully nonlinear method implemented in *UDEC* is provided. (See Section 4.2.)

The dynamic formulation can be coupled to the structural element model, thus permitting analysis of rock-structure interaction brought about by ground shaking. The dynamic feature can also be coupled to the model for fluid flow in joints. This permits, for example, analyses of the effect of dynamic loading of saturated joints. The dynamic model can likewise be coupled to the optional thermal model in order to calculate the combined effect of thermal and dynamic loading. The dynamic facility expands *UDEC*'s analytic capability to a wide range of dynamic problems in disciplines such as earthquake engineering, seismology and mine rockbursts.

This volume includes discussions on the various features and considerations associated with the dynamic option in *UDEC* (i.e., dynamic loading and boundary conditions, wave transmission and mechanical damping). These features are described separately in Section 4.3.

The user is strongly encouraged to become familiar with the operation of *UDEC* for simple mechanical, static problems before attempting to solve problems involving dynamic loading. Dynamic analysis is often very complicated, and requires a considerable amount of insight to interpret correctly. A recommended procedure for conducting dynamic numerical analysis with *UDEC* is provided in Section 4.4.

Validation and example problems illustrating the application of the dynamic model are provided in Section 4.5. *.

---

* The data files in this section are stored in the folder "ITASCA\UDEC700\Datafiles\Dynamic" with the extension ".DAT." A project file is also provided for each example. For the *GIIC*, open the project file by clicking on the FILE/OPEN PROJECT menu item and select the project file name (with ".PRJ" extension). Then click on the *Project Options* icon at the top of the *Project Tree Record*, select *Rebuild unsaved states*. For the GUI, open the project file by clicking on the FILE/OPEN PROJECT menu item and select the project file name (with ".UDPRJ" extension). Then click on the *Project* tab and select the "Master.dat" and run it

4.2 Dynamic Formulation

The finite difference formulation is identical to that described in Section 1 in **Theory and Background**, except that "real" masses are used at rigid-block centroids or deformable-block gridpoints instead of the scaled inertial masses used for optimum convergence in the static solution scheme. For deformable blocks, each triangular zone contributes one-third of its mass (computed from zone density and area) to each of the three associated gridpoints. In finite-element terminology, *UDEC* uses lumped masses and a diagonal mass matrix.

The calculation of critical timestep is identical to that given in Section 1.2.8 in **Theory and Background**. If stiffness-proportional damping is used (see Section 4.3.3.1), the timestep must be reduced, for stability. Belytschko (1983) provides a formula for critical timestep, Δt_β, that includes the effect of stiffness-proportional damping:

$$\Delta t_\beta = \left\{ \frac{2}{\omega_{\max}} \right\} \left(\sqrt{1 + \lambda^2} - \lambda \right) \tag{4.1}$$

where $\omega_{\max}$ is the highest eigenfrequency of the system, and λ is the fraction of critical damping at this frequency.

Both $\omega_{\max}$ and λ are estimated in *UDEC*, since an eigenvalue solution is not performed. The estimates are

$$\omega_{\max} = \frac{2}{\Delta t_d} \tag{4.2}$$

$$\lambda = \frac{0.4\,\beta}{\Delta t_d} \tag{4.3}$$

given

$$\beta = \xi_{\min} / \omega_{\min} \tag{4.4}$$

where $\xi_{\min}$ and $\omega_{\min}$ are the damping fraction and angular frequency specified for Rayleigh damping (see Section 4.3.3.1), and Δt_d is the timestep for dynamic runs when no stiffness-proportional damping is used. The resulting value of Δt_β is used as the dynamic timestep if stiffness-proportional damping is in operation.

4.3 Dynamic Modeling Considerations

There are three aspects that the user should consider when preparing a *UDEC* model for a dynamic analysis: (1) dynamic loading and boundary conditions; (2) wave transmission through the model; and (3) mechanical damping. This section provides guidance on addressing each aspect when preparing a *UDEC* data file for dynamic analysis. Section 4.4 illustrates the use of most of the features discussed here.

4.3.1 Dynamic Loading and Boundary Conditions

UDEC models a region of jointed material subjected to external and/or internal dynamic loading by applying a dynamic input boundary condition either at the model boundary or to internal blocks. Wave reflections at model boundaries are minimized by specifying either quiet (viscous) or free-field boundary conditions. The types of dynamic loading and boundary conditions are shown schematically in Figure 4.1; each condition is discussed in the following sections.

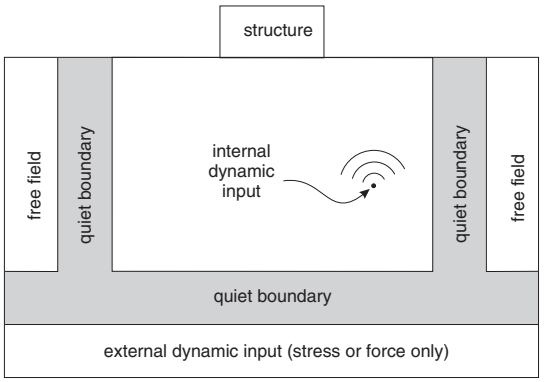

(a) Flexible base

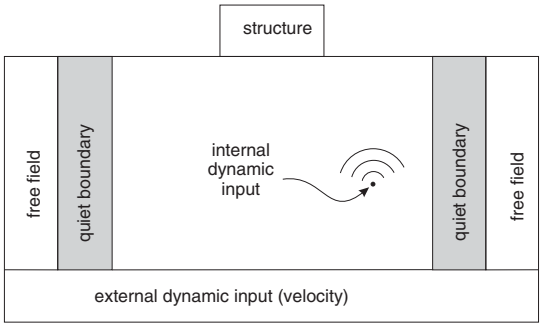

(a) Rigid base

Figure 4.1 Types of dynamic loading and boundary conditions in UDEC

4.3.1.1 *Application of Dynamic Input*

In *UDEC*, the dynamic input can be applied in one of four ways:

(a) a velocity history;

(b) a stress (or pressure) history;

(c) a force history; or

(d) a fluid pressure history within joints.

Dynamic input is usually applied to the boundaries of deformable-block models with the **block edge apply** or **block gridpoint apply** commands. Forces or pressures can also be applied to interior blocks by using the **block edge apply interior** command. Fluid pressures within joint domains are applied with the **block domain fix** command.

The history function for the input is treated as a multiplier on the value specified with the **block edge apply** or **block gridpoint apply** commands. The history multiplier is assigned with the **history** keyword, and can be in one of three forms:

(1) an harmonic function defined by the **sine** or **cosine** keyword;

(2) a table defined by the **table** command;

(3) a *FISH* function.

A sine or cosine wave is applied with a specified frequency and time period.

With **table** input, the multiplier values and corresponding time values are entered as individual pairs of numbers in the specified table; the first number of each pair is assumed to be a value of dynamic time. The time intervals between successive table entries need not be the same for all entries.

If a *FISH* function is used to provide the multiplier, the function must access dynamic time within the function, using the *UDEC* scalar variable **block.mechanical.time.total**, and compute a multiplier value that corresponds to this time. Example 4.4 provides an example of dynamic loading derived from a *FISH* function.

Dynamic input can be applied either in the x- or y-direction corresponding to the xy-axes for the model, or in the normal and shear directions to the model boundary. Histories can only be specified for input in the x- and y-directions.

Dynamic input can also be applied for rigid block models. Velocities are applied to rigid blocks by first fixing the block with the **block fix** command, and then specifying the velocity components with the *UDEC* model variable **block apply velocity-x** or **block apply velocity-y**. Forces can be applied to rigid blocks with the **block apply force-x** or **block apply force-y** command. History functions for the velocities or loads are specified via *FISH*. An application of a velocity history is illustrated in Example 4.4.

One restriction when applying velocity input to model boundaries is that this boundary condition cannot be applied along the same boundary as a "quiet" (viscous) boundary condition (compare Figure 4.1(a) to Figure 4.1(b)). To overcome this, a stress boundary condition can be used instead (i.e., a velocity record can be transformed into a stress record and applied to a quiet boundary). A velocity wave may be converted to a stress wave using

$$\sigma_n = 2(\rho\ C_p)\ v_n \tag{4.5}$$

or

$$\sigma_s = 2(\rho\ C_s)\ v_s \tag{4.6}$$

where σ_n = applied normal stress;
σ_s = applied shear stress;
ρ = mass density;
C_p = speed of p-wave propagation through medium;
C_s = speed of s-wave propagation through medium;
v_n = input normal particle velocity; and
v_s = input shear particle velocity.

C_p is given by

$$C_p = \sqrt{\frac{K + 4G/3}{\rho}} \tag{4.7}$$

and C_s is given by

$$C_s = \sqrt{G/\rho} \tag{4.8}$$

The formulae assume plane-wave conditions. The factor of two in Eqs. (4.5) and (4.6) accounts for the fact that the applied stress must be doubled to overcome the effect of the viscous boundary. The formulation is similar to that of Joyner and Chen (1975). Note that, in this case, a velocity history obtained at the boundary may be different than that from the original velocity record, because of the one-dimensional approximations of Eqs. (4.5) and (4.6).

To illustrate wave input at a quiet boundary, consider Example 4.1, in which a pulse is applied as a stress history to the bottom of a vertical, 50-m high column. The bottom of the column is declared quiet in the horizontal direction, and the top is free. The properties are chosen such that the shear wave speed is 100 m/sec, and the product, ρC_s, is 10^5. The amplitude of the stress pulse is set, therefore, to 2×10^5, according to Eq. (4.6), in order to generate a velocity amplitude of 1 m/sec

in the column. Figure 4.2 shows time histories of x-velocity at the base, middle and top of the column; the amplitude of the outgoing wave is seen to be 1 m/sec, as expected. The first three pulses in Figure 4.2 correspond, in order, to the outgoing waves at the base, middle and top. The final two pulses correspond to waves reflected from the free surface, measured at the middle and base, respectively. The velocity-doubling effect of a free surface (as well as the lack of waves after a time of about 1.3 seconds) can be seen, which confirms that the quiet base is working correctly. (See Section 4.3.1.3.) The doubling effect associated with a free surface is described in texts on elastodynamics (e.g., Graff 1991).

Example 4.1 Shear wave propagation in a vertical column

```
model new
;file: wave.dat
model title 'Shear wave propagation in a vertical column'
block tolerance corner-round-length 5E-2
block tolerance minimum-edge-length 0.1
block create polygon 0 0 0 50 1 50 1 0
block zone gen quad 0.25
block zone group 'block'
block zone cmodel assign elastic density 1E3 bulk 2E7 shear 1E7 ...
  range group 'block'
fish define wave
   if block.mechanical.time.total > 1.0 / freq
      wave = 0.0
   else
      wave = 0.5 * ...
        (1.0 - math.cos(2.0*math.pi*freq * block.mechanical.time.total))
   endif
end
fish set @freq=4.0
@wave
block gridpoint apply velocity-y 0
block gridpoint apply bulk 2.0E7 shear 1.0E7 density 1000.0
block gridpoint apply visc-x range pos-x 0 1 pos-y -0.1 0.1
block edge apply stress 0.0 -200000.0 0.0 history @wave ...
  range pos-y -0.1 0.1
block gridpoint history velocity-x 0.5 0.0
block gridpoint history velocity-x 0.5 25.0
block gridpoint history velocity-x 0.5 50.0
block mechanical history time-total
block mechanical damping 0.0 0.0
model save 'wave1.sav'
;
block cycle time 1.7
model save 'wave2.sav'
```

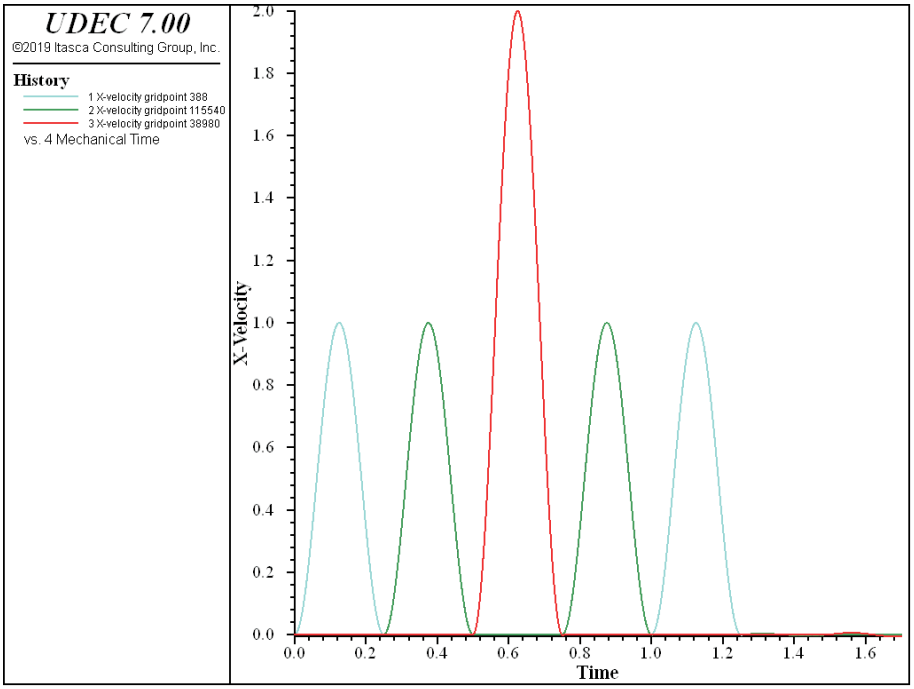

Figure 4.2 Primary and reflected waves in a bar: stress input through a quiet boundary

4.3.1.2 Baseline Correction

If a "raw" acceleration or velocity record from a site is used as a time history, the *UDEC* model may exhibit continuing velocity or residual displacements after the motion has finished. This arises from the fact that the integral of the complete time history may not be zero. For example, the idealized velocity waveform in Figure 4.3(a) may produce the displacement waveform in Figure 4.3(b) when integrated. The process of "baseline correction" should be performed, although the physics of the *UDEC* simulation usually will not be affected if it is not done. It is possible to determine a low frequency wave (for example, Figure 4.3(c)) which, when added to the original history, produces a final displacement which is zero (Figure 4.3(d)). The low frequency wave in Figure 4.3(c) can be a polynomial or periodic function, with free parameters that are adjusted to give the desired results.

Baseline correction usually applies only to complex waveforms derived, for example, from field measurements. When using a simple, synthetic waveform, it is easy to arrange the process of generating the synthetic waveform to ensure that the final displacement is zero. Normally, in seismic analysis, the input wave is an acceleration record. A baseline-correction procedure can be used to force both the final velocity and displacement to be zero. Earthquake engineering texts should be consulted for standard baseline correction procedures.

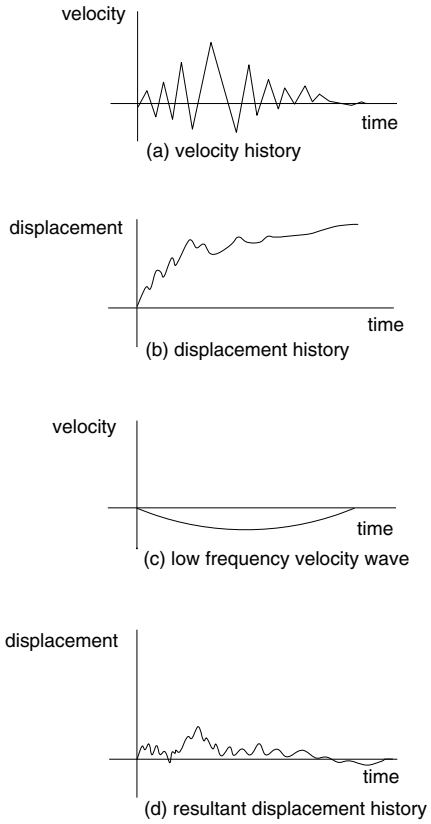

Figure 4.3 The baseline correction process

An alternative to baseline correction of the input record is to apply a displacement shift at the end of the calculation if there is a residual displacement of the entire model. This can be done by applying a fixed velocity to the mesh to reduce the residual displacement to zero. This action will not affect the mechanics of the deformation of the model. Computer codes to perform baseline corrections are available from several Internet sites (e.g., http://nsmp.wr.usgs.gov/processing.html).

4.3.1.3 Quiet Boundaries

The modeling of geomechanics problems involves media which, at the scale of the analysis, are better represented as unbounded. Deep underground excavations are normally assumed to be surrounded by an infinite medium, while surface and near-surface structures are assumed to lie on a half-space. Numerical methods relying on the discretization of a finite region of space require that appropriate conditions be enforced at the artificial numerical boundaries. In static analyses, fixed or elastic boundaries (e.g., represented by boundary-element techniques) can be realistically placed at some distance from the region of interest. In dynamic problems, however, such boundary conditions cause the reflection of outward propagating waves back into the model, and do not allow the necessary energy radiation. The use of a larger model can minimize the problem, since material damping will absorb most of the energy in the waves reflected from distant boundaries. However,

this solution leads to a large computational burden. The alternative is to use quiet (or absorbing) boundaries. Several formulations have been proposed. The viscous boundary developed by Lysmer and Kuhlemeyer (1969) is used in *UDEC*. It is based on the use of independent dashpots in the normal and shear directions at the model boundaries. The method is almost completely effective at absorbing body waves approaching the boundary at angles of incidence greater than 30°. For lower angles of incidence, or for surface waves, there is still energy absorption, but it is not perfect. However, the scheme has the advantage that it operates in the time domain. Its effectiveness has been demonstrated in both finite-element and finite-difference models (Kunar et al. 1977). A variation of the technique proposed by White et al. (1977) is also widely used.

More efficient energy absorption (particularly in the case of Rayleigh waves) requires the use of frequency-dependent elements, which can only be used in frequency-domain analyses (e.g., Lysmer and Waas 1972). These are usually termed "consistent boundaries," and involve the calculation of dynamic stiffness matrices coupling all the boundary degrees-of-freedom. Boundary element methods may be used to derive these matrices (e.g., Wolf 1985). A comparative study of the performance of different types of elementary, viscous and consistent boundaries was documented by Roesset and Ettouney (1977).

A different procedure to obtain efficient absorbing boundaries for use in time domain studies was proposed by Cundall et al. (1978). It is based on the superposition of solutions with stress and velocity boundaries in such a way that reflections are canceled. In practice, it requires adding the results of two parallel, overlapping grids in a narrow region adjacent to the boundary. This method has been shown to provide effective energy absorption, but it is difficult to implement for a blocky system with complex geometry, and thus is not used in *UDEC*.

The quiet-boundary scheme proposed by Lysmer and Kuhlemeyer (1969) involves dashpots attached independently to the boundary in the normal and shear directions. The dashpots provide viscous normal and shear tractions given by

$$t_n = -\rho\, C_p\, v_n \tag{4.9}$$

$$t_s = -\rho\, C_s\, v_s \tag{4.10}$$

where v_n and v_s are the normal and shear components of the velocity at the boundary;
ρ is the mass density; and
C_p and C_s are the p- and s-wave velocities.

These viscous terms can be introduced directly into the equations of motion of the gridpoints lying on the boundary. A different approach, however, was implemented in *UDEC*, whereby the tractions t_n and t_s are calculated and applied at every timestep in the same way boundary loads are applied. This is more convenient than the former approach, and tests have shown that the implementation is equally effective. The only potential problem concerns numerical stability, because the viscous forces are calculated from velocities lagging by half a timestep. In practical analyses to date, no reduction of timestep has been required by the use of the nonreflecting boundaries. Timestep restrictions demanded by small zones are usually more important.

Dynamic analysis starts from some in-situ equilibrium condition. If a velocity boundary is used to provide the static stress state, this boundary condition can be replaced by quiet boundaries; the boundary reaction forces will be automatically calculated and maintained throughout the dynamic loading phase. However, be careful to avoid changes in static loading during the dynamic phase. For example, if a tunnel is excavated after quiet boundaries have been specified on the bottom boundary, the whole model will start to move upward. This is because the total gravity force no longer balances the total reaction force at the bottom (calculated when the boundary was changed to a quiet one). If a *stress* boundary condition is applied for the static solution, a stress boundary condition of opposite sign must also be applied over the same boundary when the quiet boundary is applied for the dynamic phase. This will allow the correct reaction forces to be in place at the boundary for the dynamic calculation.

Quiet boundary conditions can be assigned to deformable blocks in the x- and y-directions. The boundary conditions are applied with the **block grid apply visc-x** and **block grid apply visc-y** commands. The command **block grid apply material** assigns a material property number to the far-field properties used for Eqs. (4.9) and (4.10). A quiet boundary can also be applied to a rigid block model by first creating deformable blocks at the boundary (see Example 4.4).

4.3.1.4 Free-Field Boundaries

Seismic analysis by numerical techniques of surface structures such as dams requires the discretization of a region of the material adjacent to the foundation. The seismic input is normally represented by plane waves propagating upward through the underlying material. The boundary conditions at the sides of the model must account for the free-field motion which would exist in the absence of the structure. In some cases, elementary lateral boundaries may be sufficient. For example, if only a shear wave were applied on AC (shown in Figure 4.4), it would be possible to fix the boundary along AB and CD in the y-direction only (see the example in Section 4.5.2). These boundaries should be placed at sufficient distances to minimize wave reflections and achieve free-field conditions. For soils with high material damping, this condition can be obtained with a relatively small distance (Seed et al. 1975). However, when the material damping is low, the required distance may lead to an impractical model. An alternative procedure is to "enforce" the free-field motion in such a way that boundaries retain their nonreflecting properties (i.e., outward waves originating from the structure are properly absorbed). This approach was used in the continuum finite-difference code NESSI (Cundall et al. 1980). A technique of this type was developed for *UDEC*. It involves the execution of a one-dimensional free-field calculation in parallel with the main system analysis. The lateral boundaries are coupled to the free-field grid by viscous dashpots to simulate a quiet boundary (see Figure 4.4), and the unbalanced forces from the free-field grid are applied to the deformable-block boundary at the boundary gridpoints. Both conditions are expressed in Eqs. (4.11) and (4.12), which apply to the left-hand boundary. Similar expressions may be written for the right-hand boundary.

$$F_x = -\rho C_p (v_x^m - v_x^{\text{ff}}) + \sigma_{xx}^{\text{ff}} \Delta S_y \tag{4.11}$$

$$F_y = -\rho C_s (v_y^m - v_y^{\text{ff}}) + \sigma_{xy}^{\text{ff}} \Delta S_y \tag{4.12}$$

where ρ = density of material along vertical model boundary;
C_p = p-wave speed at the left-hand boundary;
C_s = s-wave speed at the left-hand boundary;
ΔS_y = mean vertical zone size at boundary gridpoint;
v_x^m = x-velocity of gridpoint in deformable block at left boundary;
v_y^m = y-velocity of gridpoint in deformable block at left boundary;
v_x^{ff} = x-velocity of gridpoint in left free field;
v_y^{ff} = y-velocity of gridpoint in left free field;
σ_{xx}^{ff} = mean horizontal free-field stress at gridpoint; and
σ_{xy}^{ff} = mean free-field shear stress at gridpoint.

In this way, plane waves propagating upward suffer no distortion at the boundary because the free-field grid supplies conditions that are identical to those in an infinite model. If the deformable-block model is uniform, and there is no surface structure, the lateral dashpots are not exercised because the free-field grid executes the same motion as the main model. However, if the main model motion differs from that of the free field (due, say, to a surface structure that radiates secondary waves), then the dashpots act to absorb energy in a manner similar to that of quiet boundaries.

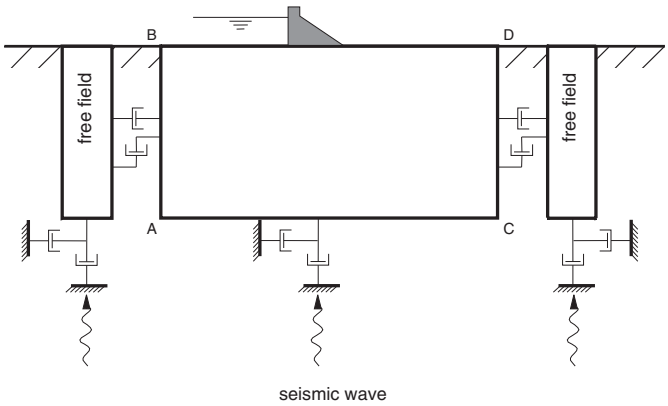

Figure 4.4 Model for seismic analysis of surface structures and free-field mesh

A free-field boundary is invoked with the **block dynamic free-field** command. The free field is created, and in-situ conditions prior to the dynamic analysis are assigned to the free field. Note that the free-field boundary conditions require that lateral boundaries of the main model *must* be vertical and straight. The free field is also connected to the main model with the **block dynamic free-field** command. The free-field grid can only be connected to deformable blocks. The **block dynamic free-field** command must be given prior to assigning the boundary that specifies the dynamic loading.

The free-field model consists of a one-dimensional "column" of unit width, simulating the behavior of the extended medium. An explicit finite-difference method was selected for the model. The

height of the free field equals the length of the lateral boundaries. It is discretized into ***n*** elements corresponding to the zones along the lateral boundaries of the *UDEC* model. Element masses are lumped at the ***n*** + 1 gridpoints. A linear variation of the displacement field is assumed within each element; the elements are, therefore, in a state of uniform strain (and stress).

The application of the free-field boundary is illustrated in Example 4.2. A shear-stress wave is applied to the base of the model. Figure 4.5 shows the resulting x-velocity at the top of the model at different locations in the free field and the main block.

Example 4.2 Shear wave loading of a model with free-field boundaries

```
model new
;File: ffield.dat
model title 'Shear wave propagation in a vertical column with free-field'
block tolerance corner-round-length 1.6E-2
block create polygon 0 0 0 10 16 10 16 0
block zone gen quad 1.0
block zone group 'block'
block zone cmodel assign elastic density 2.5E-3 bulk 6.667E4 shear 4E4 ...
  range group 'block'
model gravity 0.0 -10.0
block gridpoint apply velocity-x 0 range pos-x -0.1 0.1 pos-y -0.1 10.1
block gridpoint apply velocity-x 0 range pos-x 15.9 16.1 pos-y -0.1 10.1
block gridpoint apply velocity-y 0 range pos-x -0.1 16.1 pos-y -0.1 0.1
block solve ratio 1.0E-5
model save 'ffield1.sav'
;
;
block edge apply dynamic-free-field
block gridpoint apply bulk 66667.0 shear 40000.0 density 0.0025
block gridpoint apply visc-x visc-y range pos-y -0.1 0.1
fish define wave
  wave = 0.5 * (1.0 - math.cos(2*math.pi*block.mech.time.total/period))
end
fish set @period 0.015
block edge apply stress 0.0 -1.0 0.0 history @wave range pos-y -0.1 0.1
block mechanical time 0
block gridpoint history velocity-x 0.0 10.0
block gridpoint history velocity-x 7.6 10.0
block gridpoint history velocity-x 16.0 10.0
block dynamic free-field history velocity-x 10 2
block mechanical history time-total
block mechanical damping 0.0 0.0
fish hist @wave
block cycle time 0.02
model save 'ffield2.sav'
```

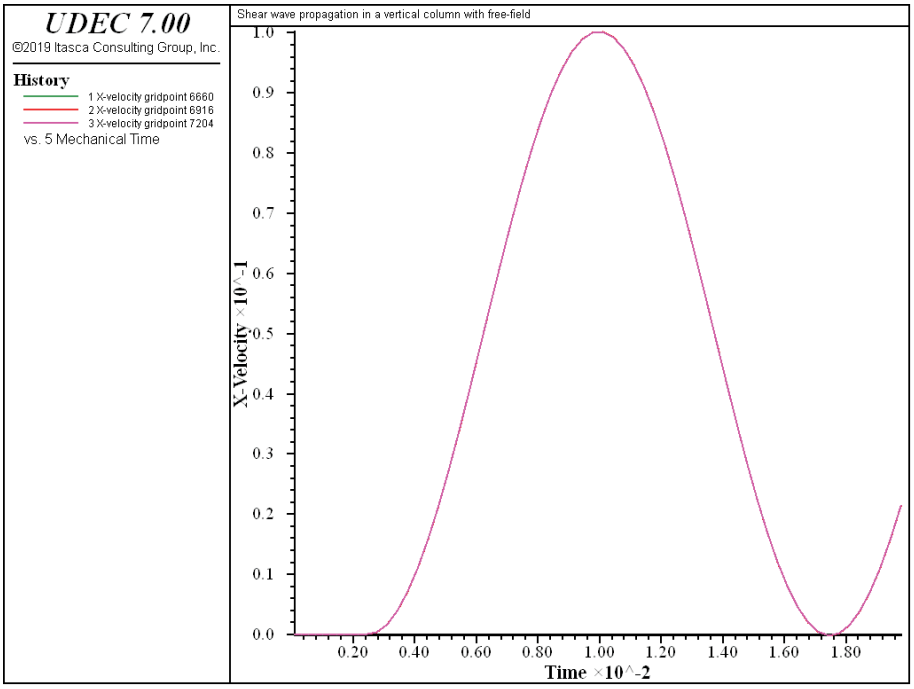

Figure 4.5 x-velocity histories at top of model with free-field boundaries

Example applications of the free-field boundary are also given in Section 3.6 in the **User's Guide** and Section 4 in the **Example Applications**.

4.3.1.5 Deconvolution and Selection of Dynamic Boundary Conditions

Design earthquake ground motions developed for seismic analyses are usually provided as outcrop motions, often rock outcrop motions.* However, for *UDEC* analyses, seismic input must be applied at the base of the model rather than at the ground surface, as illustrated in Figure 4.6. The question then arises, "What input motion should be applied at the base of a *UDEC* model in order to properly simulate the design motion?"

The appropriate input motion at depth can be computed through a "deconvolution" analysis using a 1D wave propagation code such as the equivalent-linear program *SHAKE*. This seemingly simple analysis is often the subject of considerable confusion resulting in improper ground motion input for *UDEC* models. The application of *SHAKE* for adapting design earthquake motions for *UDEC* input is described. Input of an earthquake motion into *UDEC* is typically done using one of two base types:

1. A rigid base, where an acceleration-time history is specified at the base of the *UDEC* model.

2. A compliant base, where a quiet (absorbing) boundary is used at the base of the *UDEC* model.

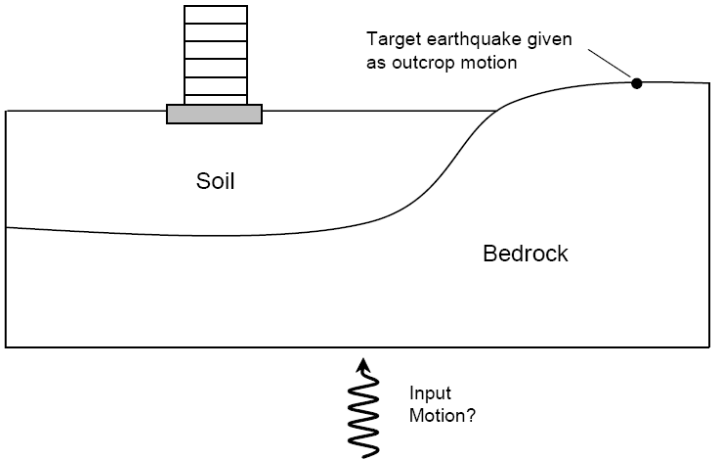

Figure 4.6 Seismic input to UDEC

For a rigid base, a time history of acceleration (or velocity or displacement) is specified for deformable-block gridpoints (or rigid-block centroids) along the base of the model. While simple to use, a potential drawback of a rigid base is that the motion at the base of the model is completely prescribed. Hence, the base acts as if it were a fixed displacement boundary reflecting downward-propagating waves back into the model. Thus, a rigid base is not an appropriate boundary for

* This section is abstracted with permission from the publication by Mejia and Dawson (2006).

general application unless a large dynamic impedance contrast is meant to be simulated at the base (e.g. low velocity sediments over high velocity bedrock).

For a compliant base simulation, a quiet boundary is specified along the base of the *UDEC* model. See Section 4.3.1.3 for a description of quiet boundaries. Note that if a history of acceleration is recorded at a point along the quiet base, it will not necessarily match the input history. The input stress-time history specifies the upward-propagating wave motion in to the *UDEC* model, but the actual motion at the base will be the superposition of the upward motion and the downward motion reflected back from the *UDEC* model.

SHAKE (Schnabel et al. 1972) is a widely used 1D wave propagation code for site response analysis. *SHAKE* computes the vertical propagation of shear waves through a profile of horizontal visco-elastic layers. Within each layer, the solution to the wave equation can be expressed as the sum of an upward-propagating wave train and a downward-propagating wave train. The *SHAKE* solution is formulated in terms of these upward- and downward-propagating motions within each layer, as illustrated in Figure 4.7:

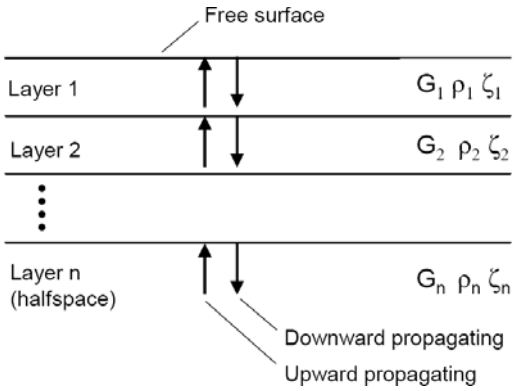

Figure 4.7 Layered system analyzed by SHAKE (layer properties are shear modulus, G, density, ρ, and damping fraction, ζ)

The relation between waves in one layer and waves in an adjacent layer can be solved by enforcing the continuity of stresses and displacements at the interface between the layers. These well-known relations for reflected and transmitted waves at the interface between two elastic materials (Kolsky 1963) can be expressed in terms of recursion formulas. In this way, the upward- and downward-propagating motions in one layer can be computed from the upward and downward motions in a neighboring layer.

To satisfy the zero shear stress condition at the free surface, the upward- and downward-propagating motions in the top layer must be equal. Starting at the top layer, repeated use of the recursion formulas allows the determination of a transfer function between the motions in any two layers of the system. Thus, if the motion is specified at one layer in the system, the motion at any other layer can be computed.

SHAKE input and output is not in terms of the upward- and downward-propagating wave trains, but in terms of the motions at a) the boundary between two layers, referred to as a "within" motion; or

b) at a free surface, referred to as an "outcrop" motion. The within motion is the superposition of the upward- and downward-propagating wave trains. The outcrop motion is the motion that would occur at a free surface at that location. Hence the outcrop motion is simply twice the upward-propagating wave-train motion. If needed, the upward-propagating motion can be computed by taking half the outcrop motion. At any point, the downward-propagating motion can then be computed by subtracting the upward-propagating motion from the within motion.

The *SHAKE* solution is in the frequency domain, with conversion to and from the time-domain performed with a Fourier transform. The deconvolution analysis discussed below illustrates the application of *SHAKE* for a linear, elastic case. *SHAKE* can also address nonlinear soil behavior approximately, through the equivalent linear approach. Analyses are run iteratively to obtain shear modulus and damping values for each layer that are compatible with the computed effective strain for the layer.

Deconvolution for a Rigid Base – The deconvolution procedure for a rigid base is illustrated in Figure 4.8 for a two-dimensional *FLAC* simulation. The same procedure also applies to *UDEC*. The goal is to determine the appropriate base input motion to *FLAC*, such that the target design motion is recovered at the top surface of the *FLAC* model. The profile modeled consists of three 20-m thick elastic layers with shear wave velocities and densities as shown in the figure. The *SHAKE* model includes the three elastic layers and an elastic half-space with the same properties as the bottom layer. The *FLAC* model consists of a column of linear elastic elements. The target earthquake is input at the top of the *SHAKE* column as an outcrop motion. Then, the motion at the top of the half-space is extracted as a within motion, and is applied as an acceleration-time history to the base of the *FLAC* model. Mejia and Dawson (2006) show that the resulting acceleration at the surface of the *FLAC* model is virtually identical to the target motion. The *SHAKE* within motion is appropriate for rigid-base input because (as described above) the within motion is the actual motion at that location, the superposition of the upward- and downward-propagating waves.

Deconvolution for a Compliant Base – The deconvolution procedure for a compliant base is illustrated in Figure 4.9 for a *FLAC* simulation. Again, the same procedure applies to *UDEC*. The *SHAKE* and *FLAC* models are identical to those for the rigid body exercise, except that a quiet boundary is applied to the base of the *FLAC* mesh. For application through a quiet base, the upward-propagating wave motion (1/2 the outcrop motion) is extracted from *SHAKE* at the top of the half-space. This acceleration-time history is integrated to obtain a velocity, which is then converted to a stress history using Eq. (4.6). Again, the resulting acceleration at the surface of the *FLAC* model is shown by Mejia and Dawson (2006) to be virtually identical to the target motion. As an additional check of the computed accelerations, they also show that the response spectra for both the compliant-base and rigid-base cases closely match the response spectra of the target motion.

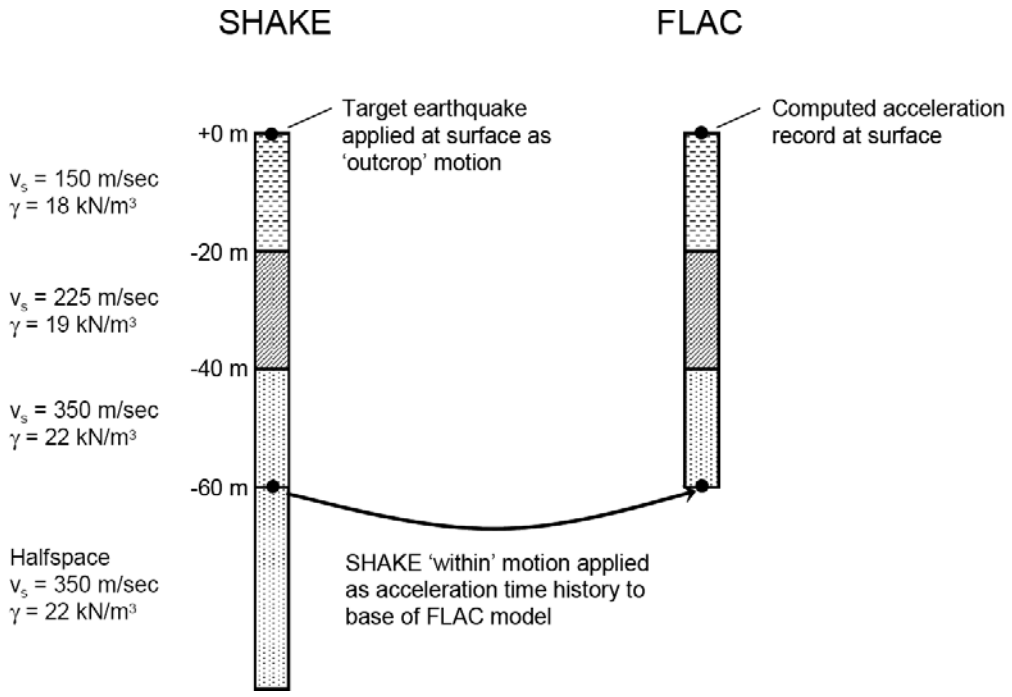

Figure 4.8 Deconvolution procedure for a rigid base (after Mejia and Dawson 2006)

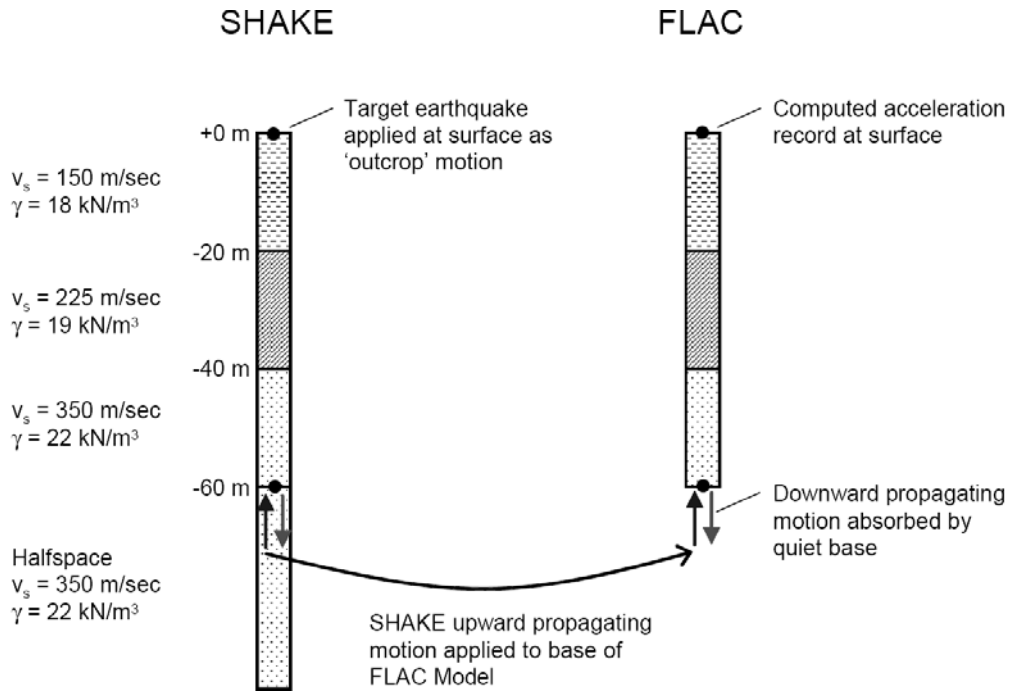

Figure 4.9 Deconvolution procedure for a compliant base (after Mejia and Dawson 2006)

Although useful for illustrating the basic ideas behind deconvolution, the previous example is not the typical case encountered in practice. The situation shown in Figure 4.10, where one or more soil layers (expected to behave nonlinearly) overlay bedrock (assumed to behave linearly), is more common. A *FLAC* or *UDEC* model for this case will usually include the soil layers and an elastic base of bedrock. To compute the correct *UDEC* compliant base input, a *SHAKE* model is constructed as shown in the figure. The *SHAKE* model includes a bedrock layer equal in thickness to the elastic base of the *UDEC* model, and an underlying elastic half-space with bedrock properties. The target motion is input to the *SHAKE* model as an outcrop motion at the top of the bedrock (point *A*). Designating this motion as outcrop means that the upward-propagating wave motion in the layer directly below point A will be set equal to 1/2 the target motion. The upward-propagating motion for input to *UDEC* is extracted at Point *B* as 1/2 the outcrop motion.

For the compliant-base case there is actually no need to include the soil layers in the *SHAKE* model, as these will have no effect on the upward-propagating wave train between points A and B. In fact, for this simple case, it is not really necessary to perform a formal deconvolution analysis, as the upward-propagating motion at point B will be almost identical to that at point A. Apart from an offset in time, the only differences will be due to material damping between the two points, which will generally be small for bedrock. Thus, for this very common situation, the correct input motion for *UDEC* is simply 1/2 of the target motion. (Note that the upward-propagating wave motion must be converted to a stress-time history using Eq. (4.6), which includes a factor of 2 to account for the stress absorbed by the viscous dashpots.)

For a rigid-base analysis, the within motion at point B is required. Since this within motion incorporates downward-propagating waves reflected off the ground surface, the nonlinear soil layers must be included in the *SHAKE* model. However, soil nonlinearity will be modeled quite differently in *UDEC* and *SHAKE*. Thus, it is difficult to compute the appropriate *UDEC* input motion for a rigid-base analysis.

Another typical case encountered in practice is illustrated in Figure 4.11. Here, the soil profile is deep, and rather than extending the *UDEC* model all the way down to bedrock, the base of the model ends within the soil profile. Note that the model must be extended to a depth below which the soil response is essentially linear. Again, the design motion is input at the top of the bedrock (point A) as an outcrop motion, and the upward-propagating motion for input to *UDEC* is extracted at point B. As in the previous example, for a compliant-base analysis there is no need to include the soil layers above point B in the *SHAKE* model. These layers have no effect on the upward-propagating motion between points A and B. Unlike the previous case, the upward-propagating motion can be quite different at points A and B, depending on the impedance contrast between the bedrock and linear soil layer. Thus, it is not appropriate to skip the deconvolution analysis and use the target motion directly.

A rigid base is only appropriate for cases with a large impedance contrast at the base of the model. However, the use of *SHAKE* to compute the required input motion for a rigid base of a *UDEC* model leads to a good match between the target surface motion and the surface motion computed by *UDEC*, *only* for a model that exhibits a low level of nonlinearity. The input motion already contains the effect of all layers above the base, because it contains the downward-propagating wave.

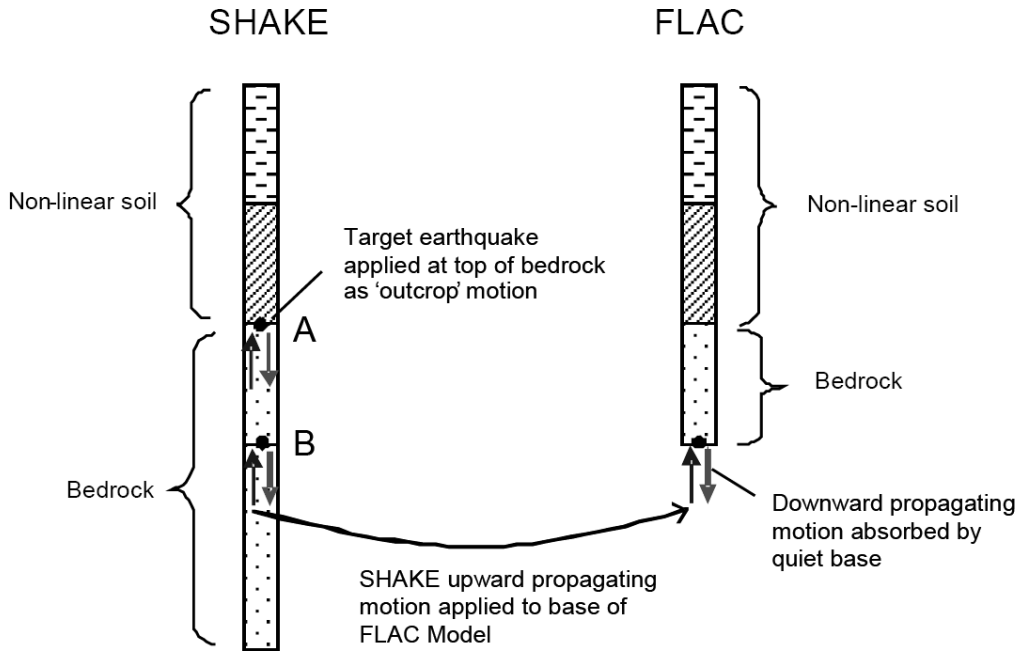

Figure 4.10 Compliant-base deconvolution procedure for a typical case (after Mejia and Dawson 2006)

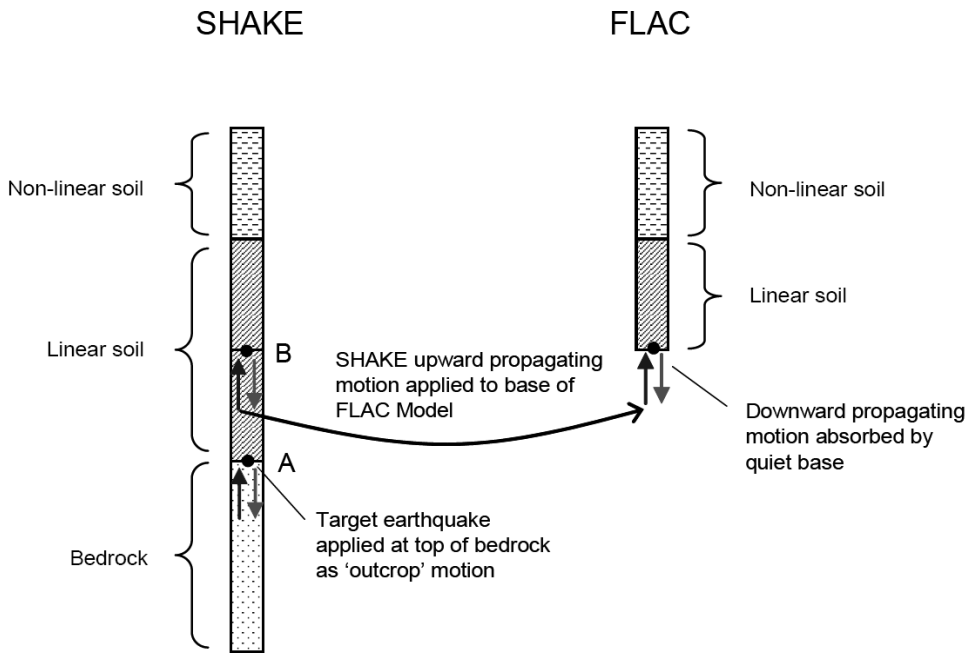

Figure 4.11 Compliant-base deconvolution procedure for another typical case (after Mejia and Dawson 2006)

A different approach must be taken if a *UDEC* model with a rigid base is used to simulate more realistic systems (e.g., sites that exhibit strong nonlinearity, or the effect of a surface or embedded structure). In the first case, the real nonlinear response is not accounted for by *SHAKE* in its estimate of base motion. In the second case, secondary waves from the structure will be reflected from the rigid base, causing artificial resonance effects.

A compliant base is almost always the preferred option because downward-propagating waves are absorbed. In this case, the quiet-base condition is selected, and only the upward-propagating wave from *SHAKE* is used to compute the input stress history. By using the upward-propagating wave only at a quiet *UDEC* base, no assumptions need to be made about secondary waves generated by internal nonlinearities or structures within the grid, because the incoming wave is unaffected by these; the outgoing wave is absorbed by the compliant base.

Although the presence of reflections from a rigid base is not always obvious in complex nonlinear *UDEC* analyses, they can have a major impact on analysis results, especially when cyclic-degradation or liquefaction-soil models are employed. Mejia and Dawson (2006) present examples from two-dimensional *FLAC* simulations that illustrate the nonphysical wave reflections calculated in models with a rigid base. One example, shown in Figure 4.12, demonstrates the difficulty with a rigid boundary. The nonphysical oscillations that result from a rigid base are shown by comparison to results for a compliant base in Figure 4.13. The inputs in both cases (rigid and compliant) were derived by deconvoluting the same surface motion.

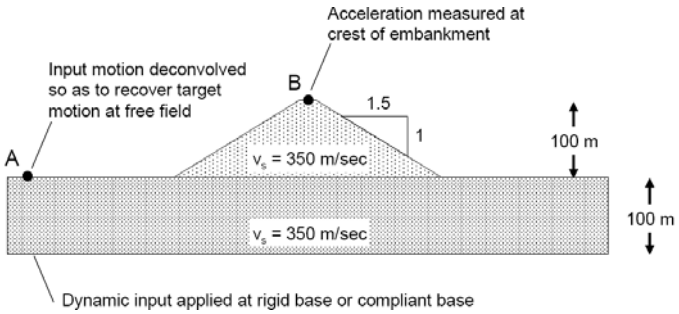

Figure 4.12 Embankment analyzed with a rigid and compliant base (after Mejia and Dawson 2006)

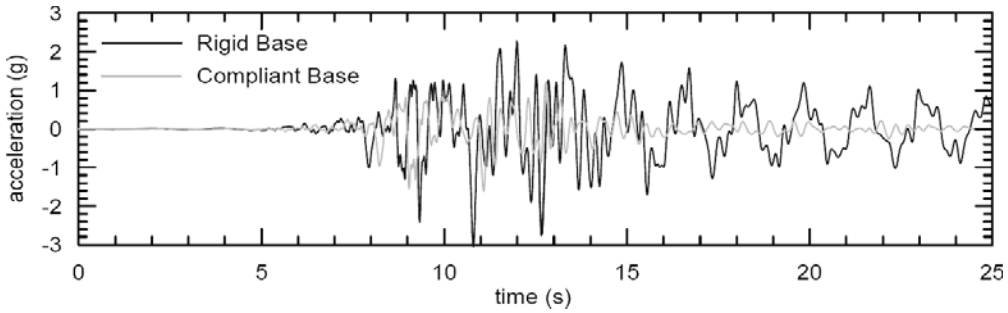

Figure 4.13 Computed accelerations at crest of embankment (after Mejia and Dawson 2006)

4.3.1.6 Hydrodynamic Pressures

The dynamic interaction between water in a reservoir and a concrete dam can have a significant influence on the performance of the dam during an earthquake. Westergaard (1933) established a mathematical basis for procedures to represent this interaction, and this approach is commonly used in engineering practice. Although the advent of computers has enabled numerical solution of coupled differential equations of fluid-structure systems, the formula proposed by Westergaard is widely used for stability analysis of smaller dams, and preliminary calculations in the design of large dams.

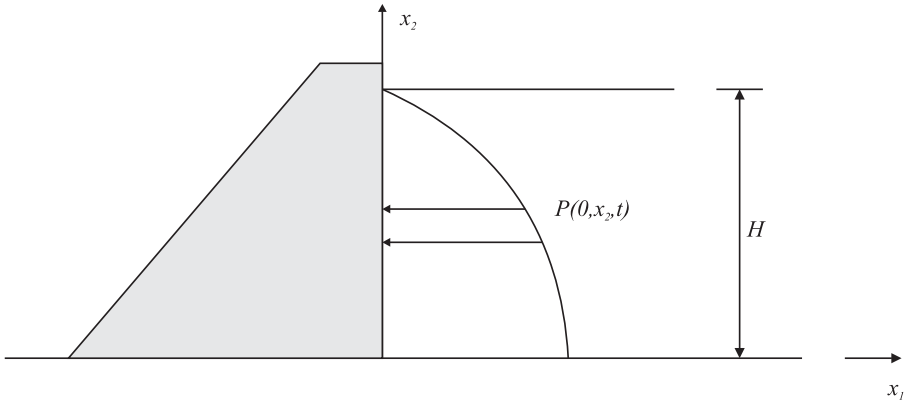

Figure 4.14 Hydrodynamic pressure acting on a rigid dam with a vertical upstream face

The hydrodynamic pressure acting on a rigid concrete dam over a reservoir height, H, is depicted in Figure 4.14. The pressure can be derived from the equation of motion for a fluid. The equation of motion for a fluid with small Reynold's number can be written as

$$c^2\left[\frac{\partial^2\Phi}{\partial x_1^2}+\frac{\partial^2\Phi}{\partial x_2^2}\right]=\frac{\partial^2\Phi}{\partial t^2} \tag{4.13}$$

where c is the speed of sound in water, and Φ is the velocity potential. The water pressure can be written as a function of the velocity potential:

$$p=\rho_w\frac{\partial\Phi}{\partial t} \tag{4.14}$$

where ρ_w is the density of water.

Additional assumptions are made, to simplify the loading condition:

1. The water is assumed to be incompressible, which reduces Eq. (4.13) to the Laplace equation: $\frac{\partial^2 \Phi}{\partial x_1^2} + \frac{\partial^2 \Phi}{\partial x_2^2} = 0$.
2. The free surface of the reservoir is assumed to be at rest. Thus, $\frac{\partial \Phi}{\partial t} = 0$ at $x_2 = H$.
3. The reservoir is assumed to be infinitely long. Therefore, as $x_1 \rightarrow \infty$, $\Phi \rightarrow 0$.
4. Hydrodynamic motion is assumed to be horizontal only: $\frac{\partial \Phi}{\partial x_2} = 0$ at $x_2 = 0$.
5. The upstream face of the dam is vertical and the dam is rigid: $\frac{\partial \Phi}{\partial x_1} = f(t)$ at $x_1 = 0$.

The solution of Eq. (4.13) with the above assumptions can be obtained for an arbitrary acceleration, $\ddot{x}_0(t)$, in the form of an infinite Fourier series:

$$p(0, x_2, t) = 8\ddot{x}_0(t)\rho_w H \sum_{n=1}^{\infty} \frac{(-1)^{n+1}}{((2n-1)\pi)^2} e^{\frac{-(2n-1)x_1}{4H}} \cos\left(\frac{(2n-1)x_2}{4H}\right) \tag{4.15}$$

Eq. (4.15) can be approximated as

$$p(0, x_2, t) = \rho_w \ddot{x}_0(t) H \frac{C_m}{2}\left[1 - \frac{x_2^2}{H^2} + \sqrt{1 - \frac{x_2^2}{H^2}}\right] \tag{4.16}$$

where $C_m = 0.743$ and $\ddot{x}$ is the horizontal acceleration at the dam face.

Eq. (4.16) is implemented in *UDEC* by adjusting the gridpoint mass on the upstream face of the dam to account for the hydrodynamic pressure. The equivalent pressure, $\bar{p}$, resulting from the inertial forces associated with the gridpoint and the hydrodynamic pressure of the water in the reservoir, averaged over the area associated with the gridpoint, can be written as

$$\bar{p}(0, x_2, t) = \rho_{ec} \ddot{x}_0(t) \frac{A_g}{\Delta x_2} \tag{4.17}$$

where A_g is the area associated with the gridpoint, and Δx_2 is the contact length on the upstream face of the dam through which the water load is applied for the gridpoint.

ρ_{ec} is the equivalent density of the gridpoint and is given by

$$\rho_{ec} = \rho_c + \rho_{sc} \tag{4.18}$$

where

$$\rho_{sc} = \rho_w \frac{H \Delta x_2}{A_g} \frac{C_m}{2} \left[1 - \frac{x_2^2}{H^2} + \sqrt{1 - \frac{x_2^2}{H^2}} \right] \tag{4.19}$$

ρ_c is the density of concrete such that the gridpoint mass is given by $m_g = A_g \rho_c$. The scaled gridpoint mass $m_{sg} = A_g \rho_{ec}$ is used only for the motion calculation in the horizontal direction; the effect of the increased mass does not influence the vertical forces.

The gridpoint mass is adjusted by adding the term (as determined from Eq. (4.19)) to account for the hydrodynamic pressure. The *FISH* gridpoint variable **block.gridpoint.dynamic.mass** is available to store the gridpoint mass adjustment. The *FISH* function **wester** is provided to apply the hydrodynamic pressures to a vertical dam face. The *FISH* function requires the following input:

dx	x_1 component of the unit vector pointing in the direction of the water
dy	x_2 component of the unit vector pointing in the direction of the water
height	height of the water in the reservoir
yb	x_2 coordinate of the base of the reservoir
den_w	density of water
c_m	pressure coefficient = 0.743

Note that this scheme for applying hydrodynamic loading can only be used when a dynamic motion is acting in the horizontal direction. The scheme does not apply for a case with vertical dynamic loading.

A simple example is presented to illustrate the effect of hydrodynamic pressures on a concrete dam. The dynamic loading is applied in two different ways. First, the dam is subjected to a dynamic loading without taking into account the hydrodynamic pressure. Then, the hydrodynamic pressure is applied as a boundary condition by means of the Westergaard scaling of the gridpoint mass, as described above. Figure 4.15 shows the model for these loading cases. The dynamic loading is a velocity sine wave applied to the base of the model. The model is first brought to a static equilibrium state with the reservoir loading applied along the upstream vertical face of the dam.

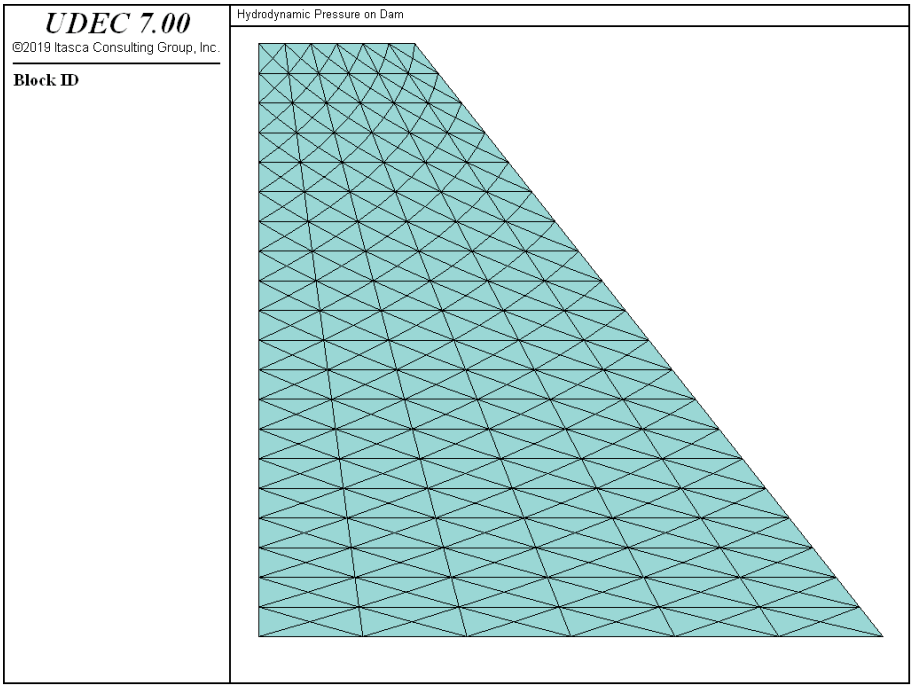

Figure 4.15 Dam model with hydrodynamic pressure boundary on upstream face

The dynamic loading is applied for a period of 10 seconds. The horizontal displacement at the top of the dam at the upstream face is monitored for both cases. The results are plotted for comparison in Figure 4.16. These results illustrate the effect on displacement of the hydrodynamic pressures.

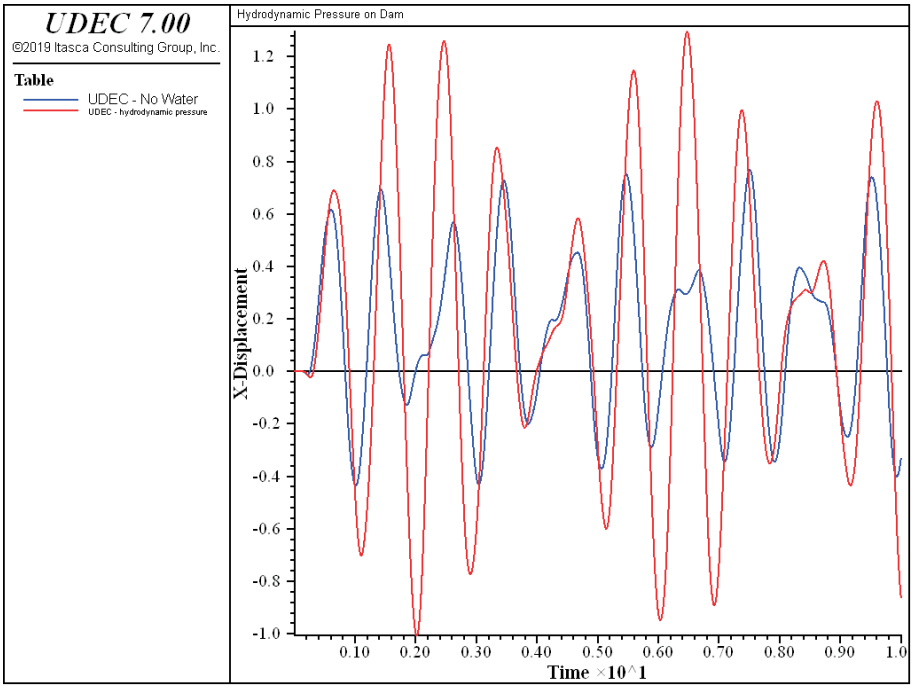

Figure 4.16 Comparison of x-displacement at top of dam

Example 4.3 Hydrodynamic pressure acting on a dam

```
model new
;File:hydrodyn.dat
; Application of hydrodynamic pressure to dam face
model Title 'Hydrodynamic Pressure on Dam'
block tolerance corner-round-length 2E-2
block tolerance minimum-edge-length 4E-2
block create polygon 30,40 30,59 35,59 50,40
block zone gen quad 1.0
block zone group 'dam'
block zone cmodel assign elastic density 2E3 bulk 1E8 shear 3E7 ...
   range group 'dam'
bl grid app velocity-x 0 range pos-x 29,51 pos-y 39.9,40.1
bl grid app velocity-y 0 range pos-x 29,51 pos-y 39.9,40.1
bl edg app stress -590000.0,0.0,0.0 gradient-x 0.0,0.0,0.0 ...
 gradient-y 10000.0,0.0,0.0 range pos-x 29.9,30.1 pos-y 39.9,59.1
block mech gravity=0.0 -10.0
block largestrain off
block solve
model save 'w1.sav'

;
; without hydrodynamic pressure
block mech damping rayleigh 0.0 0.0
block mech time 0
block gridpoint reset  vel disp
call 'sine_wave.fis'
fish set @freq=1
@sine_wave
block gridpoint history disp-x  30.0,59.0
fish history @sine_wave
block mech hist time-total
bl grid app velocity-y 0 range pos-x 29.9,50.1 pos-y 39.9,40.1
bl grid app velocity-x 1 history=@sine_wave ...
  range pos-x 29.9,50.1 pos-y 39.9,40.1
block cycle  time 10.0
call 'tabtofile.fis'
history export 1 table 1
history export 3 table 3
fish set @filename='table1.dat'
fish set @tabin 1
@tabtofile
model save 'w2.sav'
```

```
model restore 'w1.sav'
; with hydrodynamic pressure
block mech time 0
block gridpoint reset  vel disp
block mech damping rayleigh 0.0 0.0
call 'wester.fis'
fish set @dx=-1
fish set @dy=0
fish set @height=19
fish set @yb=40
fish set @c_m=0.743
fish set @den_w=1000
@westergaard
call 'sine_wave.fis'
fish set @freq=1
@sine_wave
block gridpoint history disp-x  30.0,59.0
fish history @sine_wave
block mech hist time-total
bl grid app velocity-y 0 range pos-x 29.9,50.1 pos-y 39.9,40.1
bl grid app velocity-x 1 history=@sine_wave ...
  range pos-x 29.9,50.1 pos-y 39.9,40.1
block cycle  time 10.0

history export 1 table 2
history export 3 table 3
call 'tabtofile.fis'
fish set @filename='table2.dat'
fish set @tabin 2
@tabtofile
model save 'w3.sav'


model new
;compare results
call 'table1.dat' suppress
call 'table2.dat' suppress
table 1 label 'UDEC - No Water'
table 2 label 'UDEC - hydrodynamic pressure'
model save 'compare.sav'
```

4.3.2 Wave Transmission

4.3.2.1 Accurate Wave Propagation

The physical stiffness of joints in-situ can have a substantial influence on seismic wave propagation. Myer et al. (1990) present field and laboratory test results that demonstrate the effect of the stiffness of dry natural fractures in rock on high frequency attenuation and changes in travel time of the seismic wave. It can be important to represent this effect in the discontinuum model if the wave transmission is be to modeled accurately. However, be careful to not introduce a numerical distortion of the wave that could mask the actual effect of the joints on wave propagation.

Numerical distortion of the propagating wave can occur in a dynamic analysis, whether it is based on a continuum or discontinuum program, as a function of the modeling conditions. Both the frequency content of the input wave and the wave-speed characteristics of the system will affect the numerical accuracy of wave transmission. Kuhlemeyer and Lysmer (1973) show that for accurate representation of wave transmission through a model, the spatial element size, Δl, must be smaller than approximately one-tenth to one-eighth of the wavelength associated with the highest frequency component of the input wave – i.e.,

$$\Delta l \leq \frac{\lambda}{10} \tag{4.20}$$

where λ is the wavelength associated with the highest frequency component that contains appreciable energy. For discontinuum analysis involving rigid blocks, this also applies to joint spacing (or block size).

The wavelength can be calculated from the wave speed by using Eqs. (4.29), (4.7) and (4.8) for an elastic-continuum system. For a discontinuum system containing a single set of planar joints oriented normal to the compression wave, and in which the solid material is rigid (or much stiffer than the joints), then the wave speed is only a function of joint spacing and stiffness – i.e.,

$$C_p = \sqrt{\frac{sk_n}{\rho}} \tag{4.21}$$

where s = joint spacing;
k_n = joint normal stiffness; and
ρ = mass density.

The relations can be extended to multiple-jointed media by calculating the wave speeds using closed-form solutions that have been developed to calculate effective elastic moduli as a function of the elastic moduli of the solid and the stiffnesses and spacings of the joints (see Section 3.8.2 in the **User's Guide**).

Physically measured values for normal and shear stiffnesses of a geologic structure (such as joints, faults, bedding planes, etc.) are not generally available. It is often necessary to back-calculate properties based on measured values for the elastic deformation properties of the intact material and the wave speed through the jointed system, using the formulae referenced in Section 3.8.2 in the **User's Guide**. These relations can be used to provide reasonable estimates for joint stiffness properties in *UDEC* to produce the measured shear and compressional wave speeds of the system.

In order to achieve an accurate representation of a stress wave through a distinct element model, particularly when the joint spacing is variable, the blocks should be made deformable to accommodate the element size restriction imposed by frequency and wavelength. This is accomplished in *UDEC* (as discussed in Section 1 in **Theory and Background**) by subdividing each block into a mesh of finite difference zones. These zones are then subject to the Kuhlemeyer and Lysmer restriction.

The effect of model conditions on numerical distortion of wave transmission is demonstrated by a simple analysis of a column of blocks subjected to an impulse load applied at the base (Figure 4.17). The block sizes range from approximately 1 m to 5 m (average size of 2.8 m), the contacts between blocks have a linearly elastic behavior, and the p-wave speed for the system is 4470 m/sec. A triangular-shaped impulse load, with a maximum frequency of approximately 200 Hz, is applied at the base (the solid curve in Figures 4.18 and 4.20). The wavelength associated with the highest frequency of this system is 22.4 m; thus, according to Kuhlemeyer and Lysmer, in order to transmit this wave without distortion, the element size must not exceed approximately 2 m.

A rigid block analysis is done with a constant contact normal stiffness used to produce an average wave speed of 4470 m/sec (based on the average joint spacing). A highly distorted velocity history is calculated at the top of the column, as seen by the dashed curve in Figure 4.18. This distortion can be reduced for this problem by varying the normal stiffness locally to keep the wave speed constant at contacts between blocks. However, in general, the calculation of effective (local) normal stiffnesses becomes extremely complex for a multiply jointed system, making this approach impractical.

A deformable block analysis is performed with the maximum size of the finite difference zones smaller than 2 m (see Figure 4.19). The elastic moduli for the blocks and the contact stiffness are calculated to produce the given p-wave speed. The distortion in the wave at the top of the column is now essentially eliminated, as indicated in Figure 4.20. The elastic deformation parameters represent the physical properties of the blocks and contacts separately in this case, and do not have to be adjusted locally.

The data file for this model is contained in Example 4.4.

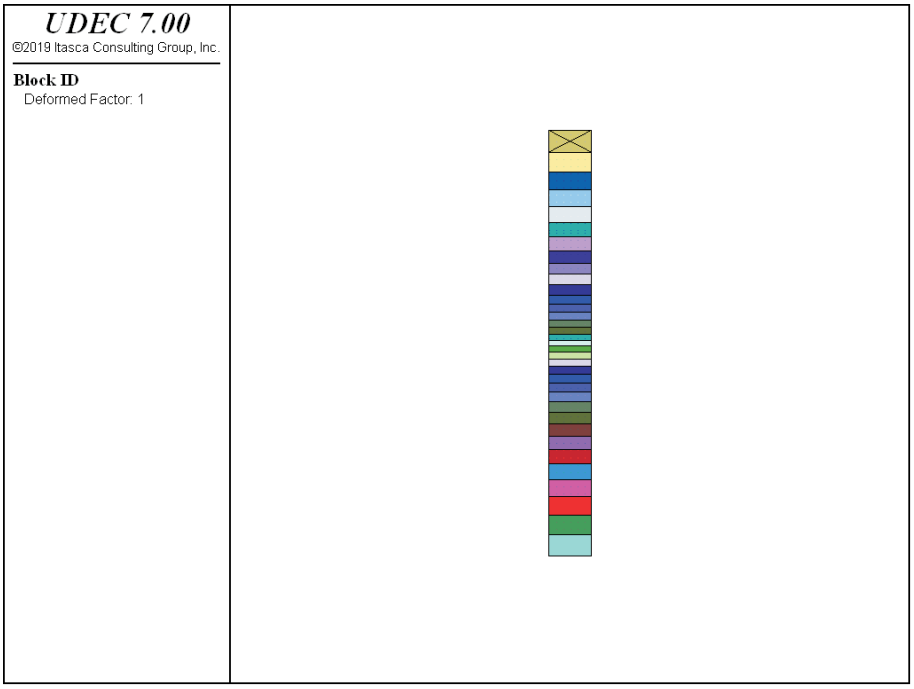

Figure 4.17 Column of variable-sized blocks subjected to triangular-shaped impulse load at base

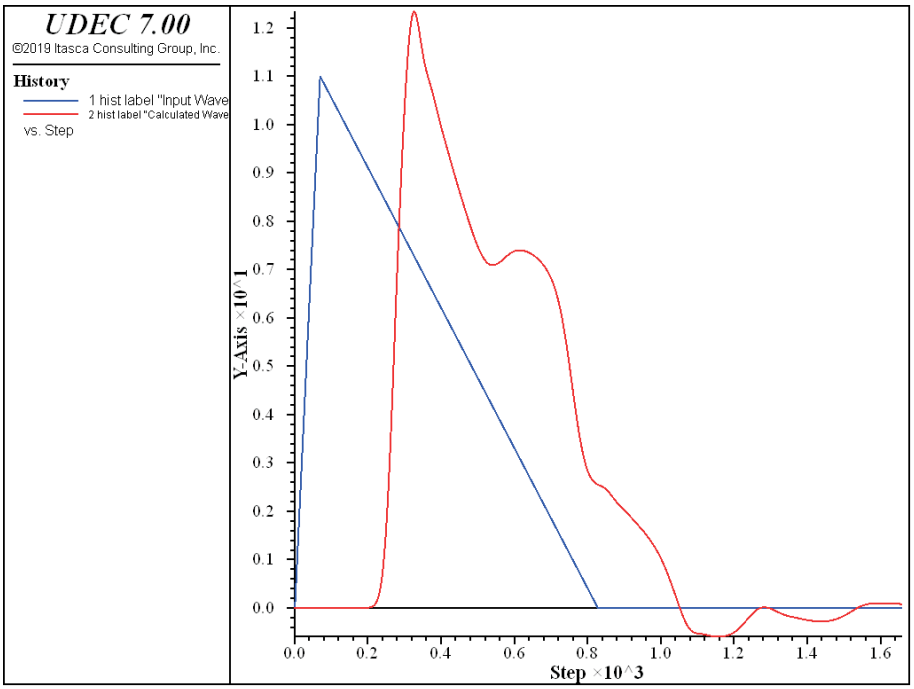

Figure 4.18 Input wave (solid) at base and calculated wave (dashed) at top of column of rigid block model

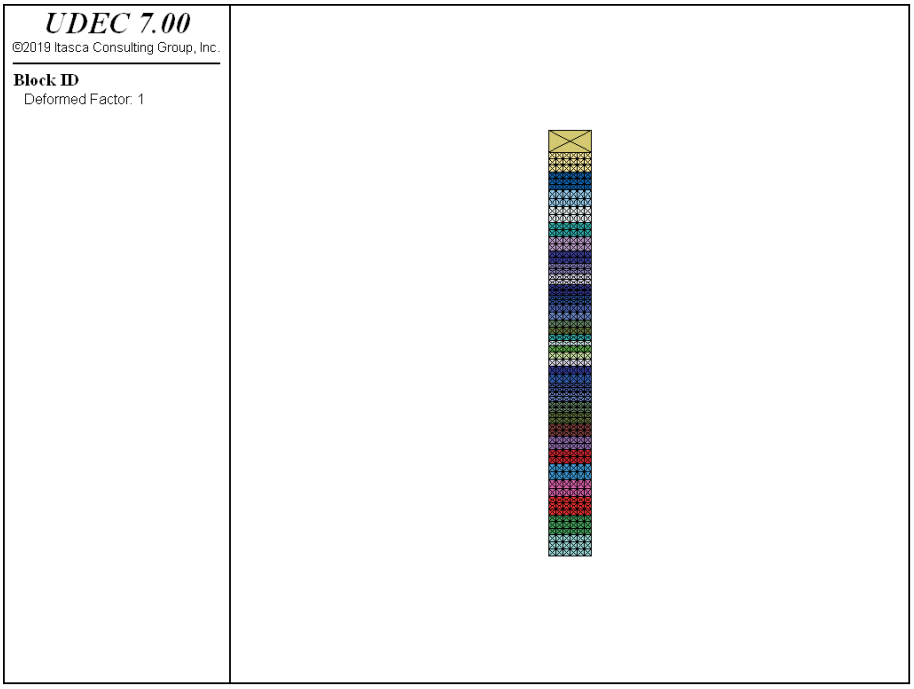

Figure 4.19 Column of variable-sized blocks subdivided into finite difference zones

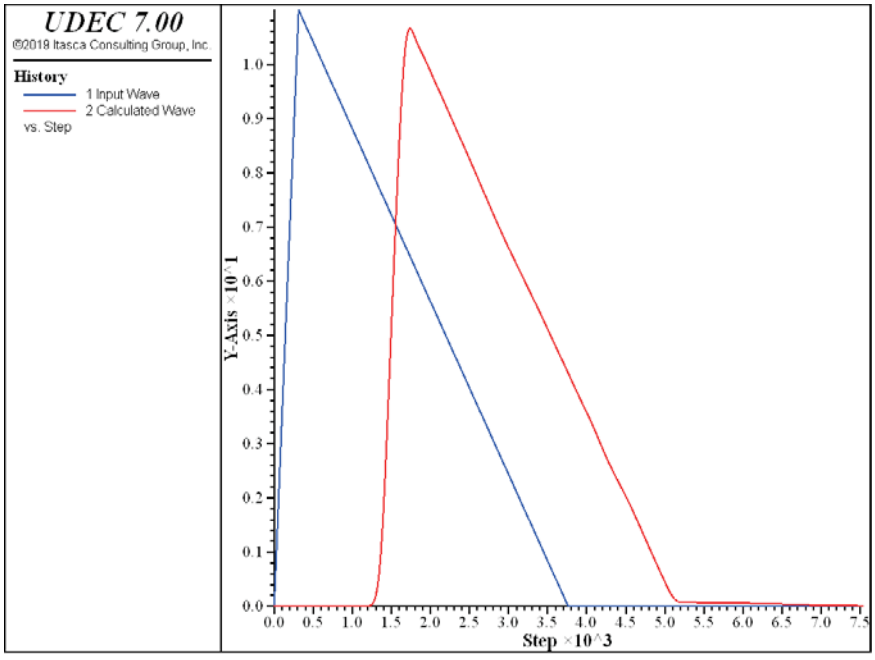

Figure 4.20 Input wave (solid) at base and calculated wave (dashed) at top of column of deformable block model

Example 4.4 Column of variable-sized blocks subjected to impulse load at base

```
model new
;file: impulse.dat
block tolerance corner-round-length 0.1
Model title 'Impulse Load with Rigid Blocks'
block create polygon 0 0 0 100 10 100 10 0
fish define var_cut
  ntot = 80
  nc = 1
  rat = 1.08
  ycut = 5.0
  yloc = ycut
  loop while nc < ntot
     command
       block cut crack 0 @yloc 10 @yloc
     endcommand
     if yloc < 50.0 then
        ycut = ycut / rat
     else
        ycut = ycut * rat
     endif
     yloc = yloc + ycut
     nc = nc + 1
  endloop
end
@var_cut
block zone gen quad 20 range pos-x 0 10 pos-y 95 100
; in order to apply viscous boundary
;
; properties for rigid block model
block property material 1 density 1000
block contact property material 1 stiffness-normal 10e9 ...
  stiffness-shear 10e9 coh 1e10 ten 1e10
block prop mat 1 bulk 1e10 shear 7.5e9
;
;  impulse load
;
fish define find_block
  _iab = block.near(5.0,3.0)
end
@find_block
;
fish define pulse
   whilestepping
```

```
    _dytime = block.mechanical.time.total
    ypulse = vmax / tpeak * _dytime
    if _dytime > tpeak then
       ypulse = vmax - (vmax / (tend - tpeak)) * (_dytime - tpeak)
    endif
    if _dytime > tend then
       ypulse = 0.0
    endif
    block.vel.y(_iab) = ypulse ; velocity assigned to rigid block at base
;    pulse = ypulse  ; velocity history for zoned model
end
fish set @vmax = 11.0 @tpeak = 0.005 @tend = 0.06
; fix bottom block to apply impulse for rigid block model
block fix all range position-x 0 10 position-y 0 5
; velocity boundary for zoned model
; quiet boundary at top for both rigid and deformable block models
block gridpoint apply viscous-y range position-x 0 10 position-y 99 101
block edge apply property material 1
block gridpoint apply velocity-x 0.0
; monitor velocities at bottom and top
history interval 1
block gridpoint history velocity-y 0 0
block gridpoint history velocity-y 0 95
fish history @pulse
hist name 1 label 'hist label "Input Wave'
hist name 2 label 'hist label "Calculated Wave'
; add 5% stiffness damping
block mechanical damping 0.05 200 stiff
block cycle time 0.12
model sav 'rig.sav'
return
```

4.3.2.2 Filtering

For dynamic input with a high peak velocity and short rise-time, the Kuhlemeyer and Lysmer requirement may necessitate a very fine spatial mesh and a corresponding small timestep. The consequence is that reasonable analyses may be prohibitively time- and memory-consuming. In such cases, it may be possible to adjust the input by recognizing that most of the power for the input history is contained in lower frequency components (e.g., use "FFT.FIS" in the FISH library in the Help in *UDEC* .)

By filtering the history and removing high frequency components, a coarser mesh may be used without significantly affecting the results.

The filtering procedure can be accomplished with a low-pass filter routine such as the fast Fourier transform technique. For example, the unfiltered velocity record shown in Figure 4.21 represents a typical waveform containing a very high frequency spike. The highest frequency of this input exceeds 50 Hz but, as shown by the power spectral density plot of Fourier amplitude versus frequency (Figure 4.22), most of the power (approximately 99%) is made up of components with frequencies of 15 Hz or lower. It can be inferred, therefore, that by filtering this velocity history with a 15 Hz low-pass filter, less than 1% of the power is lost. The input filtered at 15 Hz is shown in Figure 4.23, and the Fourier amplitudes are plotted in Figure 4.24. The difference in power between unfiltered and filtered input is less than 1%, while the peak velocity is reduced 38% and the rise time is shifted from 0.035 to 0.09 seconds. Analyses should be performed with input at different levels of filtering to evaluate the influence of the filter on model results.

If a simulation is run with an input history that violates Eq. (4.20), the output will contain spurious "ringing" (superimposed oscillations) that are nonphysical, as illustrated in Figure 4.18. The input spectrum *must* be filtered in this case before being applied to a *UDEC* model. This limitation applies to all numerical models in which a continuum is discretized; it is not just a characteristic of *UDEC*. Any discretized medium has an upper limit to the frequencies that it can transmit, and this limit must be respected in order for the results to be meaningful. Users of *UDEC* commonly apply sharp pulses or step waveforms to a *UDEC* grid; this is *not* acceptable, since these waveforms have spectra that extend to infinity. It is a simple matter to apply, instead, a smooth pulse that has a limited spectrum.

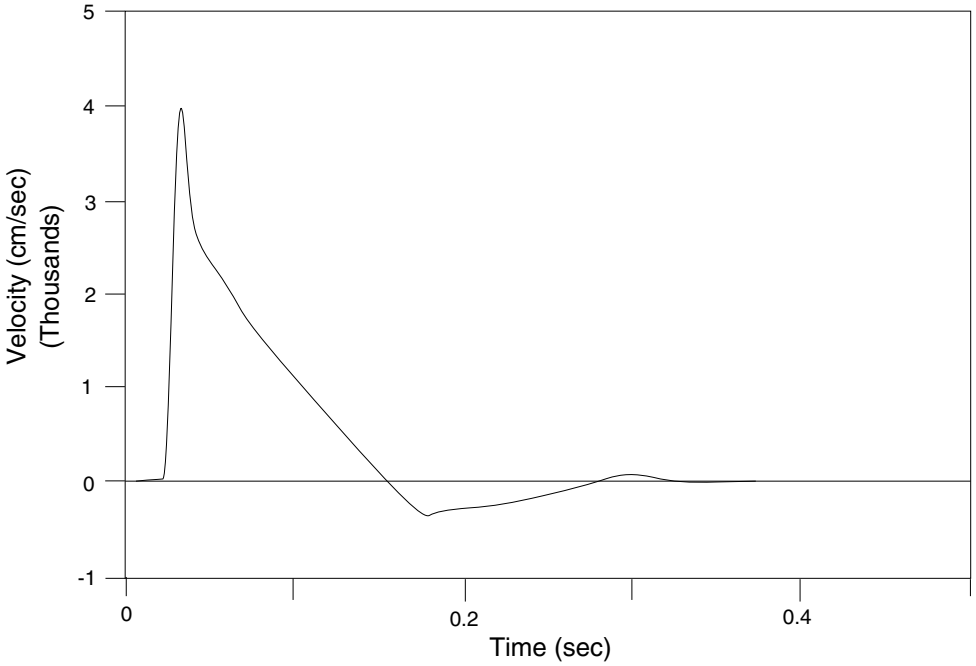

Figure 4.21 Unfiltered velocity history

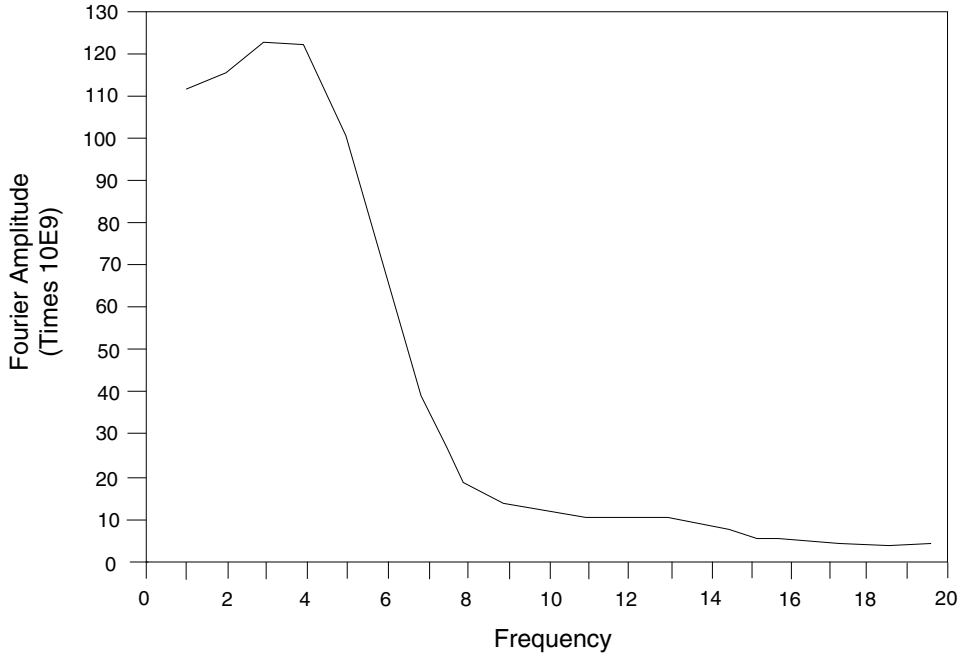

Figure 4.22 Unfiltered power spectral density plot

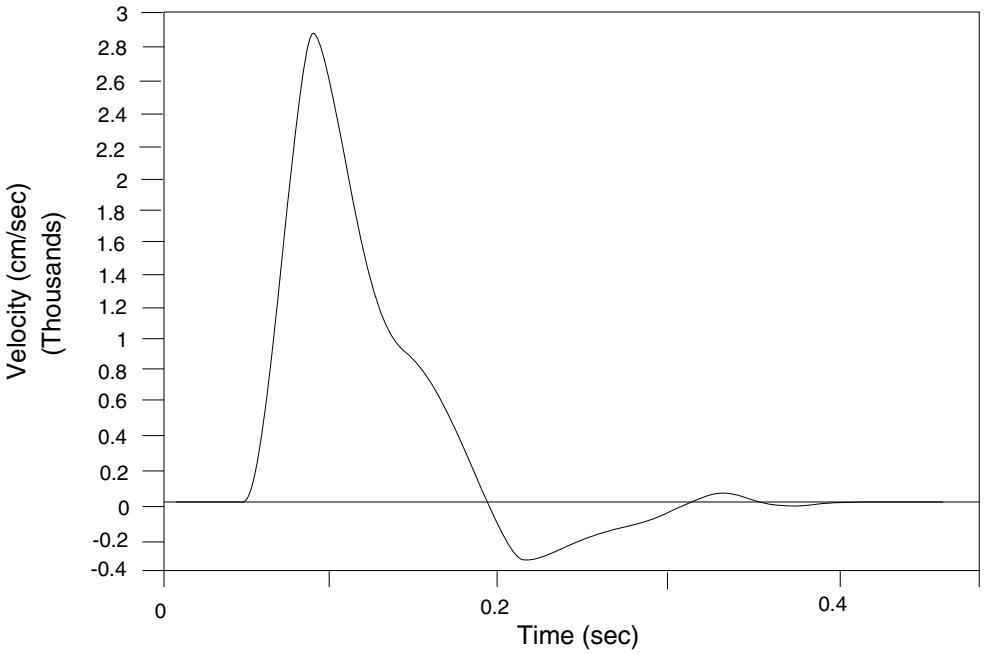

Figure 4.23 Filtered velocity history at 15 Hz

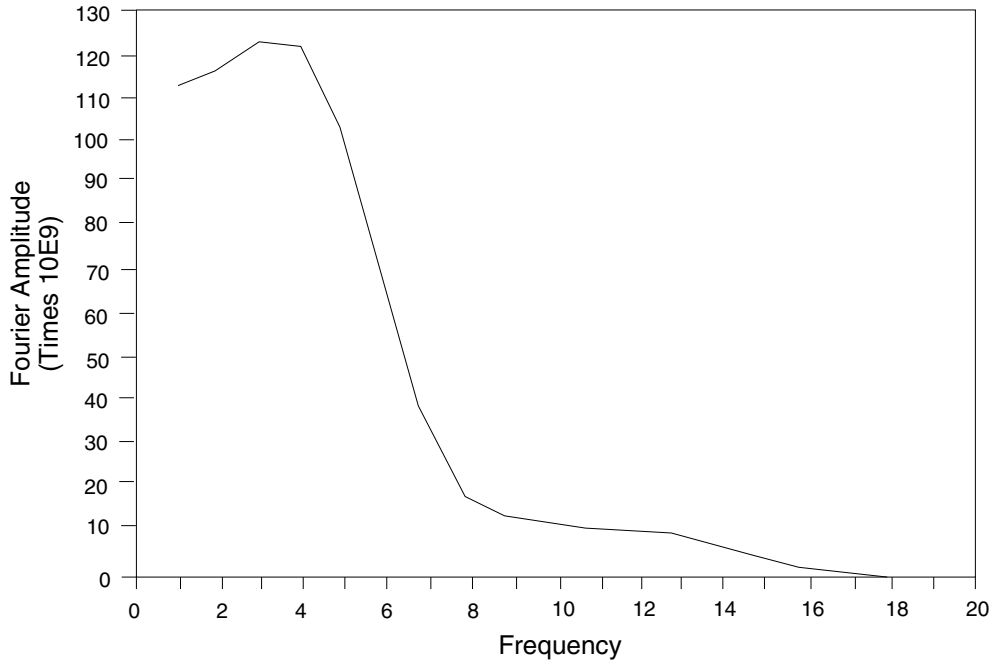

Figure 4.24 Results of filtering at 15 Hz

4.3.3 Mechanical Damping

Natural dynamic systems contain some degree of damping of the vibration energy within the system; otherwise, the system would oscillate indefinitely when subjected to driving forces. Damping is due, in part, to energy loss as a result of internal friction in the intact material and slippage along interfaces within the system.

UDEC uses a dynamic algorithm for solution of two general classes of mechanical problems: quasi-static and dynamic. Damping is used in the solution of both classes of problems, but quasi-static problems require more damping. The damping for static solutions is discussed in Section 1.2.7 in **Theory and Background**.

For a dynamic analysis, the damping in the numerical simulation should attempt to reproduce the energy losses in the natural system when subjected to dynamic loading. In soil and rock, natural damping is mainly hysteretic (i.e., independent of frequency – see Gemant and Jackson 1937; Wegel and Walther 1935). It is difficult to reproduce this type of damping numerically because of at least two problems (see Cundall 1976). First, many simple hysteretic functions do not damp all components equally when several waveforms are superimposed. Second, hysteretic functions lead to path dependence, which makes results difficult to interpret. However, if a constitutive model that contains an adequate representation of the hysteresis that occurs in a real material is found, then *no additional damping* is necessary in a *UDEC* run. The current built-in models in *UDEC* are not considered to model dynamic hysteresis well enough to omit additional damping completely.

In time domain programs, *Rayleigh damping* is commonly used to provide damping that is approximately frequency-independent over a restricted range of frequencies. Although Rayleigh damping embodies two viscous elements (in which the absorbed energy is dependent on frequency), the frequency-dependent effects are arranged to cancel out at the frequencies of interest. Rayleigh damping is described in Sections 4.3.3.1 through 4.3.3.3.

Alternatively, the *local damping* embodied in *UDEC*'s static solution scheme may be used dynamically, but with a damping coefficient appropriate to wave propagation. Local damping in dynamic problems is useful as an approximate way to include hysteretic damping. However, it becomes increasingly unrealistic as the complexity of the waveforms increases (i.e., as the number of frequency components increases). Local damping cannot properly capture the energy loss of multiple frequency cyclic loading. Local damping is described in more detail in Section 4.3.3.4.

4.3.3.1 Rayleigh Damping

Rayleigh damping was originally used in the analysis of structures and elastic continua, to damp the natural oscillation modes of the system. The equations, therefore, are expressed in matrix form.

A damping matrix, C, is used, with components proportional to the mass (M) and stiffness (K) matrices:

$$C = \alpha\ M + \beta\ K \tag{4.22}$$

where α = the mass-proportional damping constant; and

β = the stiffness-proportional damping constant.

The mass-proportional term is analogous to a dashpot connecting each *UDEC* corner or gridpoint to "ground." The stiffness-proportional term is analogous to a dashpot connected across each *UDEC* zone (responding to the strain rate). Although both terms are frequency-dependent, an approximately frequency-independent response can be obtained over a limited frequency range, with the appropriate choice of parameters, as discussed below.

For a multiple degree-of-freedom system, the critical damping ratio, ξ_i, at any angular frequency of the system, ω_i, can be found from (Bathe and Wilson 1976):

$$\alpha + \beta\ \omega_i^2 = 2\ \omega_i\ \xi_i \tag{4.23}$$

or

$$\xi_i = \frac{1}{2}\left(\frac{\alpha}{\omega_i} + \beta\ \omega_i\right) \tag{4.24}$$

The critical damping ratio, ξ_i, is also known as the fraction of critical damping for mode i with angular frequency, ω_i.

Figure 4.25 shows the variation of the normalized critical damping ratio with angular frequency, ω_i. Three curves are given: mass and stiffness components only, and the sum of both components. As shown, mass-proportional damping is dominant at lower angular frequencies, while stiffness-proportional damping dominates at higher angular frequencies. The curve representing the sum of both components reaches a minimum at

$$\begin{aligned} \xi_{\min} &= (\alpha\ \beta)^{1/2} \\ \omega_{\min} &= (\alpha/\beta)^{1/2} \end{aligned} \tag{4.25}$$

or

$$\alpha = \xi_{\min}\ \omega_{\min}$$
$$\beta = \xi_{\min}/\omega_{\min} \tag{4.26}$$

The center frequency is then defined as

$$f_{\min} = \omega_{\min}/2\pi \tag{4.27}$$

Note that at frequency $\omega_{\min}$ (or $f_{\min}$) (and *only* at that frequency), mass damping and stiffness damping each supply half of the total damping force.

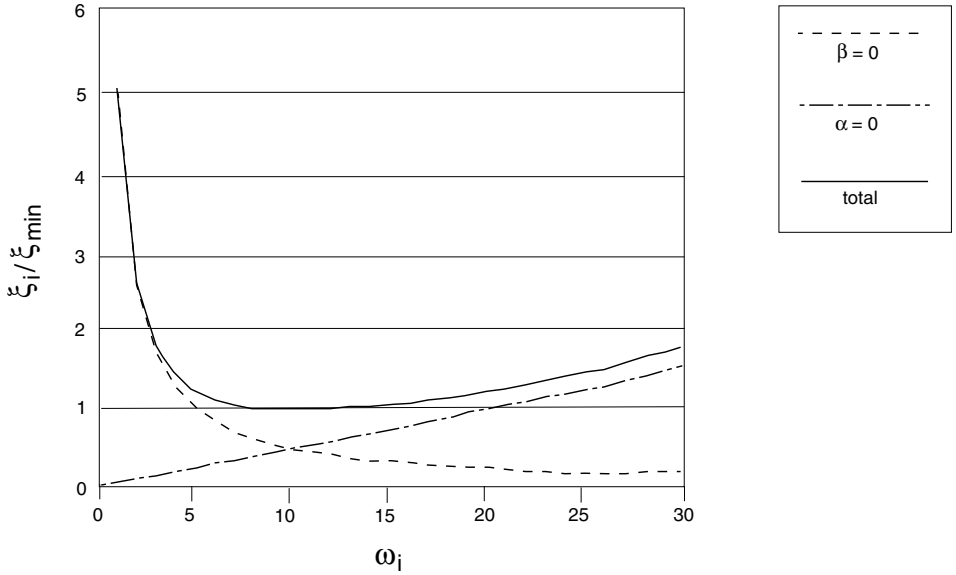

Figure 4.25 Variation of normalized critical damping ratio with angular frequency

Rayleigh damping is specified in *UDEC* with the parameters $f_{\min}$ (input parameter ***freq***) in Hertz (cycles per second) and $\xi_{\min}$ (input parameter ***fcrit***), both specified with the **block mechanical damping** command.

Stiffness-proportional damping causes a reduction in the critical timestep for the explicit solution scheme (see Eq. (4.1)). In *UDEC*, the internal timestep calculation takes stiffness-proportional damping into account, but it is still possible for instability to occur if very large block deformation occurs. If this happens, it is necessary to reduce the timestep manually (via the **block mechanical timestep-factor** command). For the case shown in Figure 4.25, $\omega_{\min} = 10$ radians per second. It is evident that the damping ratio is almost constant over at least a 3:1 frequency range (e.g., from 5

to 15). Since damping in geologic media is commonly independent of frequency, as discussed in Section 4.3.3, ω_{min} is usually chosen to lie in the center of the range of frequencies present in the numerical simulation – either natural frequencies of the model or predominant input frequencies or a combination of both. Hysteretic damping is thereby simulated in an approximate fashion.

4.3.3.2 Example Application of Rayleigh Damping

In order to demonstrate how Rayleigh damping works in *UDEC*, the results of the following four damping cases can be compared; the example consists of a block sitting on a fixed block with gravity suddenly applied. The conditions are

(a) undamped;

(b) Rayleigh damping (both mass and stiffness damping);

(c) mass damping only; and

(d) stiffness damping only.

Example 4.5 provides data corresponding to each case in turn.

Example 4.5 Block under gravity – undamped and 3 critically damped cases

```
model new
;file: Dampedblock.dat
block tolerance corner-round-length 0.01
block tolerance minimum-edge-length 0.02
block create polygon 0,0 0,10 10,10 10,0
block cut crack (0,5) (10,5)
block contact group 'joint'
block contact cmodel assign area stiffness-shear 5E7 ...
  stiffness-normal 5E7 range group 'joint'
; new contact default
block contact cmodel default area stiffness-shear=5E7 ...
  stiffness-normal=5E7
block change mat 1
block property mat 1 density 1E3
block fix vel-y range pos-x 0,10 pos-y 0,5
block mechanical gravity=0 -10
history interval 1
block gridpoint history vel-y  0.0,10.0
block gridpoint history disp-y 0.0,10.0
block mechanical hist time-total

model save 'damp1.sav'

model restore 'damp1.sav'
```

```
; --- undamped ---
model title 'Dynamic Rayleigh Damping - Undamped'
block mechanical damping rayleigh 0.0 0.0
block cycle  time 0.3
model save 'damp2.sav'

model restore 'damp1.sav'
; --- mass and stiffness damped
model title 'Dynamic Rayleigh Damping - Mass and Stiffness Damping'
block mechanical damping rayleigh 1.0 16.0
block cycle  time 0.3
model save 'damp3.sav'

model restore 'damp1.sav'
; --- mass damped ---
model title 'Dynamic Rayleigh Damping - Only Mass Damping'
block mechanical damping rayleigh 2.0 16.0 mass
block cycle  time 0.3
model save 'damp4.sav'

model restore 'damp1.sav'
; --- stiffness damped ---
model title 'Dynamic Rayleigh Damping - Only Stiffness Damping'
block mechanical damping rayleigh 2.0 16.0 stiffness
block cycle  time 0.3
model save 'damp5.sav'

ret
```

In the first case, with no damping, a natural frequency of oscillation of approximately 16 Hertz is observed (see Figure 4.26). The theoretical period of oscillation is given by

$$\text{frequency} = \frac{1}{2\pi}\left(\frac{kl}{m}\right)^{1/2} = 15.9 \text{ cycles/second} \tag{4.28}$$

where l = joint length (10 m, in this case);
k = joint stiffness (50 MPa/m); and
m = mass of upper block (50,000 kg).

The problem should be critically damped if: (1) a fraction of critical damping, $\xi_{\min}$, of 1 is specified; (2) the natural frequency of oscillation, $f_{\min}$, of 16 Hertz is specified; and (3) both mass and stiffness damping are used.

The results in Figure 4.27 show that the problem is critically damped. If only mass or stiffness damping is used, then ξ_{min} must be doubled to obtain critical damping (since each component contributes one-half to the overall damping). Figures 4.28 and 4.29 again show that the system is critically damped.

Note that the timestep is different for the three damped simulations. This is a result of the influence of stiffness-proportional damping, as discussed above.

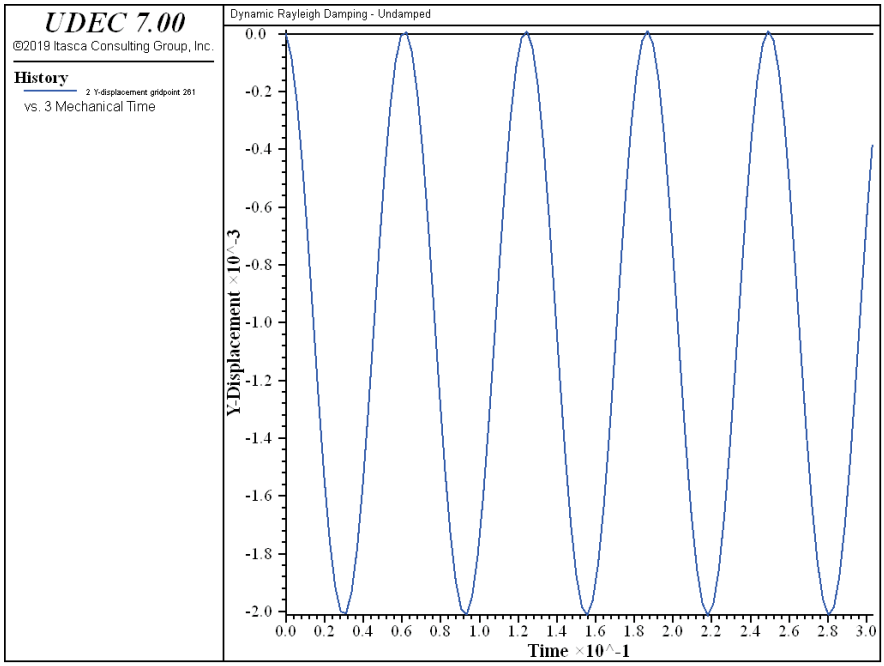

Figure 4.26 Plot of vertical displacement versus time, for a single block contacting on a rigid base with gravity suddenly applied (no damping)

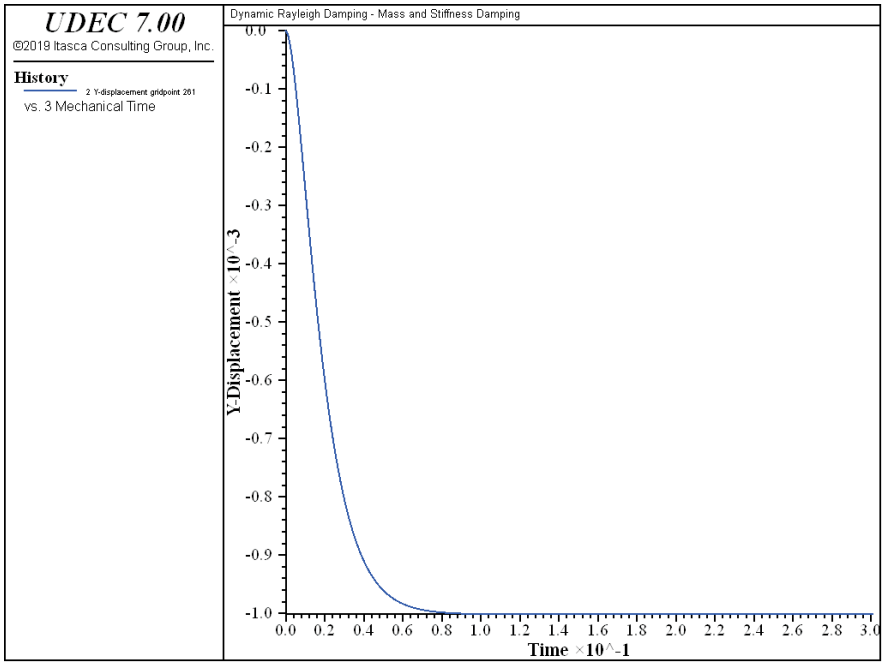

Figure 4.27 Plot of vertical displacement versus time, for a single block contacting on a rigid base with gravity suddenly applied (mass and stiffness damping)

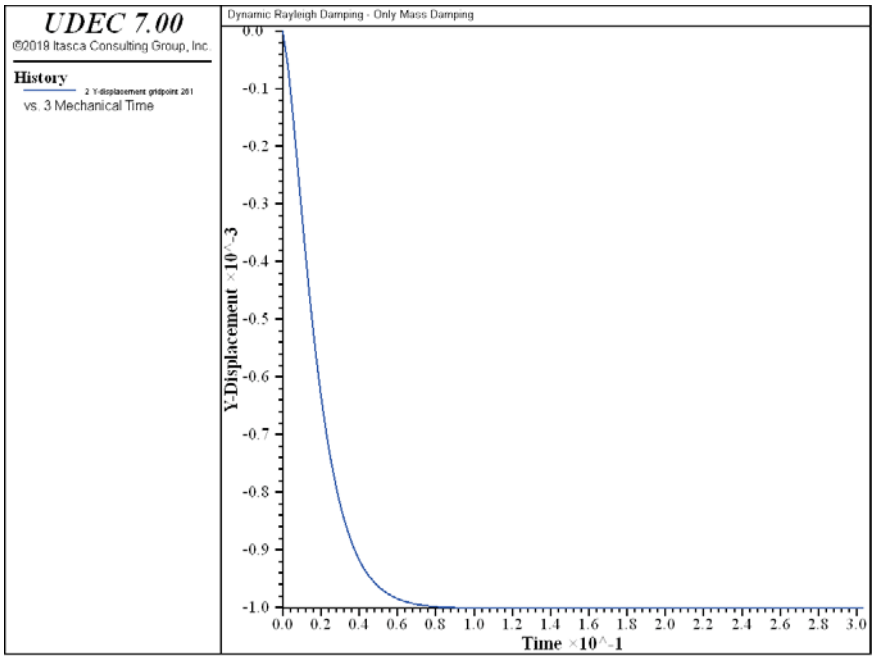

Figure 4.28 Plot of vertical displacement versus time, for a single block contacting on a rigid base with gravity suddenly applied (mass damping only)

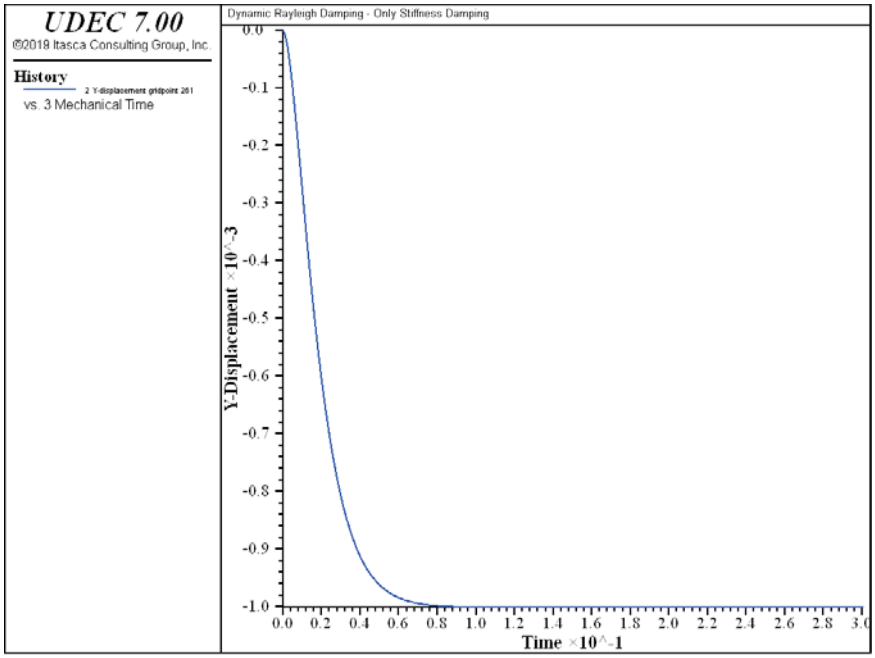

Figure 4.29 Plot of vertical displacement versus time, for a single block contacting on a rigid base with gravity suddenly applied (stiffness damping only)

4.3.3.3 Guidelines for Selecting Rayleigh Damping Parameters

Damping Ratio, $\xi_{\min}$

What is normally attempted in a dynamic analysis is the reproduction of the *frequency-independent* damping of materials at the correct level. For geological materials (e.g., soils), damping commonly falls in the range of 2 to 5% of critical; for structural systems, 2 to 10% is representative (Biggs 1964). In analyses that use one of the block plasticity models (e.g., Mohr-Coulomb), a considerable amount of energy dissipation can occur during plastic flow. Energy dissipation can also occur during joint slip. Thus, for many dynamic analyses that involve large block deformation or large joint displacement, only a minimal percentage of damping (e.g., 0.5%) may be required. Further, dissipation will increase with amplitude for stress/strain cycles that involve plastic flow or joint slip. $\xi_{\min}$ is adjusted to coincide with the correct physical damping ratio.

Center Frequency, $f_{\min}$

Rayleigh damping is frequency-dependent but has a "flat" region that spans about a 3:1 frequency range, as shown in Figure 4.25. For any particular problem, a spectral analysis of typical velocity records might produce a response such as shown in Figure 4.30.*

---

* A spectral analysis based on a fast Fourier transform is supplied as a *FISH* library function in Help in*UDEC* . – see "FFT.FIS."

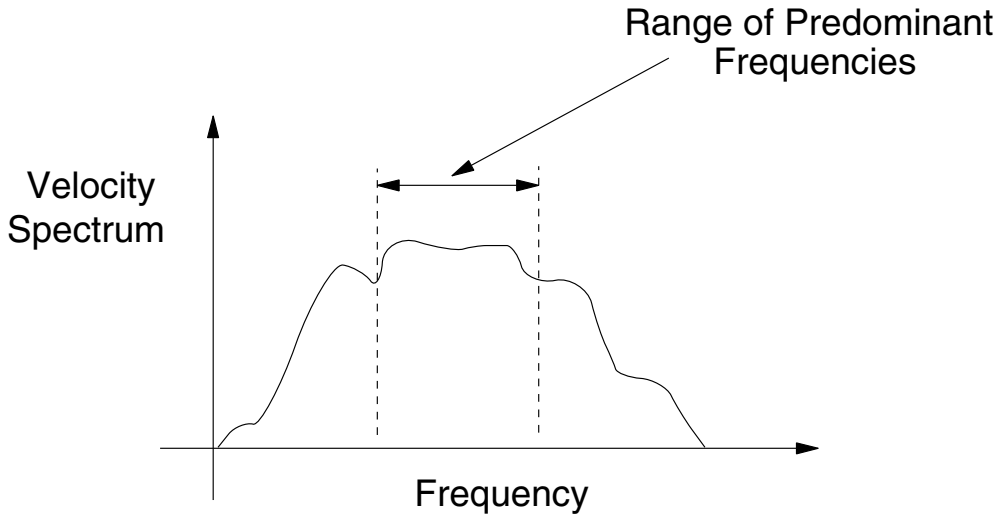

Figure 4.30 Plot of velocity spectrum versus frequency

If the highest predominant frequency is three times greater than the lowest predominant frequency, then there is a 3:1 span or range that contains most of the dynamic energy in the spectrum. The idea in dynamic analysis is to adjust $f_{\min}$ of the Rayleigh damping so that its 3:1 range coincides with the range of predominant frequencies in the problem. $\xi_{\min}$ is adjusted to coincide with the correct physical damping ratio. The "predominant frequencies" are neither the input frequencies nor the natural modes of the system, but a combination of both. The idea is to try to get the right damping for the *important* frequencies in the problem.

For many problems, the important frequencies are related to the natural mode of oscillation of the system. Examples of this type of problem include seismic analysis of surface structures such as dams or dynamic analysis of underground excavations. The fundamental frequency, f, associated with the natural mode of oscillation of a system is

$$f = \frac{C}{\lambda} \tag{4.29}$$

where C = speed of propagation associated with the mode of oscillation; and

λ = longest wavelength associated with the mode of oscillation.

For deep underground structures, the frequency of interest is usually given by the applied input wave. In this situation, the input wave contains the dominant frequencies.

For a continuous, elastic system (e.g., a one-dimensional elastic bar), the speed of propagation, C_p, for p-waves is given by Eq. (4.7), and for s-waves by Eq. (4.8). If shear motion of the bar gives rise to the lowest natural mode, then C_s is used in the above equation; otherwise, C_p is used if motion parallel to the axis of the bar gives rise to the lowest natural mode.

The longest wavelength (or characteristic length or fundamental wavelength) depends on boundary conditions. Consider a solid bar of unit length with boundary conditions, as shown in Figure 4.31(a). The fundamental mode shapes for cases (1), (2) and (3) are as shown in Figure 4.31(b). If a wavelength for the fundamental mode of a particular system cannot be estimated in this way, then a preliminary run may be made with zero damping (for example, see Figure 4.26). A representative natural period may be estimated from time histories of velocity or displacement. Section 4.4.2 contains another example in which natural periods are estimated by undamped simulations.

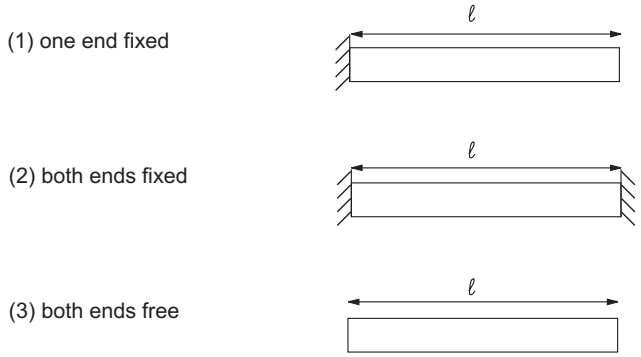

(a) boundary (end) conditions

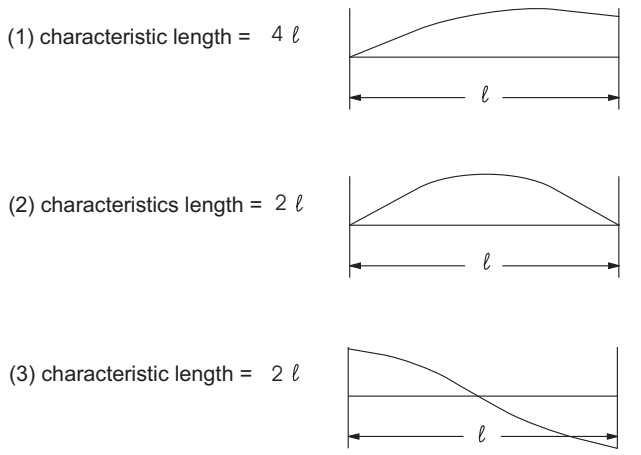

(b) characteristic lengths or fundamental wavelengths

Figure 4.31 Comparison of fundamental wavelengths for bars with varying end conditions

4.3.3.4 Local Damping for Dynamic Simulations

Local damping (see Section 1 in **Theory and Background**) was originally designed as a way to equilibrate static simulations. However, it has some characteristics that make it attractive for dynamic simulations. It operates by adding or subtracting mass from a gridpoint or structural node at certain times during a cycle of oscillation; there is overall conservation of mass, because the amount added is equal to the amount subtracted. Mass is added when the velocity changes sign, and subtracted when it passes a maximum or minimum point. Hence, increments of kinetic energy are removed twice per oscillation cycle (at the velocity extremes). The amount of energy removed, ΔW, is proportional to the maximum, transient strain energy, W, and the ratio $\Delta W / W$ is independent of rate and frequency. Since $\Delta W / W$ may be related to fraction of critical damping, D (Kolsky 1963), we obtain the expression

$$\alpha_L = \pi D \tag{4.30}$$

where α_L is the local damping coefficient. Thus, the use of local damping is simpler than Rayleigh damping, because we do not need to specify a frequency. To compare the two types of damping, we repeat Example 4.5 with 5% damping. Example 4.6 provides the data file. A similar run is done with local damping, with the coefficient set to 0.1571 ($= 0.05\pi$) – see Example 4.7. We adjust the timestep for the second run to match the timestep for the first (using the **block mechanical timestep-factor** command) so that we can execute the same number of steps in each to obtain the same elapsed time. Displacement histories from the two runs are given in Figures 4.32 and 4.33, respectively. The results are quite similar.

Example 4.6 Continuation of Example 4.5 with 5% Rayleigh damping

```
;file: rayldamp.dat
model rest 'damp1.sav'
;
model title 'Dynamic Damping - 5% Rayleigh Damping'
block mechanical damping rayleigh 0.05 16
block cycle time 1.2
model save 'rayl.sav'
```

Example 4.7 Continuation of Example 4.5 with 5% local damping

```
;file: localdamp.dat
model rest 'damp1.sav'

model title 'Dynamic Damping - 5% Local Damping'
block mechanical damping local 0.1571  ;  pi * 0.05
block mechanical timestep-factor 0.084
block cycle time 1.2
model save 'local.sav'
```

CAUTION: Local damping appears to give good results for a simple case because it is frequency-independent and needs no estimate of the natural frequency of the system being modeled. However, this type of damping should be treated with caution, and the results compared to those with Rayleigh damping for each application. There is some evidence to suggest that, for complicated waveforms, local damping underdamps the high frequency components, and may introduce high frequency "noise."

Local damping is *not* recommended for seismic simulations, because this type of damping cannot properly represent the energy loss of multiple cyclic loading completely.

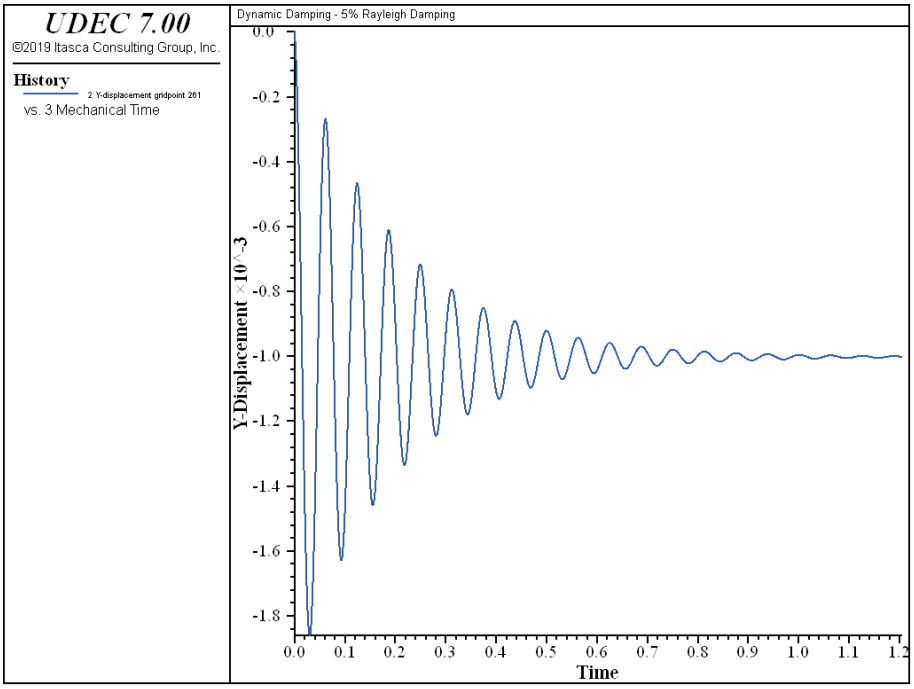

Figure 4.32 Displacement history – 5% Rayleigh damping

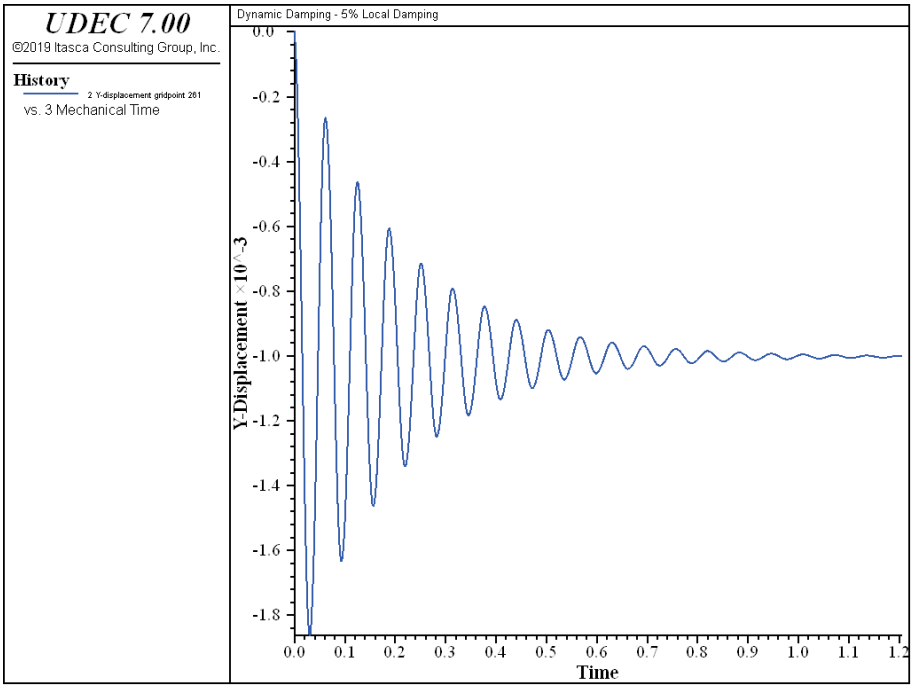

Figure 4.33 Displacement history – 5% local damping

4.4 Solving Dynamic Problems

In this section, an approach for modeling dynamic problems is described. The general methodology is described first, followed by an example application in which the various stages in the analysis are illustrated. Section 3.6 in the **User's Guide** and Section 4 in the **Example Applications** also contain examples that demonstrate this approach for dynamic analysis with *UDEC*.

4.4.1 General Methodology

Dynamic analysis is viewed as a loading condition on the model, and as a distinct stage in a modeling sequence, as described in Section 3.6 in the **User's Guide**. A static equilibrium calculation *always* precedes a dynamic analysis. There are generally four components to the dynamic analysis stage:

1. Ensure that model conditions satisfy the requirements for accurate wave transmission (by adjusting zone sizes within blocks with the **block zone generate** command; see Section 4.3.2). This check must be performed even before the static solution is performed, because blocks cannot be rezoned after the calculation starts.

2. Specify appropriate mechanical damping, representative of the problem materials and input frequency range (use the **block mechanical damping** command as described in Section 4.3.3).

3. Apply dynamic loading and boundary conditions (by using the **block edge apply** or **block gridpoint apply** command – see Section 4.3.1). A given time history may need to be filtered in order to comply with the requirements noted in Section 4.3.2.

4. Set up facilities to monitor the dynamic response of the model (by using the **block gridpoint history** command).

4.4.2 Illustration of Procedures: Stability of a Jointed-Rock Slope

The procedure for dynamic analysis is illustrated in Example 4.8, and then in Example 4.9. The model is greatly simplified for rapid execution, but still demonstrates the steps in a dynamic analysis. The example application is a stability analysis of an open cut in a jointed rock mass. The slope is 10 m high and is cut in rock containing two continuous joint sets with dip angles of 20° and 80°. The intact material is elastic, and the joints have a friction angle of 45°. The cut is initially stable for the given slope angle of 31°.

The data file for the initial static loading state is given below. The stress state of the model at equilibrium is shown in Figure 4.34.

Example 4.8 Initial conditions for the slope problem

```
model new
;file: slopestable.dat
model title 'Dynamic Slope Stability'
block tolerance corner-round-length 5.0E-2
block create polygon 0,-5 0,0 5,0 10,10 22,10 22,-5
block cut joint-set angle 20 trace 100 spacing 2 origin 5,0
block cut joint-set angle 80 trace 100 spacing 4 origin 5,0
block zone gen quad 4.0,4.0
block zone gen edge 4.0
block zone group 'block'
block zone cmodel assign elastic density 2.5E-3 bulk 1.6667E4 ...
  shear 1E4 range group 'block'
block contact group 'joint'
block contact cmodel assign area stiffness-shear 2E5 ...
  stiffness-normal 2E5 friction 45 range group 'joint'
; new contact default
block contact cmodel default area stiffness-shear=2E5 ...
  stiffness-normal=2E5 friction=45
block insitu stress -0.125,0.0,-0.25 gradient-x 0.0,0.0,0.0 ...
  gradient-y 0.0125,0.0,0.025
bl grid app velocity-x 0 range pos-x -0.1,0.1  pos-y -5.1,0.1
bl grid app velocity-x 0 range pos-x 21.9,22.1 pos-y -5.1,10.1
bl grid app velocity-y 0 range pos-x -0.1,22.1 pos-y -5.1,-4.9
block mechanical gravity=0 -10
```

```
block gridpoint history disp-x  11.0,10.0
block gridpoint history disp-y 11.0,10.0
block mechanical history unbalanced
block solve ratio 1.0E-5
model save 'slope0.sav'
```

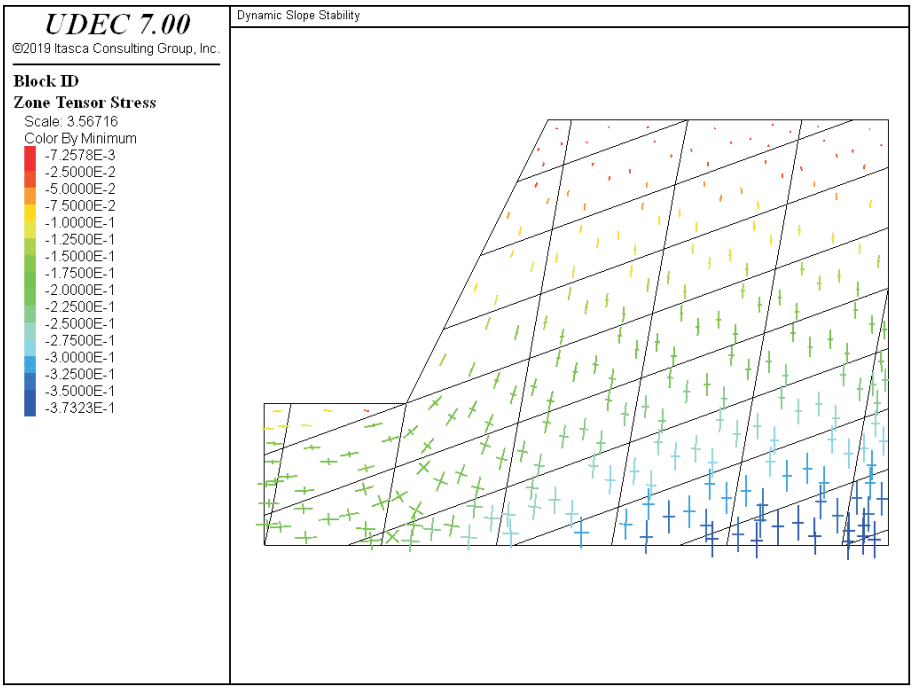

Figure 4.34 Initial equilibrium of slope cut in jointed rock

The slope is subjected to ground shaking as a result of shear and normal dynamic waves applied to the base of the model. The four steps identified previously are now followed to prepare the dynamic analysis:

1. **Check Wave Transmission** – The dynamic loading for this problem is given as a shear sinusoidal velocity record. The shear wave has a frequency of 10 Hz and an amplitude of 2 m/sec. The duration of the dynamic loading is 0.1 sec.

   There are two aspects of this analysis that must be considered with respect to wave transmission. First, as discussed in Section 4.3.2, numerical accuracy of the model is controlled by the relation between element size (joint spacing for rigid blocks and zone size for deformable blocks) and wavelength of peak velocities. Second, because the wave speed is affected by the joint characteristics, the joint structure may introduce a physically real distortion in the wave transmission.

   In order to evaluate the numerical accuracy, we ignore the presence of the joint structure by setting the joint stiffnesses to high values, based upon the limiting relation given by

Eq. (3.7) in the **User's Guide**. The shear wave speed is then calculated from the intact block elastic moduli and is (from Eq. (4.8))

$$C_s = 2000 \text{ m/sec}$$

The largest zone dimension in this model is approximately 4.5 m. Based upon Eqs. (4.29) and (4.20), the maximum frequency that can be modeled accurately is

$$f = \frac{C_s}{\lambda} = \frac{C_s}{10\ \Delta l} \approx 44 \text{ Hz}$$

Therefore, the zone size is small enough to allow waves at the input frequency to propagate accurately.

In order to evaluate the influence of the joint structure on wave transmission, it is necessary to have field measurements of the waveform (e.g., from accelerometer tests). Since physically measured values for joint stiffnesses are difficult to obtain, stiffnesses can be back-calculated to best-fit the wave transmission calculated in the model to that measured in the field.

In this example, the joint stiffnesses are assumed to be 200 GPa/m; these stiffnesses have a negligible effect on the wave transmission. This can be seen by setting the joint strengths to high values and applying the input velocities to the model, without the slope cut, and with free-field boundaries on the sides. We monitor the velocities at the bottom and top boundaries; the results shown in Figure 4.35 illustrate that no distortion of the wave has occurred.

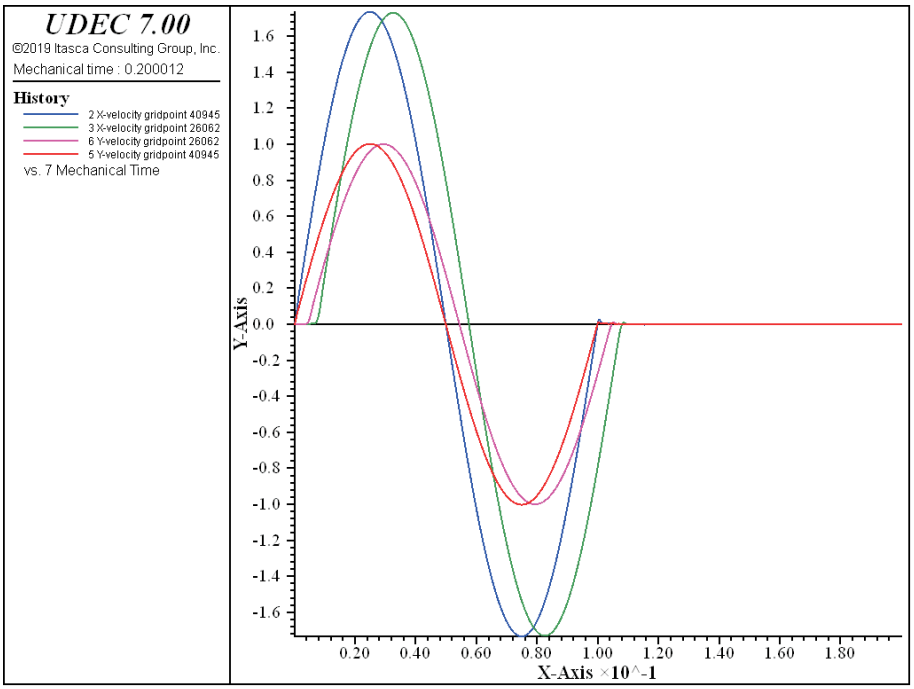

Figure 4.35 Input velocity (history 2) and calculated velocity (history 3) at top of model without slope

2. **Specify Damping** – Energy is dissipated as the joints slip and separate during the dynamic loading, which tends to make the selection of damping parameters less critical to the outcome of the analysis. This model was run with a very small amount of Rayleigh damping (0.1% at the natural frequency) to minimize the influence of high-frequency components. The dominant natural frequency is defined by the input wave frequency for this problem. This can be shown by running the model with high strength properties and no damping, and monitoring the velocity history at different locations in the model.

3. **Apply Dynamic Loading and Boundary Conditions** – The base of the model is considered to be flexible, so we must convert the input velocity to shear stresses in order to apply the dynamic loading with a quiet boundary for the flexible foundation (see Section 4.3.1.1). A *FISH* function, **`convert`**, supplies the conversion factor to convert the velocity input into stress input, based on Eq. (4.6). The boundary stress is then applied to the base of the model in the shear direction using the **block edge apply** command with the velocity wave input applied as a multiplier via the **history** keyword. The *FISH* function **`wave`** supplies the sinusoidal velocity history defined by a 1 m/sec amplitude, 10 Hz frequency and 0.1 sec. duration. Free-field boundaries are assigned along the left and right boundaries to absorb energy.

4. **Monitor Dynamic Response** – Velocity histories are located at various locations in the model: at the position of the applied input wave, along the slope face, and within the interior of the model.

The data file for the dynamic stage is reproduced in Example 4.9:

Example 4.9 Dynamic excitation of the slope problem

```
;file: slopedy.dat
model restore 'slope0.sav'

fish def convert
  c_p = math.sqrt((b_mod + (4.0 * sh_mod / 3.0)) / m_dens)
  c_s = math.sqrt(sh_mod / m_dens)
  norm_str  = -2.0 * m_dens * c_p
  shear_str = 2.0*(-2.0 * m_dens * c_s)
end
fish set @m_dens=0.0025
fish set @b_mod=16667
fish set @sh_mod=10000
@convert
fish def wave
  if block.mech.time.total > env_time
```

```
    wave = 0.0
  else
    wave = ampl * math.sin(2.0*math.pi*freq*block.mech.time.total)
  endif
end
fish set @freq =10
fish set @ampl=1.0
fish set @env_time=0.1
@wave

block edge apply dynamic-free-field
block edge property bulk=16667.0 shear=10000.0 density=0.0025
block grid apply visc-x visc-y range pos-y -5.1,-4.9
bl edg app stress 0.0,@norm_str,@norm_str history=@wave ...
  range pos-y -5.1,-4.9
history reset
block mechanical reset time
block gridpoint reset disp
fish history @wave
block gridpoint history vel-x  10.0,-5.0
block gridpoint history vel-x  8.0,6.0
block gridpoint history vel-x  18.0,-2.0
block gridpoint history vel-y  10.0,-5.0
block gridpoint history vel-y  22.0,10.0
block mech hist time-total
block mechanical damping rayleigh 0.0010 10.0

model save 'slopedy.sav'

block cycle  time 0.2
model save 'slope02.sav'

block cycle  time 0.2
model save 'slope03.sav'

block cycle  time 0.3
model save 'slope04.sav'
```

The response of the slope at 0.7 seconds (0.6 second after the dynamic wave is stopped) is shown in Figure 4.36. Sliding failure of the blocks is occurring along the slope face. The x-velocity histories in Figure 4.37 illustrate the influence of the joint structure on the input history (at $x = 10$, $y = -5$, history 2), the movement at the slope face (at $x = 8$, $y = 6$, history 3), and the return to equilibrium at a position remote from the slope (at $x = 20$, $y = -20$, history 4). History 3 velocity levels off at a nonzero value, indicating that the slope block is moving. Note that there are still some high frequency components in the velocity response.

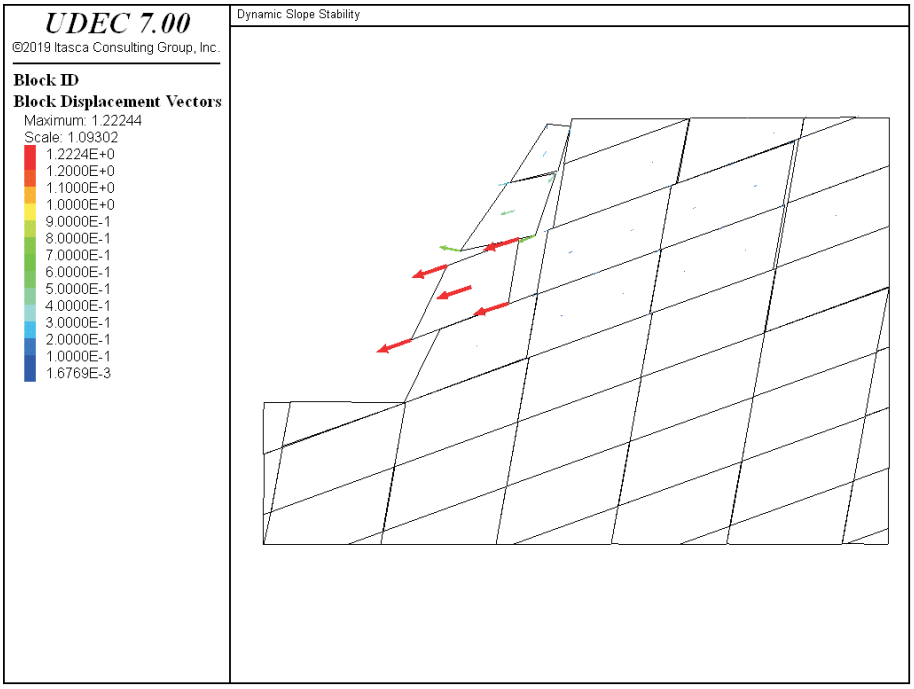

Figure 4.36 Slope failure resulting from dynamic loading

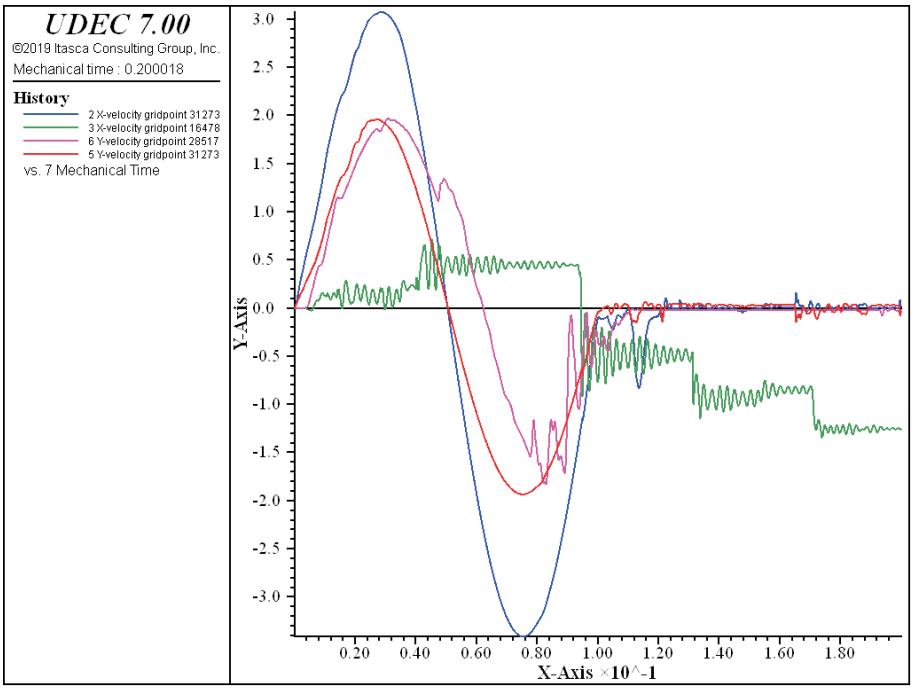

Figure 4.37 x-velocity histories at base, slope face and remote from slope

4.5 Validation Examples

Several examples are presented to validate and demonstrate the dynamic option in *UDEC*. The data files for these examples are contained in the "ITASCA\UDEC700\datafiles\Dynamic" directory.

4.5.1 Natural Periods of an Elastic Column

A column of elastic material resting on a rigid base has natural periods of vibration, depending on the mode of oscillation and the confining conditions. Three cases are examined: an unconfined column, a confined column in compression and a column in shear.

The column is loaded by applying gravity in either the x- or y-direction and observing the oscillations with zero damping. The case of confined compression is modeled by inhibiting lateral displacement along the vertical boundaries, which prevents lateral deformation of the model. For unconfined compression, lateral displacement is not inhibited. For the column in shear, vertical motion is inhibited, to eliminate bending modes; the loading is applied laterally.

The theoretical value for natural period of oscillation, T, is given by Eq. (4.31):

$$T = 4L\sqrt{\frac{\rho}{E^*}} \tag{4.31}$$

where E^* is the appropriate modulus selected from Table 4.1.

Table 4.1 Moduli appropriate to various deformation modes

Confined Compression	Unconfined Compression	Shear
$K + (4/3)\ G$	$4G\left[\frac{(1/3)\ G+K}{K+(4/3)\ G}\right]$ (plane strain, Young's modulus)	G
2.5714×10^4	1.4286×10^4	1.0×10^4

UDEC data files for the three cases are given in Examples 4.10, 4.11 and 4.12. Material properties are given below.

Table 4.2 Material properties

Properties	Symbol	Value	Comment
bulk modulus	K	2.0×10^4	for compression tests
shear modulus	G	0.428562×10^4	
Poisson's ratio	ν	0.4	
bulk modulus	K	1.0×10^4	for shear tests
shear modulus	G	1.0×10^4	
Poisson's ratio	ν	0.125	
density	ρ	1.0	
applied gravity	g_y	-1.0	for compression tests
	g_x	0.1	for shear tests
column height	L	800	
column width	W	100	

Table 4.3 compares the theoretical periods and calculated (*UDEC*) natural periods of oscillation, averaged over several periods by the *FISH* function **`crossings`** – see Example 4.13.

Table 4.3 Comparison of theoretical and calculated (UDEC) dynamic period T of oscillation for three modes

	Confined Compression	Unconfined Compression	Shear
Theoretical	19.96	26.77	32.00
UDEC	19.68	25.62	32.05

Example 4.10 Data file for confined compression

```
model new
;file: confined.dat
block tolerance corner-round-length 0.8
block create poly -50,-400 -50,400 50,400 50,-400
block cut joint-set angle 0 trace 100 spacing 100 origin 0,0  join
block zone gen quad 200.0
block mechanical damping rayleigh 0.0 0.0
block zone group 'block'
block zone cmodel assign elastic density 1 bulk 2E4 shear 4.28562E3 ...
  range group 'block'
block mechanical gravity=0 -1
history interval 1
block gridpoint history velocity-y  50.0,400.0
block gridpoint apply velocity-y 0 range pos-x -51,51 pos-y -401,-399
block gridpoint apply velocity-x 0
block cycle time 100.0
call 'avper.fis'
model save 'confined.sav'
```

Example 4.11 Data file for unconfined compression

```
model new
;file: unconfined.dat
block tolerance corner-round-length 0.8
block create polygon -50,-400 -50,400 50,400 50,-400
block cut joint-set angle 0 trace 100 spacing 100 origin 0,0  join
block zone gen quad 200.0
block mechanical damping rayleigh 0.0 0.0
model save 'base.sav'

block zone group 'block'
block zone cmodel assign elastic density 1 bulk 2E4 shear 4.28562E3 ...
  range group 'block'
block mechanical gravity=0 -1
history interval 1
block gridpoint history vel-y  50.0,400.0
block gridpoint apply velocity-y 0 range pos-x -51,51 pos-y -401,-399
block cycle time 100.0
call 'avper.fis'
model save 'unconfined.sav'
```

Example 4.12 Data file for shear

```
model new
;file: shear.dat
block tolerance corner-round-length 0.8
block create polygon -50,-400 -50,400 50,400 50,-400
block cut joint-set angle 0 trace 100 spacing 100 origin 0,0  join
block zone gen quad 200.0
block mechanical damping rayleigh 0.0 0.0
block zone group 'block'
block zone cmodel assign elastic density 1 bulk 1E4 shear 1e4 ...
  range group 'block'
block mechanical gravity=1 0
history interval 1
block gridpoint history vel-x  50.0,400.0
block gridpoint apply velocity-x 0 range pos-x -51,51 pos-y -401,-399
block gridpoint apply velocity-y 0
block cycle time 100.0
call 'avper.fis'
model save 'shear.sav'
```

Example 4.13 Listing of "avper.fis": function to compute average period

```
hist export 1 table 1  ; Note: velocity history must be number 1
fish define crossings
  _dytime      = block.mechanical.time.total
  ndif        = 0
  dif         = 0.0
  t_cross_old = 0.0
  sign        = 1.0
  delta_t     = block.mechanical.timestep
  loop n (1,global.step)
    if math.sgn(table.y(1,n)) # math.sgn(sign)
      sign        = -sign
      t_cross = (n - 1) * delta_t
      if t_cross_old # 0.0
        dif  = dif + t_cross - t_cross_old
        ndif = ndif + 1
      endif
      t_cross_old = t_cross
    endif
  end_loop
  ii = io.out(' Crossings = '+string(ndif))
```

```
  ii = io.out(' Average period = '+string(2.0*dif/ndif))
end
@crossings
;
```

4.5.2 Slip Induced by Harmonic Shear Wave

This problem concerns the effects of a planar discontinuity on the propagation of an incident shear wave. Two homogeneous, isotropic, semi-infinite elastic regions, separated by a planar discontinuity with a limited shear strength, are shown in Figure 4.38. A normally incident, plane harmonic, shear wave will cause slip at the discontinuity, resulting in frictional energy dissipation. Thus, the energy will be reflected, transmitted and absorbed at the discontinuity. The problem is modeled with *UDEC*, and the results are used to determine the coefficients of transmission, reflection and absorption. These coefficients are compared with ones given by an analytical solution (Miller 1978).

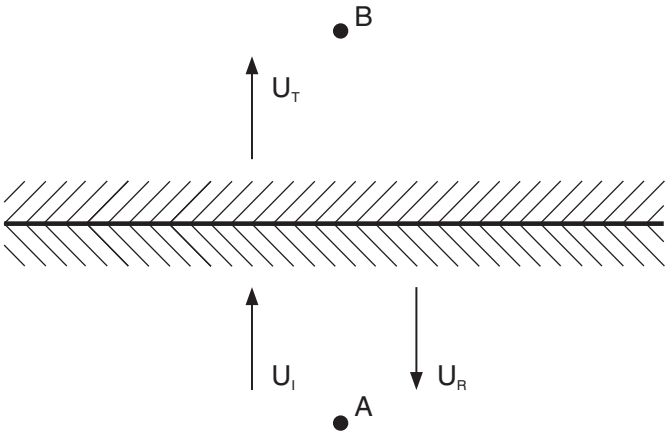

Figure 4.38 Transmission and reflection of incident harmonic wave at a discontinuity

The coefficients of reflection (R), transmission (T) and absorption (A) given by Miller (1978) for the case of uniform material are

$$R = \sqrt{\frac{E_R}{E_I}} \tag{4.32}$$

$$T = \sqrt{\frac{E_T}{E_I}} \tag{4.33}$$

$$A = \sqrt{1 - R^2 - T^2} \tag{4.34}$$

where E_I, E_T and E_R represent the energy flux per unit area per cycle of oscillation associated with the incident, transmitted and reflected waves, respectively. The coefficient A is a measure of the energy absorbed at the discontinuity. The energy flux E_I is given by

$$E_I = \int_{t_1}^{t_1+T} \sigma_s \, v_s \, dt \tag{4.35}$$

where T = $(2\pi)/\omega$ = the period for the incident wave;

σ_s = shear stress;

v_s = particle velocity in the x-direction; and

ω = frequency of incident wave (radian/sec).

For elastic media,

$$\sigma_s = \rho \, c \, v_s \tag{4.36}$$

Hence,

$$E_I = \rho \, c \int_{t_1}^{t_1+T} v_s^2 \, dt \tag{4.37}$$

in which c is the velocity of the propagating shear wave.

The energy flux of the incident wave, E_I, is evaluated at point A (see Figure 4.38) for no slip at the discontinuity. The energy flux of the transmitted wave, E_T, is evaluated at point B for the case of slip at the discontinuity. The energy flux of the reflected wave, E_R, is calculated by determining the difference of velocities in two cases: slip and no slip.

Figure 4.39 shows the numerical model, which consists of two sub-grids connected by an interface EF, which has high stiffness and simulates the discontinuity. The conditions used are as follows.

Boundary Conditions

- Nonreflecting viscous boundaries are located at GH and CD.
- Vertical motion is prevented along lateral boundaries GC and DH.

Loading Conditions

- Shear stresses corresponding to the incident wave are applied along CD.
- The maximum stress of the incident wave is 1 MPa and the frequency is 1 Hz.

Material Conditions

- elastic media

  ρ = 2.65 × 10^3 kg/m^3

  K = 16,667 MPa

  G = 10,000 MPa

- interface

  k_x = k_s = 10,000 MPa/m

  C = cohesion = 2.5 MPa for no-slip = 0.5, 0.1, 0.02 MPa for slip case

Note that the magnitude of the incident wave must be doubled in the numerical model to account for the simultaneous presence of the nonreflecting boundary (see Section 4.3.1.1).

Example 4.14 provides a data file that makes four complete simulations of the problem: the first simulation is for a fully elastic case, and the remaining simulations correspond to the various values of cohesion. Computed values for R, T and A are written to the log file "UDEC.LOG" if the model is run in command-driven mode. If run in *GIIC* mode, the computed values are displayed in the *Console* pane.

The initial assumption of an elastic discontinuity is achieved by assigning a high cohesion (2.5 MPa, in this case) to the interface. Figure 4.40 shows the time variation of shear stress near points A and B. From the amplitude of the stress histories at A and B, it is clear that there is perfect transmission of the wave across the discontinuity. It is also clear from Figure 4.40 that the viscous boundary condition provides perfect absorption of normally incident waves. Following the execution of the elastic case, the velocity history at point A is saved in table 1, to be used later for calculating E_I used in the equations for energy coefficients.

The cohesion of the discontinuity is then set, successively, to 0.5, 0.1 and 0.02 MPa to permit slip to occur. The recorded shear stresses at points A and B for the three cases are shown in Figures 4.41, 4.42 and 4.43, respectively. The peak stress at point A is the superposition of the incident wave and the wave reflected from the slipping discontinuity. It can be seen in Figures 4.41 through 4.43 that the shear stress of point B is limited by the discontinuity strength.

After each inelastic simulation, the velocity histories at points A and B are saved in tables 2 and 3, and the energy flux and coefficients R, T and A are computed by the *FISH* function **`energy`** and written to the log file. All conditions are then reset to zero, and requested histories are deleted, in preparation for the next simulation; this is done in function **`common`**. It was determined that at least five cycles of the input wave were necessary before the computed coefficients settled down to steady-state values. Even then, there is a periodic fluctuation in the values. In order to obtain mean values, the coefficient values were averaged over the final 100 timesteps: the *FISH* variable

i_mean controls the step number at which this averaging process starts. Figure 4.44 compares the numerical results with the exact solution for the coefficients for three values of the dimensionless parameter:

$$\frac{\omega \gamma U}{\tau_s}$$

where τ_s = discontinuity cohesion;

U = displacement amplitude of the incident wave;

γ = $\sqrt{\rho G}$; and

ω = frequency of incident wave (1 Hz).

The displacement amplitude for the incident wave (U) was obtained by monitoring the horizontal displacement at point A for non-slipping discontinuities. As can be seen, the *UDEC* results agree well with the analytical solution.

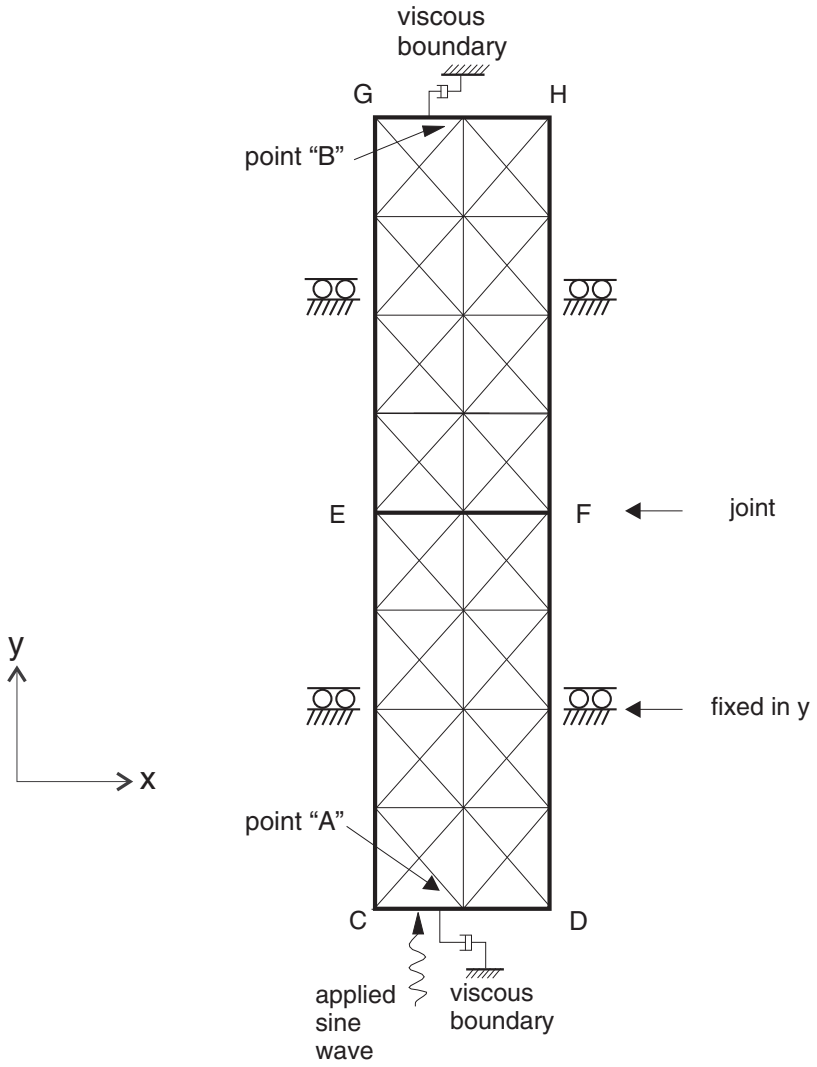

Figure 4.39 Problem geometry and boundary conditions for the problem of slip induced by harmonic shear wave

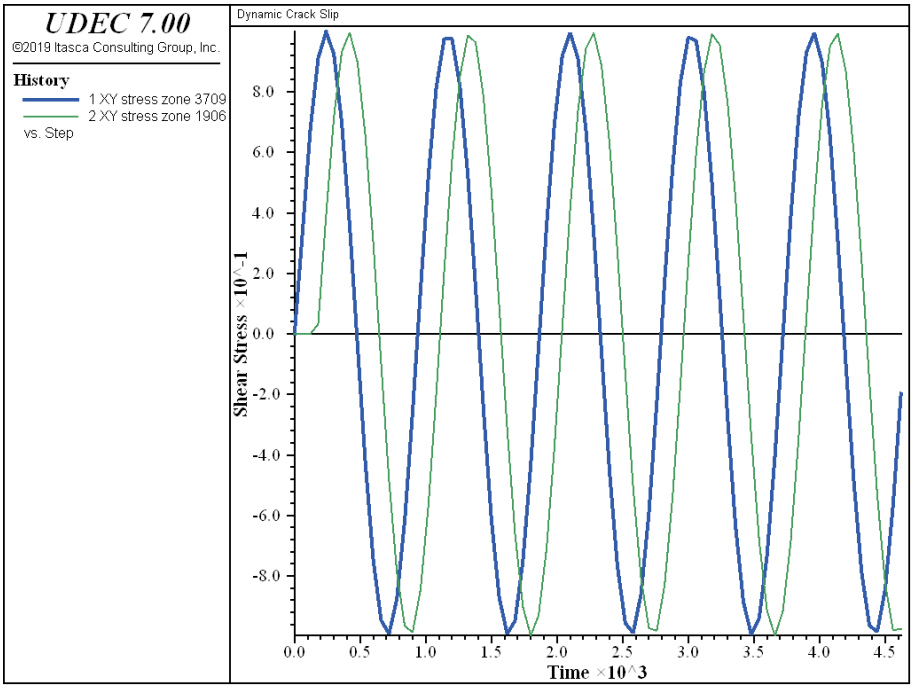

Figure 4.40 Time variation of shear stress at points A and B for elastic discontinuity (cohesion = 2.5 MPa)

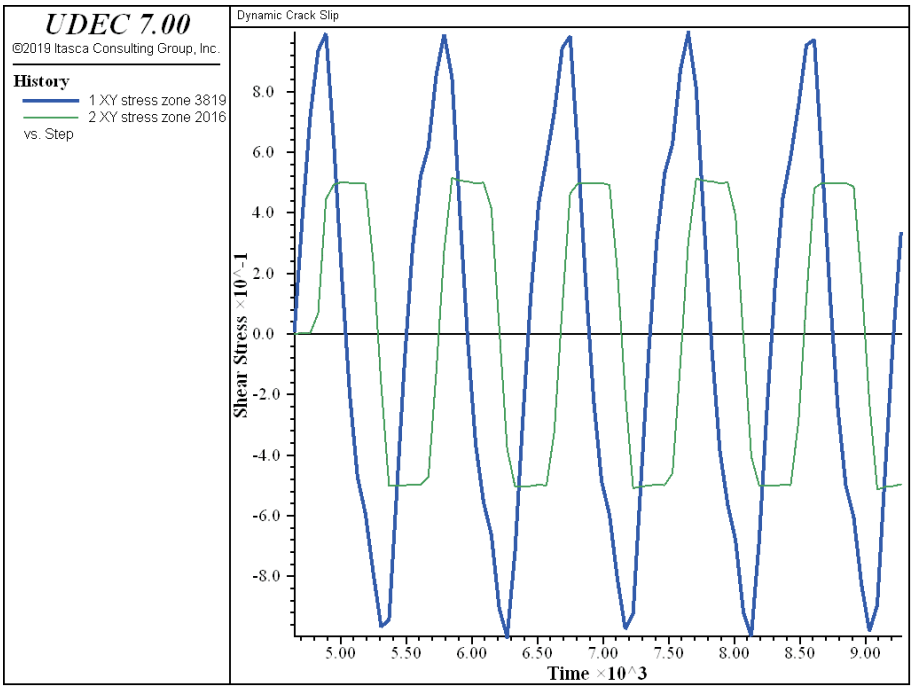

Figure 4.41 Time variation of shear stress at points A and B for slipping discontinuity (cohesion = 0.5 MPa)

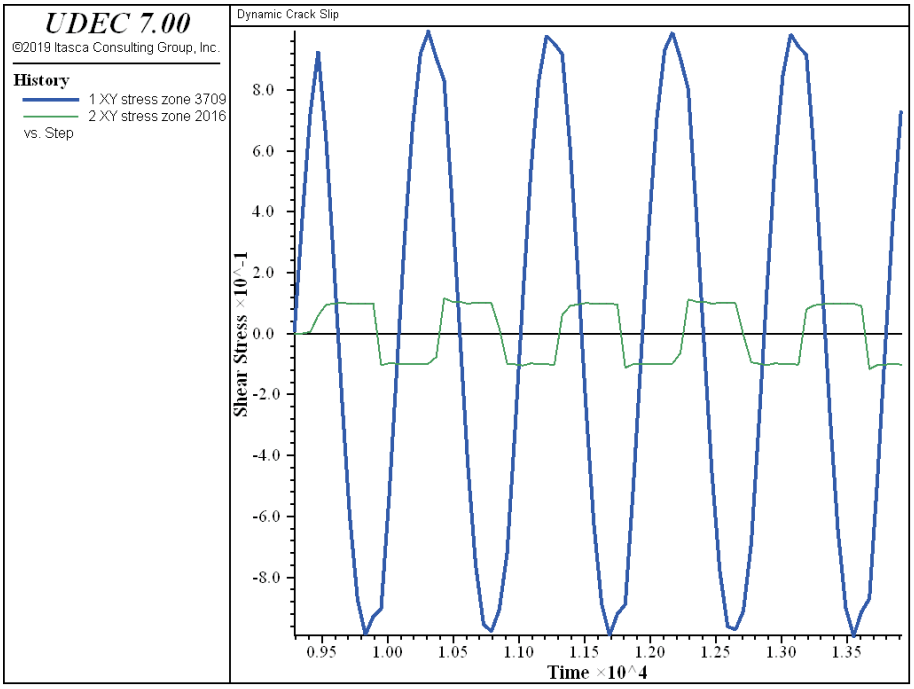

Figure 4.42 Time variation of shear stress at points A and B for slipping discontinuity (cohesion = 0.1 MPa)

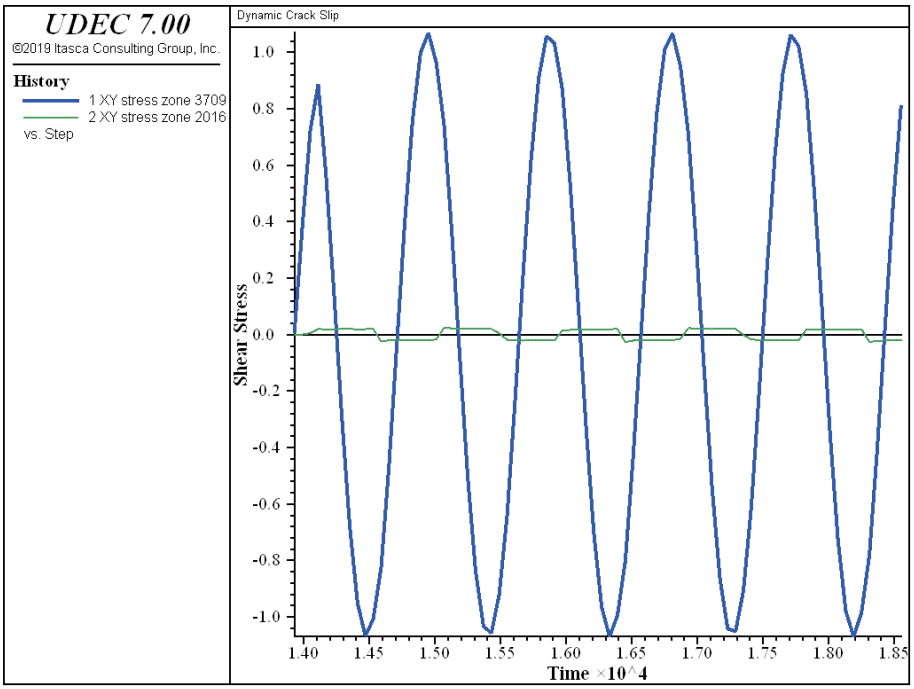

Figure 4.43 Time variation of shear stress at points A and B for slipping discontinuity (cohesion = 0.02 MPa)

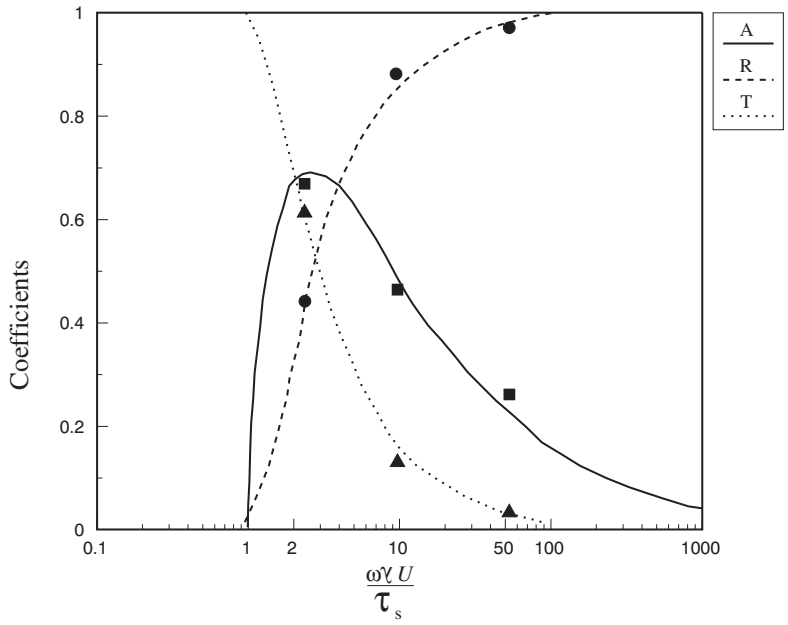

Figure 4.44 Comparison of transmission, reflection and absorption coefficients; points denote UDEC results

Example 4.14 Verification of dynamic slip – four complete simulations

```
model new
;file: dynslip.dat
model title 'Dynamic Crack Slip'
block tolerance corner-round-length 0.1
block create polygon -200 -200 -200 200  -120 200 -120 -200
block cut crack -210,0 201 0
block zone gen edge 60
block mech damp rayleigh 0.005 1 stiff
;
fish def setup
   mat_shear = 10000.0
   mat_dens  = 0.00265
   freq      = 1.0
   tload     = 10.0
   w         = 2.0 * math.pi * freq
end
fish def fsin
   if block.mech.time.total <= tload then
      fsin = math.sin(w*block.mech.time.total)
   else
```

```
      fsin = 0.0
   endif
end
fish def common
   command
      hist reset
      block gridpoint reset disp vel
      block mechanical time  0
      block zone reset stress
      block contact reset stress
      block edge apply free-x free-y
      block edge property bulk=16667 shear=@mat_shear density=@mat_dens
      block gridpoint apply visc-x range pos-y  -201,-199
      block gridpoint apply visc-y range pos-y  -201,-199
      block gridpoint apply visc-x range pos-y   199, 201
      block gridpoint apply visc-y range pos-y   199, 201
      block edge apply stress 0,2,0 hist @fsin  range  pos-y  -201,-199
      block gridpoint apply vel-y = 0           range  pos-x  -201,-199
      block gridpoint apply vel-y = 0           range  pos-x  -121,-119
      block zone hist           stress-xy -160,-200
      block zone hist           stress-xy -160,200
      block gridpoint hist      vel-x (-160,-200)
      block gridpoint hist      vel-x (-160,200)
      block gridpoint hist      dis-x (-160,-200)
      block gridpoint hist      dis-x (-160,200)
      block mechanical hist time-total
      block insitu stress 0 0 -1e-6
      block step time 5.0
   endcommand
end
;
fish def energy
;- compute energy coefficients for slipping-joint example -
;;
;; table 1 - x-velocity at point A for elastic joint case
;; table 2 - x-velocity at point A for slipping joint case
;; table 3 - x-velocity at point B for slipping joint case
;; table 4 - model mechanical time
;; Ei - energy flux for incident wave
;; Et - energy flux for transmitted wave
;; Er - energy flux for reflected wave
;; AAA  - a measure of energy absorbed at the interface
;; items - no. of items in tables
;;
   Cs     = math.sqrt(mat_shear / mat_dens)
   factor = mat_dens * Cs
```

```
   Ei    = 0.0
   Et    = 0.0
   Er    = 0.0
   t_n_1 = 0.0
   nac   = 0
   AAA   = 0.0
   TTT   = 0.0
   RRR   = 0.0
   loop i (1,items)
      t_n = table.y(4,i+1)
      d_t  = t_n - t_n_1
      t_n_1 = t_n
      Vsa_e = table.y(1,i+1)
; NOTE:
;  i+1 accounts for zero inserted at
;  the beginning of the first history
      Vsa_s = table.y(2,i+1)
      Vsb_s = table.y(3,i+1)
      Ei = Ei + factor * Vsa_e * Vsa_e * d_t
      Et = Et + factor * Vsb_s * Vsb_s * d_t
      Er = Er + factor * (Vsa_s-Vsa_e) * (Vsa_s-Vsa_e) * d_t
      if i > i_mean
         nac = nac + 1
         RRR = RRR + math.sqrt(Er/Ei)
         TTT = TTT + math.sqrt(Et/Ei)
      endif
   end_loop
   RRR = RRR / float(nac)
   TTT = TTT / float(nac)
   AAA = AAA + math.sqrt(1.0-RRR*RRR-TTT*TTT)
   command
      log on
   end_command
   ii = io.out(' R = '+string(RRR))
   ii = io.out(' T = '+string(TTT))
   ii = io.out(' A = '+string(AAA))
   command
      log off
   end_command

end
@setup

;hist export 3 table 1  ; model save elas incident wave
;
block zone group 'block'
```

```
block zone cmodel assign elastic density @mat_dens bulk 16667 ...
  shear @mat_shear  range group 'block'
;
block contact group 'joint'
block contact cmodel assign area stiffness-shear 10000 ...
  stiffness-normal 10000 cohesion=2.5 tens=1e6 ...
  range group 'joint'

; new contact default
block contact cmodel default area stiffness-shear=10000 ...
  stiffness-normal=10000 cohesion=0 tens=1e6
;
fish set @items 460
fish set @i_mean=360
@common
hist export 3 table 1  ; model save elas incident wave
model save 'dinte.sav'

block contact cmodel assign area stiffness-shear 10000 ...
  stiffness-normal 10000 cohesion=0.5 tens=1e6 ...
  range group 'joint'
@common
hist export 3 table 2
hist export 4 table 3
hist export 7 table 4
@energy
model save 'dintp5.sav'

;
block contact cmodel assign area stiffness-shear 10000 ...
  stiffness-normal 10000 cohesion=0.1 tens=1e6 ...
  range group 'joint'
@common
hist export 3 table 2
hist export 4 table 3
hist export 7 table 4
@energy
model save 'dintp1.sav'

;
block contact cmodel assign area stiffness-shear 10000 ...
  stiffness-normal 10000 cohesion=0.02 tens=1e6 range group 'joint'
@common
hist export 3 table 2
hist export 4 table 3
hist export 7 table 4
```

```
@energy
model save 'dintp02.sav'

ret
```

4.5.3 Line Source in an Infinite Elastic Medium with a Single Discontinuity

This verification problem consists of an infinite elastic medium containing a single planar discontinuity, and subject to a line source of compression parallel to the discontinuity. The closed-form solution was derived by Day (1985) as a special symmetric condition for the general problem of slip of an interface due to a dynamic point source (Salvado and Minster 1980). The solution assumes that the discontinuity has a viscous behavior in shear, and is rigid in the normal direction.

The problem geometry, shown in Figure 4.45, is defined by a planar crack of infinite lateral extent and infinitesimal thickness, ϵ, in an elastic medium, and a dynamic load at some distance, $y = h$, from the discontinuity. The y-axis is a line of symmetry.

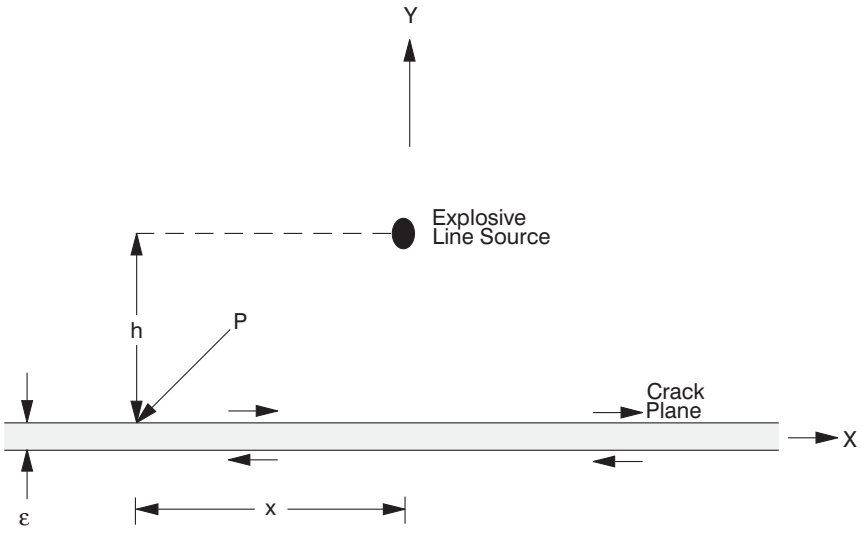

Figure 4.45 Problem geometry for an explosive source near a slip-prone discontinuity

The closed-form solution for crack slip as a function of time, as derived by Day (1985) is given by

$$\delta u(x,t) = \frac{2\, m_o\, \beta^2}{\pi\, \rho\, \alpha^2}\, Re\left[\frac{p\, \eta_\alpha\, \eta_\beta}{R(p)}\right]\left(\tau + \frac{2r}{\alpha}\right)^{-1/2} \tau^{-1/2}\, H(\tau) \tag{4.38}$$

where

$$R(p) = (1 - 2\,\beta^2\, p^2)^2 + 4\,\beta^4\, \eta_\alpha\, \eta_\beta\, p^2 + 2\,\beta\, \eta_\beta\, \gamma$$

$$p = \frac{1}{r^2}\left[\left(\tau + \frac{r}{\alpha}\right) x + i\left(\tau + \frac{2r}{\alpha}\right)^{1/2} \tau^{1/2}\, h\right]$$

and r = $(x^2 + h^2)^{1/2}$, distance from the point source to the point on the crack where the slip is monitored;
$H(\tau)$ = step function;
τ = $t - (r/\alpha)$
m_o = source strength;
α = velocity of pressure wave;
β = velocity of shear wave;
ρ = density;
η_α = $(\alpha^{-2} - p^2)^{1/2}$, $Re\ \eta_\alpha \geq 0$;
η_β = $(\beta^{-2} - p^2)^{1/2}$, $Re\ \eta_\beta \geq 0$;
γ = dimensionless bonding parameter,

The slip response of the discontinuity for any source history $S(t)$ can be obtained by convolution of Eq. (4.38) and the source function $S(t)$. Figure 4.46 shows the dimensionless analytical results of slip history at a point P for a smooth step function

$$S(t) = \begin{cases} 0.5\ (1 - \cos(\pi t/0.6)) & \text{t} < 0.6 \\ 1.0 & \text{t} \geq 0.6 \end{cases} \tag{4.39}$$

and for the values of the variables α, x and γ:

α^2 = $3\ \beta^2$
x = h
γ = 0

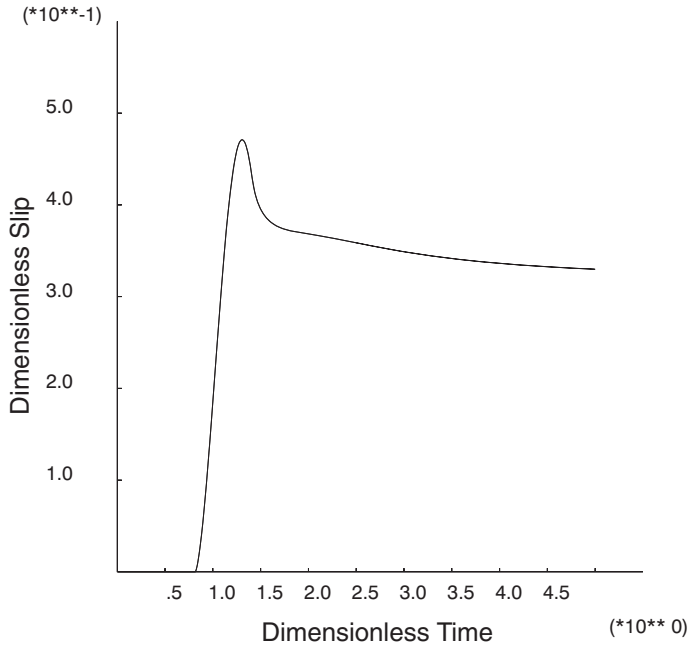

Figure 4.46 Dimensionless analytical results for slip history at point P (Day 1985) (dimensionless slip = $(4h\ \rho\ \beta^2/m_o)\ \delta u$; dimensionless time = $t\beta/h$)

Figure 4.47 shows the problem geometry modeled by *UDEC*. The source is located at the origin of the coordinate axes and the discontinuity is located at $y = -h$. The y-axis is a line of symmetry, and quiet boundaries are used on the other three sides of the model. The dynamic input is applied at the semicircular boundary of radius 0.05 h. The slip movement is monitored at point P on the discontinuity.

The continuous medium is modeled with seven elastic deformable blocks, as shown in Figure 4.48. All joints except the discontinuity at $y = -h$ are construction joints, in order to produce a continuous elastic medium. The discontinuity is assigned zero shear strength, high normal stiffness and high tensile strength in order to meet the assumptions given in the analytical solution.

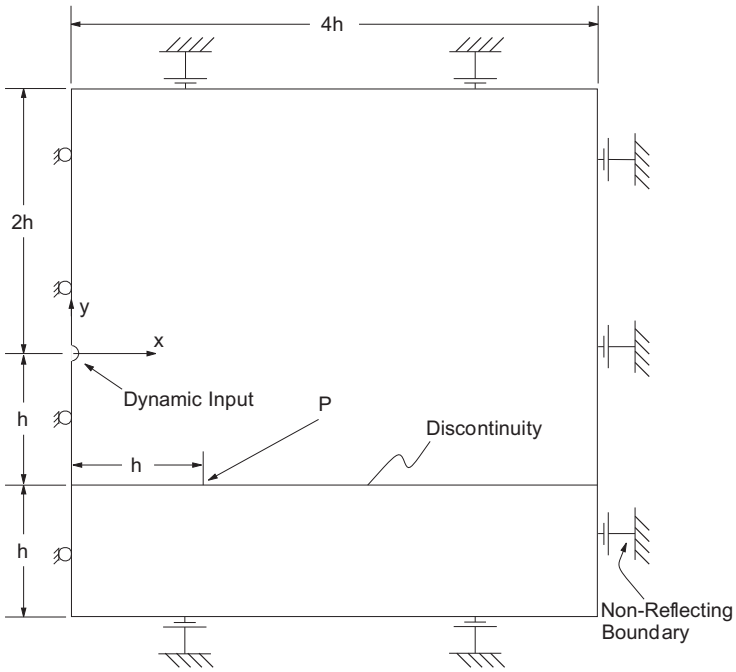

Figure 4.47 Problem geometry and boundary conditions for the UDEC analysis

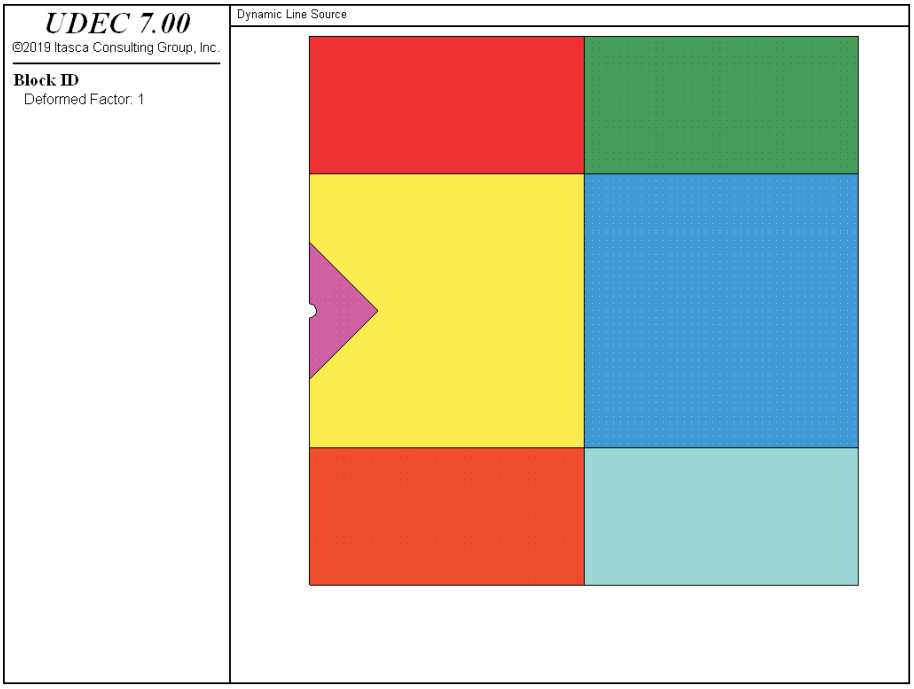

Figure 4.48 UDEC model showing semicircular source and joints

The following properties are assigned to the *UDEC* model.

Block Properties

		Units
Geometric Scale:	h = 10	(m)
Material Properties:	mass density (ρ) = 1	(kg / m^3)
	shear modulus (G) = 100	(Pa)
	bulk modulus (K) = 166.67	(Pa)
	Poisson's ratio (ν) = 0.25	
	p-wave velocity (α) = 17.32	(m / sec)
	s-wave velocity (β) = 10.00	(m / sec)

Joint Properties

The following joint constitutive models are used:

(i) Coulomb slip model; and

(ii) Continuously yielding model.

The specific *UDEC* parameters used for each joint model are as follows.

(i) Coulomb slip model (**block contact cmodel assign area**)

	Units
st-n = 10,000	(Pa/m)
st-s = 0.1	(Pa/m)
fric = 0	

(ii) Continuously yielding model (**block contact cmodel assign c-y**)

	Units
st-n = 10,000	(Pa/m)
st-s = 0.1	(Pa/m)
fric = 1.0×10^{-5}	(degrees)
exp-n = 0	
exp-s = 0	
fric-init = 1.0×10^{-10}	(degrees)
rough = 1.0×10^{-4}	(m)

Radial velocities corresponding to the dynamic solution for a line source in an infinite medium are applied at the semicircular boundary. The velocities are calculated in the following manner.

The solution for the displacement due to a center of dilation in an infinite medium (Achenbach 1975) is described by the expression

$$u_i = \frac{1}{4\pi\ {C_p}^2}\ \frac{\partial}{\partial x_i}\left[\ \frac{1}{r}\ f\left(\ t - \frac{r}{C_p}\ \right)\ \right] \tag{4.40}$$

where $r^2 = x^2 + y^2 + z^2$;

C_p = p-wave velocity; and

f(t) = source time history.

Integration of Eq. (4.40) along the z-axis leads to the solution for a line source of compression (Lemos 1987) when f(t) is taken as a step function,

$$f(t) = \begin{cases} 0, & t < 0 \\ 1, & t \geq 0 \end{cases} \tag{4.41}$$

The two-dimensional solution for radial displacement becomes

$$u = -\frac{1}{2\pi\ C_p}\ \frac{t}{r^2}\left[\ \frac{t^2\ {C_p}^2}{r^2} - 1\ \right]^{-1/2}\ ,\quad t > \frac{r}{C_p} \tag{4.42}$$

where $r^2 = x^2 + y^2$.

The corresponding velocity is

$$v = -\frac{1}{2\pi\ C_p}\ \frac{1}{r^2}\left[\ \frac{t^2\ {C_p}^2}{r^2} - 1\ \right]^{-3/2}\ ,\quad t > \frac{r}{C_p} \tag{4.43}$$

The actual input velocity record at $r = 0.05\ h$, as shown in normalized form in Figure 4.49, is obtained by convoluting Eqs. (4.43) and (4.39).

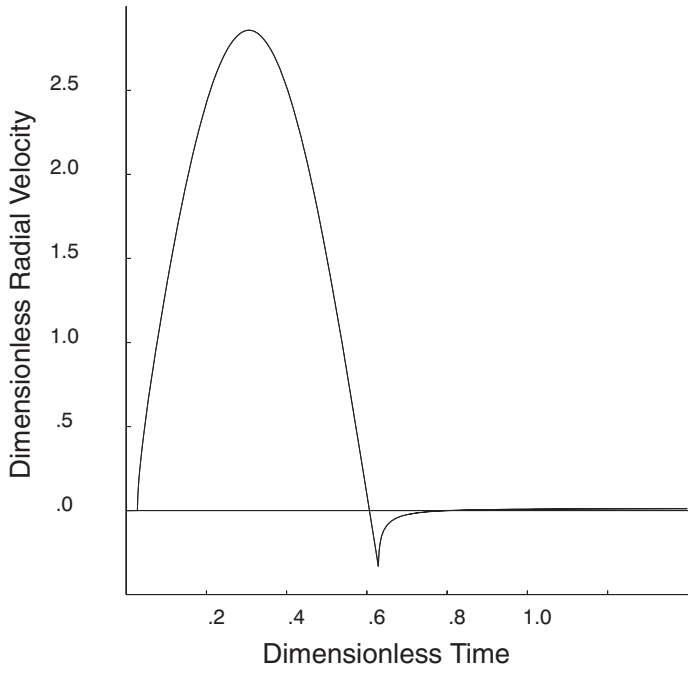

Figure 4.49 Input radial velocity time history prescribed at r = 0.05 h (dimensionless velocity = $(h^2\ \rho\ \beta/m_o)\ v$; dimensionless time = $t\ \beta/h$)

Example 4.15 contains the *UDEC* data file for this problem. The velocity input is calculated in the *FISH* function **vel_inp** (see Example 4.16); the velocity is input as a history multiplier from table number 1. The analytical solution is calculated and stored in table number 4, using *FISH* function **ana_slp** (see Example 4.17). The *UDEC* results are stored in table number 8 for comparison to the analytical solution.

The results for dynamic slip are compared in dimensionless form in Figure 4.50 for the Coulomb slip model, and Figure 4.51 for the continuously yielding joint model. The difference at peak slip between numerical and analytical results is 3% for the Coulomb model. The results for the continuously yielding model are virtually identical. The analyses for both joint models are for a *UDEC* mesh of maximum zone length equal to 0.033 h. The slip response on the discontinuity involves higher frequency components because of zero friction along the crack. This requires a very fine mesh for accurate representation, as discussed in Section 4.3.2. A spectral analysis of the slip response at P suggests that at least 35 zones within the distance of the dominant wavelength of the input wave are required to provide good accuracy.

Both figures show a disturbance in the *UDEC* results at a dimensionless time of approximately 2.5. This indicates the effectiveness of the quiet boundaries. These boundaries cannot be fully effective in a problem involving dynamic slip in a discontinuity that actually crosses the boundary. However, the results are still considerably better than those obtained without nonreflecting boundaries. If the boundaries are placed farther away from the source, then improved performance may be expected. In a practical problem, material damping would reduce the importance of these partial boundary reflections.

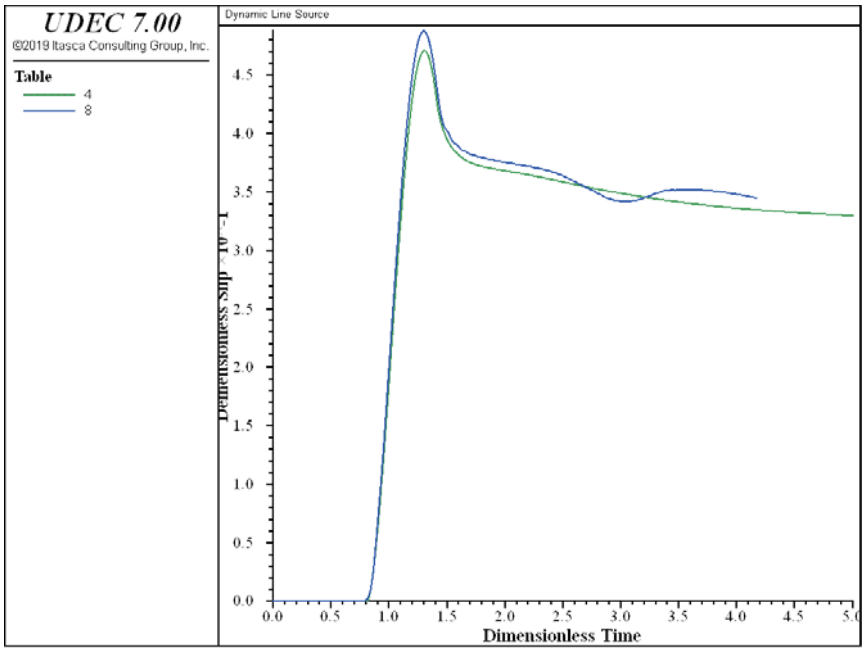

Figure 4.50 Comparison of analytical results (history 4) and numerical results (history 8) for dynamic slip at point P, using the Coulomb joint model

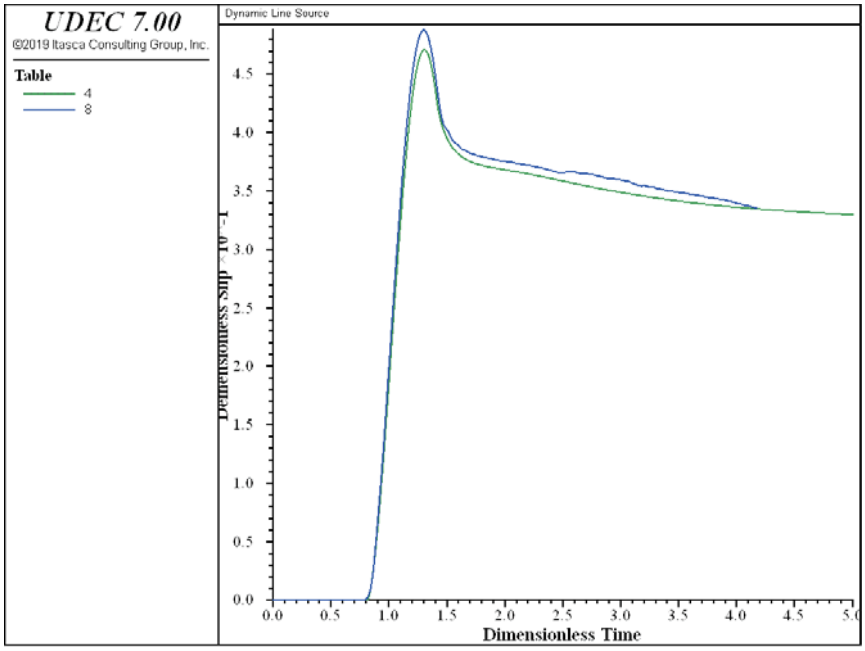

Figure 4.51 Comparison of analytical results (history 4) and numerical results (history 8) for dynamic slip at point P, using the continuously yielding model

Example 4.15 Line source in an infinite elastic medium with a discontinuity

```
model new
;file: linesource.dat
model title 'Dynamic Line Source'
;-----------------------------------------------------------------
; create block geometry with maximum zone length of 0.033h
; Coulomb block contact cmodel assign
block tolerance corner-round-length 0.002
block create polygon 0,-20 0,-.5 0.1913,-0.4619 0.3536,-0.3536 ...
  0.4619,-0.1913 0.5,0 0.4169,0.1913 0.3536,0.3536 0.1913,0.4619 ...
  0,0.5 0,20 40,20 40,-20
;
;  construction joints
block cut crack -5,10 45,10  join
block cut crack 20,-21 20,21 join
block cut crack -1,-6 6,1    join
block cut crack -1,6 6,-1    join
;
;  discontinuity
block cut crack -5,-10 45,-10
;
```

```
;  create finite difference zones
gen  edge 0.33 range pos-x 0,40 pos-y -20,20
model save 'line1.sav'
model restore 'line1.sav'
;
block zone group 'elastic block'
block zone cmodel assign elastic density 1 bulk 166.67 shear 100 ...
  range group 'elastic block'
;
block contact group 'joint'
block contact cmodel assign area stiffness-normal 1E4 ...
  stiffness-shear 0.1 tension 1E6 range group 'joint'
; new contact default
block contact cmodel default area stiffness-normal=1E4 ...
  stiffness-shear=0.1 tension=1E6
;
block gridpoint apply  bulk=166.67 shear=100.0 density=1.0
block gridpoint apply  visc-x  range pos-x -1,41 pos-y -20.1,-19.9
block gridpoint apply  visc-x  range pos-x -1,41 pos-y 19.9,20.1
block gridpoint apply  visc-x  range pos-x 39.9,40.1 pos-y -21,21
block gridpoint apply  visc-y  range pos-x -1,41 pos-y -20.1,-19.9
block gridpoint apply  visc-y  range pos-x -1,41 pos-y 19.9,20.1
block gridpoint apply  visc-y  range pos-x 39.9,40.1 pos-y -21,21
call 'VEL_INP.FIS'
;  set velocity boundary conditions along the semi-circular boundary,
;  applying the history as TABLE 1 from VEL_INP.FIS
bl gr ap v-x=0     v-y=-1.0   hi tab 1 ra p-x -0.05 0.05 p-y -0.55 -0.45
bl gr ap v-x=0.383 v-y=-0.924 hi tab 1 ra p-x  0.17 0.21 p-y -0.48 -0.45
bl gr ap v-x=0.707 v-y=-0.707 hi tab 1 ra p-x  0.33 0.37 p-y -0.37 -0.33
bl gr ap v-x=0.924 v-y=-0.383 hi tab 1 ra p-x  0.43 0.47 p-y -0.21 -0.17
bl gr ap v-x=1.0   v-y= 0.0   hi tab 1 ra p-x  0.48 0.52 p-y -0.05  0.05
bl gr ap v-x=0.924 v-y= 0.383 hi tab 1 ra p-x  0.41 0.45 p-y  0.17  0.21
bl gr ap v-x=0.707 v-y= 0.707 hi tab 1 ra p-x  0.33 0.37 p-y  0.33  0.37
bl gr ap v-x=0.383 v-y= 0.924 hi tab 1 ra p-x  0.17 0.21 p-y  0.43  0.47
bl gr ap v-x=0     v-y= 1.0   hi tab 1 ra p-x -0.05 0.05 p-y  0.45  0.55
; set symmetry boundary conditions along the remaining side
bl grid apply  vel-x=0      range pos-x -0.1,0.1 pos-y -21,21
block insitu stress -1.0e-9,0,-1.0e-9
;  set histories
;  contact address at coordinate 10,-10
hist interval = 10
block gridpoint history vel-y  (0,.5)
block gridpoint history vel-x  (.5,0)
block gridpoint history vel-x  (.35,0)
block gridpoint history vel-y  (.35,.35)
block gridpoint history vel-x  (.19,-.46)
```

```
block gridpoint history vel-y  (.19,-.46)
block contact history displacement-shear 10,-10
;
block mech damp rayleigh 0,0
model save 'line2.sav'
;
block cycle  8000
model save 'line3.sav'
;
;  calculate analytical solution for dynamic slip
call 'ana_slp.fis'
;
; calculate dimensionless numerical solution
hist EXPORT 7 table 7
fish def num_slp
  h_step = 800
  h_n    = 10.0
  rho_n  = 1.0
  vs_n   = 10.0
  m0_n   = 1.0
  loop n (1,h_step)
    table.y(8,n) = (4.0*h_n*rho_n*vs_n*vs_n/m0_n)*table.y(7,n)
    table.x(8,n) = (vs_n / h_n) * table.x(7,n) * block.mechanical.timestep
  endloop
end
@num_slp
model save 'line4.sav'
;
model new
;
;-----------------------------------------------------------------
; create block geometry with maximum zone length of 0.033h
; Continuously yielding block contact cmodel assign
model restore 'line1.sav'

;
block zone group 'elastic block'
block zone cmodel assign elastic density 1 bulk 166.67 shear 100 ...
  range group 'elastic block'
;
block contact group 'cy discontinuity'
block contact cmodel assign cy friction 1E-5 friction-initial 1E-10 ...
 roughness 0.0001 stiffness-shear 0.1 stiffness-normal 1E4 ...
 range group 'cy discontinuity'
; new contact default
block contact cmodel default cy friction=1E-5 friction-initial=1E-10 ...
```

```
  roughness=0.0001 stiffness-shear=0.1 stiffness-normal=1E4
;
block gridpoint apply bulk=166.67 shear=100.0 density=1.0
block grid apply visc-x range pos-x -1,41 pos-y -20.1,-19.9
block grid apply visc-x range pos-x -1,41 pos-y 19.9,20.1
block grid apply visc-x range pos-x 39.9,40.1 pos-y -21,21
block grid apply visc-y range pos-x -1,41 pos-y -20.1,-19.9
block grid apply visc-y range pos-x -1,41 pos-y 19.9,20.1
block grid apply visc-y range pos-x 39.9,40.1 pos-y -21,21
call 'VEL_INP.FIS'
;  set velocity boundary conditions along the semi-circular boundary,
;  applying the history as TABLE 1 from VEL_INP.FIS
bl gr ap v-x=0     v-y=-1.0   hi tab 1 ra p-x -0.05 0.05 p-y -0.55 -0.45
bl gr ap v-x=0.383 v-y=-0.924 hi tab 1 ra p-x  0.17 0.21 p-y -0.48 -0.45
bl gr ap v-x=0.707 v-y=-0.707 hi tab 1 ra p-x  0.33 0.37 p-y -0.37 -0.33
bl gr ap v-x=0.924 v-y=-0.383 hi tab 1 ra p-x  0.43 0.47 p-y -0.21 -0.17
bl gr ap v-x=1.0   v-y= 0.0   hi tab 1 ra p-x  0.48 0.52 p-y -0.05  0.05
bl gr ap v-x=0.924 v-y= 0.383 hi tab 1 ra p-x  0.41 0.45 p-y  0.17  0.21
bl gr ap v-x=0.707 v-y= 0.707 hi tab 1 ra p-x  0.33 0.37 p-y  0.33  0.37
bl gr ap v-x=0.383 v-y= 0.924 hi tab 1 ra p-x  0.17 0.21 p-y  0.43  0.47
bl gr ap v-x=0     v-y= 1.0   hi tab 1 ra p-x -0.05 0.05 p-y  0.45  0.55
; set symmetry boundary conditions along the remaining side
block gridpoint apply vel-x=0      range pos-x -0.1,0.1 pos-y -21,21
block insitu stress -1.0e-9,0,-1.0e-9
;  set histories
;  contact address at coordinate 10,-10
hist interval =10
block gridpoint history vel-y  (0,.5)
block gridpoint history vel-x  (.5,0)
block gridpoint history vel-x  (.35,0)
block gridpoint history vel-y  (.35,.35)
block gridpoint history vel-x  (.19,-.46)
block gridpoint history vel-y  (.19,-.46)
block contact history displacement-shear 10,-10
;
block mechanical damp rayleigh 0,0
model save 'line2_cy.sav'

;
block cycle  8000
model save 'line3_cy.sav'
;
;  calculate analytical solution for dynamic slip
call 'ana_slp.fis'
;
; calculate dimensionless numerical solution
```

```
hist export 7 table 7
fish def num_slp
  h_step = 800
  h_n    = 10.0
  rho_n  = 1.0
  vs_n   = 10.0
  m0_n   = 1.0
  loop n (1,h_step)
    table.y(8,n) = (4.0*h_n*rho_n*vs_n*vs_n/m0_n)*table.y(7,n)
    table.x(8,n) = (vs_n / h_n) * table.x(7,n) * block.mechanical.timestep
  endloop
end
@num_slp
model save 'line4_cy.sav'

ret
```

Example 4.16 Listing of "VEL_INP.FIS": function to calculate velocity input

```
; ------------------------------------------------------------------------
; Fish function for generating the radial velocity input profile at r=0.05h
;
;  Input:
;         vl   --- P-wave velocity
;         per  --- period of wave
;         tt   --- total time
;         xd   --- horizontal distance
;         nt   --- total number of dat points
;
;  Output:
;         velocity profile stored in table 1
; ------------------------------------------------------------------------
def ini_par
    vl = 0.0
    per = 0.0
    tt = 0.0
    xd = 0.0
    nt = 1000
    _vtab  = 1 ; table storing velocity profile
    _fptab = 2
    _vhtab = 3
    table.x(_vtab,  nt) = 0.0
    table.x(_fptab, nt) = 0.0
    table.x(_vhtab, nt) = 0.0
end
@ini_par

def vel_inp
   if xd <= 0.0
      exit
   endif
   if per <= 0.0
      exit
   endif
   _w  = 2.0*math.pi/per
   _dt = tt/float(nt)
   _ca = -1./(2.0*math.pi*vl)
   _cb = _ca/(xd * xd)
   _cc = _cb * _dt
;
; Obtain velocity record by performing convolution
; using the radial displacement for a step function
```

```
; and second derivative of the pressure history
;
   loop _n (1, nt)
      _t = float(_n-1) * _dt
      table.x(_fptab, _n) = _t
      if _t < 0.5*per
          table.y(_fptab, _n) = 0.5*_w*_w*math.cos(_w*_t)
          _nfp = _n
      else
          table.y(_fptab, _n) = 0.0
      endif
   end_loop
;
;   --- displacement -----
;
   _t0 = xd/vl
   _j0 = int(_t0/_dt)
   _j0 = _j0 + 1
   loop _n (1, nt)
      _t = float(_n-1) * _dt
      if _n < _j0
           table.y(_vhtab, _n) = 0.0
      else
           _t     = _t0 + 0.5*_dt + float(_n-_j0)*_dt
           _cf    = _t*vl/xd
           _cf2   = _cf * _cf
           _cs    = math.sqrt(_cf2 - 1.0)
           _cg    = _cs / _t
           table.y(_vhtab, _n) = _cc / _cg
      endif
      table.x(_vhtab, _n) = _t
   end_loop
;
;   ---- velocity ---------
;
   table.y(_vtab, 1) = 0.0
   table.x(_vtab, 1) = 0.0
   loop _n (2, nt)
       _vn = 0.0
       _j1 = math.min(_nfp, _n-1)
       loop _n1 (1, _j1)
          _vn = _vn + table.y(_fptab, _n1) * table.y(_vhtab, (_n - _n1))
       end_loop
       table.y(_vtab, _n) = _vn
   end_loop
;
```

```
; Change sign for pressures source
;
   _vmax = -1e20
   _vmin =  1e20
   loop _n (1, nt)
       table.y(_vtab, _n) = -1.0*table.y(_vtab, _n)
       _vi   =  table.y(_vtab, _n)
       vmin = math.min(_vmin, _vi)
       vmax = math.max(_vmax, _vi)
       table.x(_vtab, _n) = float(_n-1)*_dt
   end_loop
;  oo = out(' vmin, vmax = ', string(vmin), ',', string(vmax))
end
fish set @vl=17.32
fish set @per=1.2
fish set @tt=1.4
fish set @xd=0.5
fish set @nt=1000
@vel_inp
```

Example 4.17 Listing of "ANA_SLP.FIS": function to calculate Day solution for dynamic slip

```
; ========================================================================
;   This function evaluates the dynamic response of the slip of a
;   single discontinuity of infinite extent caused by an explosive
;   loading. Analytical solution of a line source in an elastic medium
;   with a discontinuity is given by S. M. Day (1985)
;
;   Input: _nt    --- total number of data points to be created
;          _dt    --- time increment
;          _xd    --- horizontal distance, x
;          _hd    --- vertical distance, _hd
;          per   --- period of input function
;          rho   --- density
;          m0    --- source strength
;          gamma --- ???
;          _vp   --- velocity of pressure wave
;          _vs   --- velocity of shear wave
;
;   Output: Dimensionless relation, (4*_hd*rho*_vs^2/m0)du vs. t*_vs/_hd,
;           stored in table 4. Non-normalized values are stored in table 6.
;
; ========================================================================
fish define add_complex
; Summation of two complex variables
; Input : Za, Zb
; Output: Z = Re(Z) + Im(Z)
  Re_z = Re_a + Re_b
  Im_z = Im_a + Im_b
end
;
fish define mult_complex
; multiplication of two complex variables
; Input : Za, Zb
; Output: Z = Re(Z) + Im(Z)
  Re_z = Re_a*Re_b - Im_a*Im_b
  Im_z = Re_a*Im_b + Im_a*Re_b
end
;
fish define divi_complex
; division of complex variables Za/Zb
  _deno = Re_b * Re_b + Im_b * Im_b
  if _deno = 0.0
     divi_compex = 1
```

```
      exit
    endif
    Re_z = (Re_a*Re_b + Im_a*Im_b)/_deno
    Im_z = (Im_a*Re_b - Re_a*Im_b)/_deno
  end
  ;
  fish define sqrt_complex
  ; squart root of a complex variable
  ; Input : Zx
  ; Output: Zr = Re(Zr) + Im(Zr)
  ; _theta = atan2(Im_x, Re_x) * 0.5
    _arg   = float(Im_x/Re_x)
    _theta = math.atan(_arg) * 0.5
    _sqrtr = math.sqrt(math.sqrt(Re_x*Re_x + Im_x*Im_x))
    Re_zr   = _sqrtr*math.cos(_theta)
    Im_zr   = _sqrtr*math.sin(_theta)
  end
  ;
  fish define ana_slp
  ;
  ; Input _nt, _dt, _xd, _hd, gamma, per, rho
  ;
    _dt = float(_dt)
    _xd = float(_xd)
    _hd = float(_hd)
    gamma = float(gamma)
    per   = float(per)
    rho   = float(rho)

    _utab  = 4       ; table for normal-displacement vs time
    _ftab  = 5
    _uftab = 6

    _vs2  = _vs*_vs
    _vs4  = _vs2*_vs2
    _2vs2 = 2.0 * _vs2
    _4vs4 = 4.0 * _vs4
    _r    = math.sqrt(_xd*_xd + _hd*_hd)
    _r2   = _r * _r
    loop _n (1, _nt)
      _t = float(_n) * _dt
      _tau = _t - _r/_vp
      if _tau > 0.0
         _t2r2 = math.sqrt(_t*_t - (_r/_vp)*(_r/_vp))
         Re_cp =    _t*_xd / _r2
         Im_cp = _t2r2*_hd / _r2
```

```
Re_a  =  Re_cp
Im_a  =  Im_cp
Re_b  =  Re_cp
Im_b  =  Im_cp
mult_complex            ; Z^2 ---> Re(Z) + Im(Z)
Re_z2 = Re_z
Im_z2 = Im_z

Re_x  =  1.0/(_vp*_vp) - Re_z2
Im_x  = -1.0 * Im_z2
sqrt_complex            ; sqrt(Zx)
Re_cetap = Re_zr
Im_cetap = Im_zr

Re_x  =  1.0/(_vs*_vs) - Re_z2
Im_x  = -1.0 * Im_z2
sqrt_complex            ; sqrt(Zx)
Re_cetas = Re_zr
Im_cetas = Im_zr

Re_a = 1.0 - _2vs2 * Re_z2
Im_a = -1.0 * _2vs2 * Im_z2
Re_b = Re_a
Im_b = Im_a
mult_complex           ; (1. - 2.*vs^2*cp^2) ^ 2
Re_temp1 = Re_z
Im_temp1 = Im_z

Re_a = Re_cetap
Im_a = Im_cetap
Re_b = Re_cetas
Im_b = Im_cetas
mult_complex           ; cetap * cetas
Re_a = Re_z
Im_a = Im_z
Re_b = Re_z2
Im_b = Im_z2
mult_complex           ; cetap * cetas * cp^2
Re_temp2 = _4vs4 * Re_z
Im_temp2 = _4vs4 * Im_z

Re_cr = Re_temp1 + Re_temp2
Im_cr = Im_temp1 + Im_temp2
Re_cr = Re_cr + 2.0 * _vs * gamma * Re_cetas
Im_cr = Im_cr + 2.0 * _vs * gamma * Im_cetas
_dut = 2.0*m0*_vs*_vs/(math.pi*rho*_vp*_vp)
```

```
        ; note Re_a, Im_a store (cetap*cetas)
        Re_b = Re_cp
        Im_b = Im_cp
        mult_complex           ; cetap * cetas * cp

        Re_a = Re_z
        Im_a = Im_z
        Re_b = Re_cr
        Im_b = Im_cr
        if divi_complex = 1    ; cetap * cetas * cp / cr
             oo = io.out(' divided by zero')
             exit
        endif
        _dut = _dut * Re_z / _t2r2
        table.y(_utab, _n) = _dut
     else
        table.y(_utab, _n) = 0.0
     endif
  end_loop
;
  _nf = int(per/_dt + 0.0001)
  _sum = 0.0
  loop _n (1, _nf)
    _ph = float(_n) * _dt / per
    if _ph < 1.0
       table.y(_ftab, _n) = math.sin(math.pi * _ph)
    else
       table.y(_ftab, _n) = 0.0
    endif
    _sum = _sum + table.y(_ftab, _n)
  end_loop
;
;   du vs. time relation
;
  loop _i (1, _nt)
     _uf = 0.0
     _n = math.min(_nf, _i)
     loop _j (1, _n)
          _uf = _uf + table.y(_utab,_i-_j+1)*table.y(_ftab,_j)
     end_loop
     table.y(_uftab, _i) = _uf / _sum
     table.x(_uftab, _i) = float(_i) * _dt
  end_loop
;
;   Dimensionless relation
;
```

```
  loop _n (1, _nt)
     table.y(_utab, _n) = (4.0*_hd*rho*_vs*_vs/m0)*table.y(_uftab, _n)
     table.x(_utab, _n) = float(_n) * _dt * _vs / _hd
  end_loop
;
end
;
fish set @_nt=1000
fish set @_dt=0.005
fish set @_xd=1.0
fish set @_hd=1.0
fish set @_vs=1.0
fish set @_vp=1.7320508
fish set @gamma=0.0
fish set @per=0.6
fish set @rho=1.0
fish set @m0=1.0
@ana_slp
;
;
```

4.6 Dynamic Wizard

4.6.1 Signal Preprocessing for Seismic Analysis

An example application of the Tools->Dynamic Input Wizard is presented here. The seismic loading is from the 1987 Loma Prieta earthquake in California. The input record (i.e., the upward-propagating motion from the deconvolution analysis; *SHAKE-91* is used in this example to estimate the appropriate motion at depth corresponding to the target (surface) motion) is in the file named "ACC_DECONV.HIS", and is shown in Figure 4.52. The estimated peak acceleration is approximately 5.8 ft/sec^2.

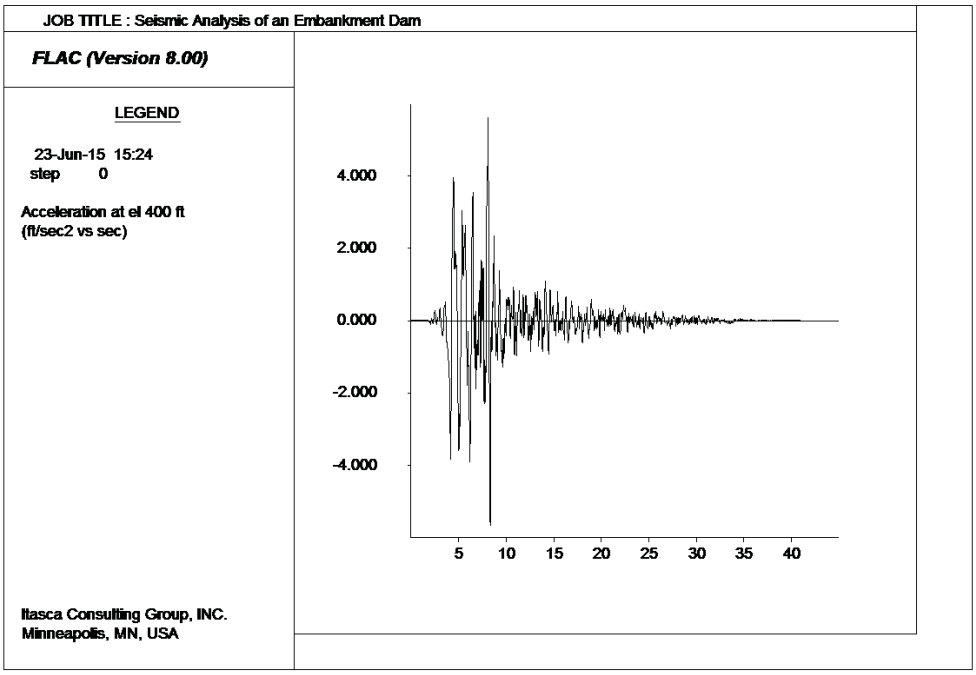

Figure 4.52 Horizontal acceleration time history at elevation of 400 ft (upward-propagating motion from deconvolution analysis)

Step 1: Import the Data File into the Wizard

To import the upward-propagating motion from the deconvolution analysis, press the "file open" button, select the file named "ACC_DECONV.HIS" and then press the SELECT button as shown in Figure 4.53. Choose "history" as the file format, select " Acceleration" as the ground motion type and choose the imperial unit (ft/s^2), then press the NEXT button for filtering.

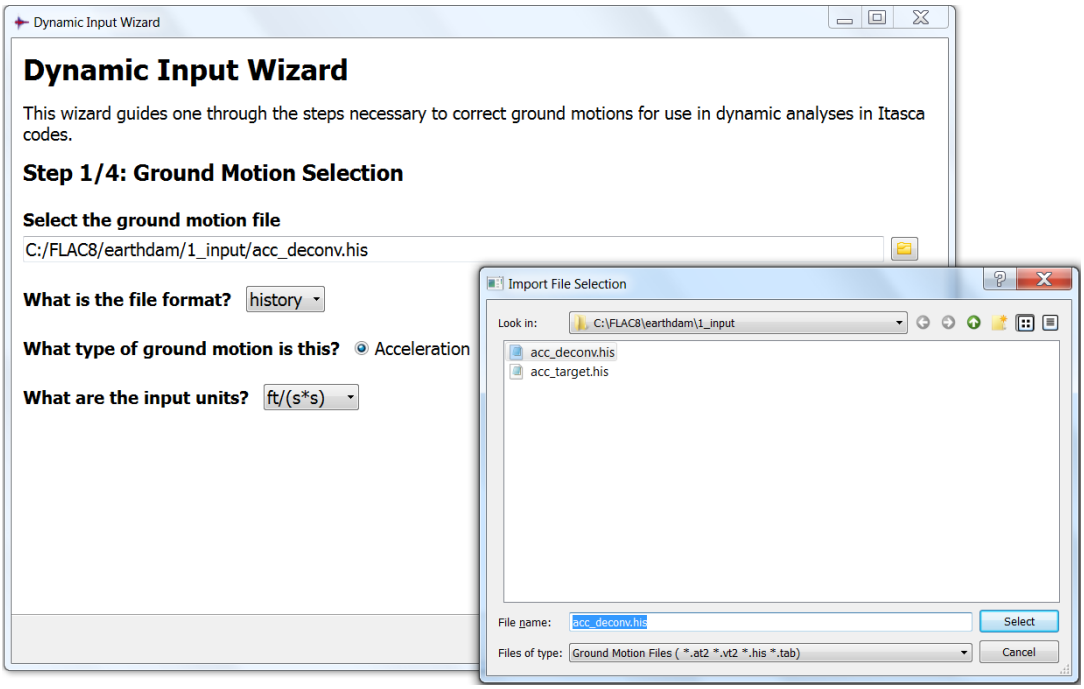

Figure 4.53 Import input into the wizard

Step 2: Filtering

The acceleration input record is integrated to produce a velocity record, which is then integrated again to get a displacement record. Those records are shown on the left section of the window.

A fast Fourier transform (FFT) analysis of the input acceleration record results in an amplitude spectrum as shown in Figure 4.54.

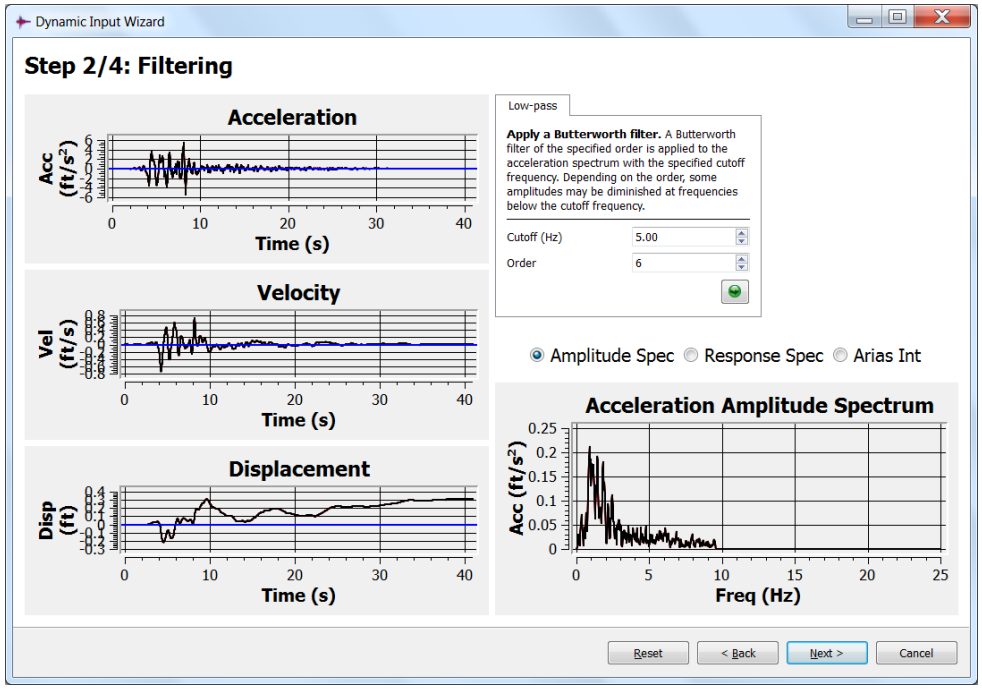

Figure 4.54 Original input records, amplitude spectrum and filter

This figure indicates that the dominant frequency is approximately 1 Hz, the highest frequency component is less than 10 Hz, and the majority of the frequencies are less than 5 Hz. Most energy of the input is contained in lower frequency components. A Butterworth-type low-pass filter with a cutoff frequency of 5 Hz is applied to remove the frequency components above 5 Hz. The input records are updated after the circular green "start" button is pressed as shown in Figure 4.55.

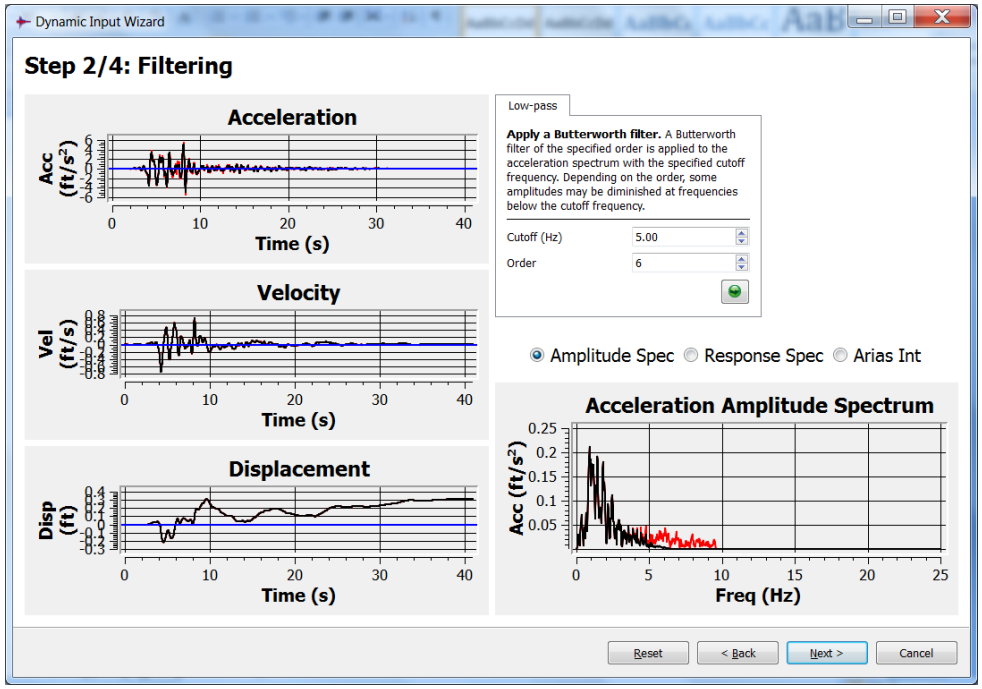

Figure 4.55 Filtered input records, amplitude spectrum

Step 3: Baseline correction

The baseline correction window will appear by hitting the NEXT button as shown in Figure 4.56. Four tabbed panes are provided to perform baseline correction. First press the MEAN tab to remove the mean acceleration. This may not be necessary if the ground motion has been corrected. Next, remove the displacement drift via a low-frequency sinusoid function. The final displacement drift is found to be approximately 0.3 ft as shown in Figure 4.56. By pressing the green circular "start" button, the drift is removed and the final displacement is corrected to zero, as shown in Figure 4.57.

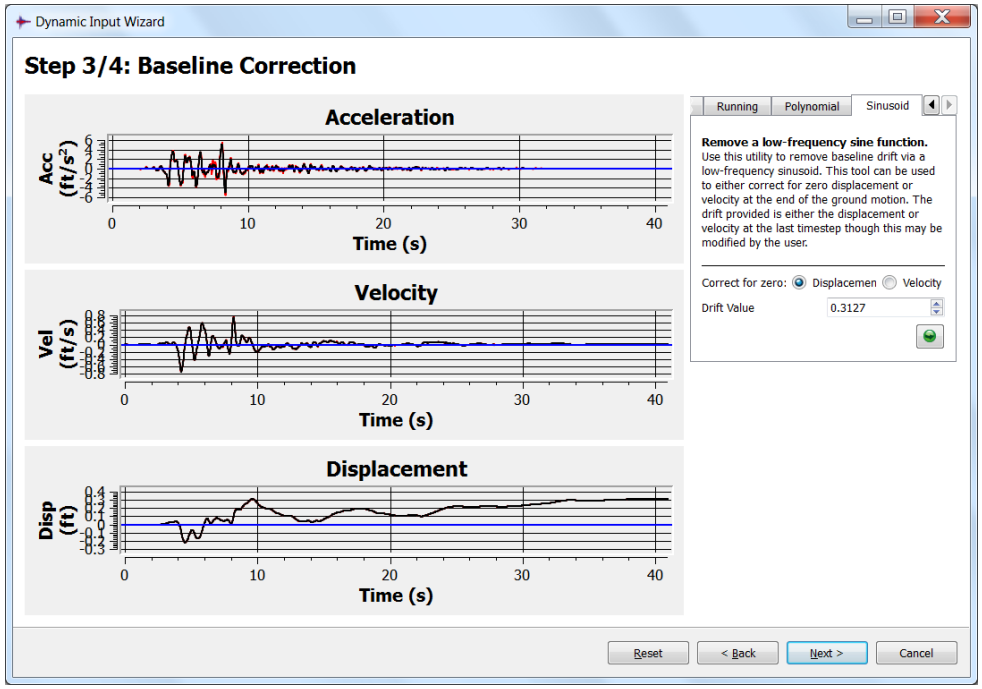

Figure 4.56 Waveform before baseline correction

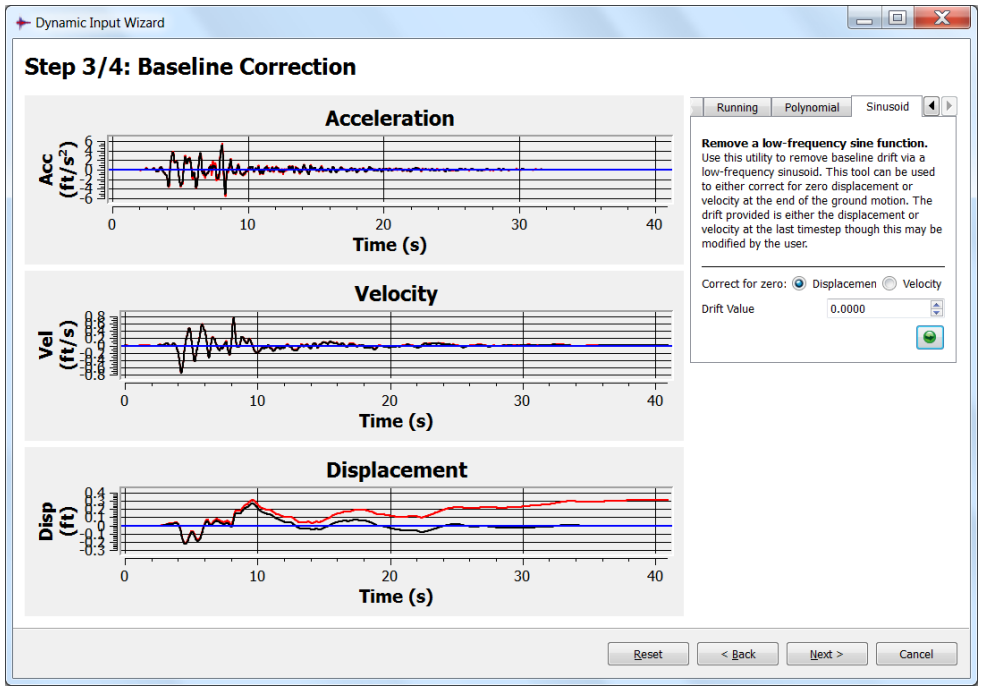

Figure 4.57 Waveform after baseline correction

Step 4: Export data for dynamic analysis

The processed data can be saved by pressing the "save" button. Name the file "INPUT.TAB", press the SELECT button, choose "Velocity" as motion type and then press the EXPORT button to export the data as shown in Figure 4.58.

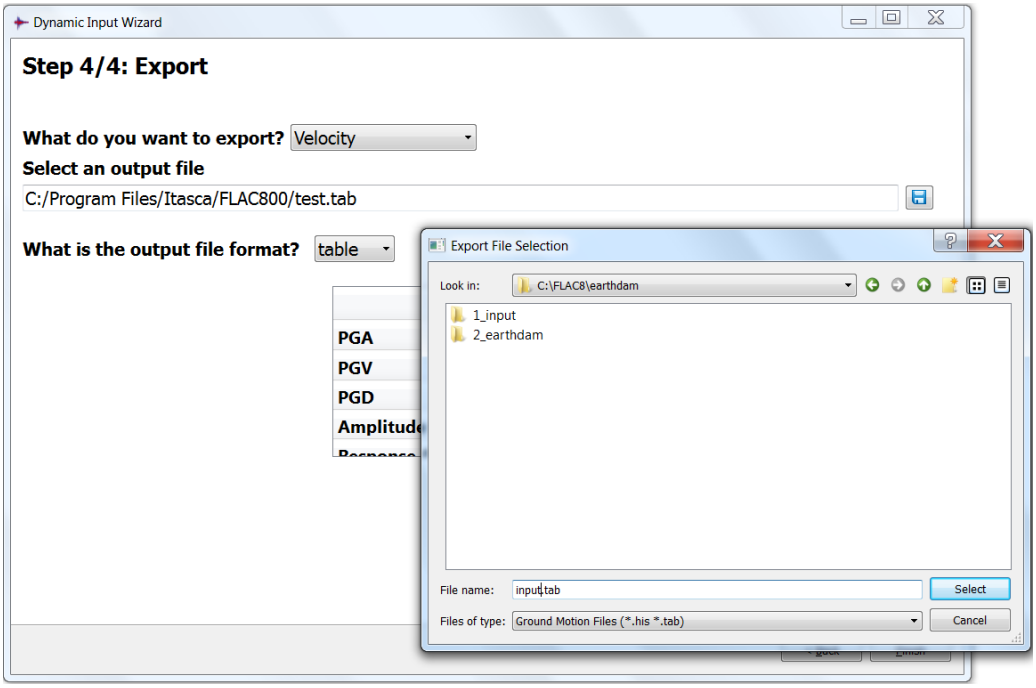

Figure 4.58 Save processed velocity in a table

The corrected velocity table can be read into *UDEC* for dynamic analysis as shown in Figure 4.59

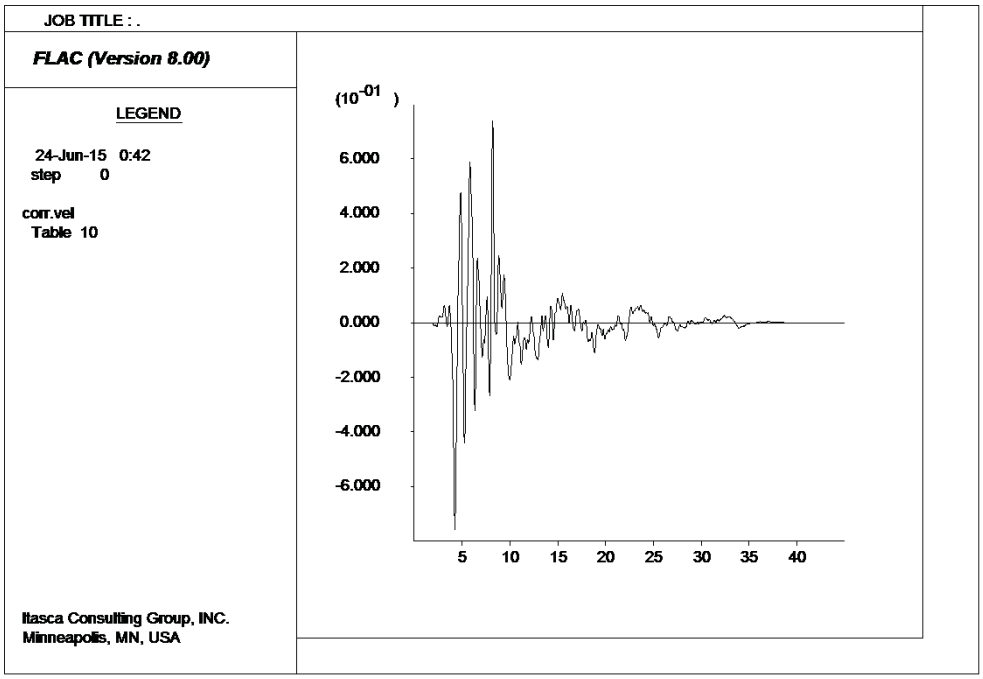

Figure 4.59 Processed velocity record

4.7 References

Achenbach, J. D. ***Wave Propagation in Elastic Solids***. New York: North-Holland Publishing Company (1975).

Bathe, K.-J., and E. L. Wilson. ***Numerical Methods in Finite Element Analysis***. Englewood Cliffs, New Jersey: Prentice-Hall Inc. (1976).

Belytschko, T. "An Overview of Semidiscretization and Time Integration Procedures," ***Computational Methods for Transient Analysis***, Ch. 1, pp. 1-65. New York: Elsevier Science Publishers, B.V. (1983).

Biggs, J. M. ***Introduction to Structural Dynamics***. New York: McGraw-Hill (1964).

Cundall, P. A. "Adaptive Density-Scaling for Time-Explicit Calculations," in ***Proceedings of the 4th International Conference on Numerical Methods in Geomechanics (Edmonton, Canada, 1982)***, Vol. 1, pp. 23-26. Z. Eisenstein, ed. Rotterdam: A. A. Balkema (1982).

Cundall, P. A. "Explicit Finite Difference Methods in Geomechanics," in ***Numerical Methods in Engineering (Proceedings of the EF Conference on Numerical Methods in Geomechanics, Blacksburg, Virginia, June, 1976)***, Vol. 1, pp. 132-150 (1976).

Cundall, P. A., et al. "Solution of Infinite Domain Dynamic Problems by Finite Modelling in the Time Domain," in ***Proceedings of the 2nd International Conference on Applied Numerical Modelling (Madrid, September 1978)***, pp. 341-351. London: Pentech Press (1979).

Cundall, P. A., et al. "Computer Modeling of Jointed Rock Masses," U.S. Army, Engineer Waterways Experiment Station, Technical Report WES-TR-N-78-4 (August 1978).

Cundall, P. A., et al. "NESSI – Soil Structure Interaction Program for Dynamic and Static Problems," Norwegian Geotechnical Institute, Report 51508-9 (December 1980).

Day, S. M. "Test Problem for Plane Strain Block Motion Codes," S-Cubed Memorandum to Itasca (May 1 1985).

Gemant, A., and W. Jackson. "The Measurement of Internal Friction in Some Solid Dielectric Materials," *The London, Edinburgh, and Dublin Philosophical Magazine & Journal of Science*, ***XXII***, 960-983 (1937).

Gerrard, C. M. "Elastic Models of Rock Masses Having One, Two and Three Sets of Joints," *Int. J. Rock Mech. Min. Sci. & Geomech. Abstr.*, ***19***, 15-23 (1982).

Graff, K. G. ***Wave Motion in Elastic Solids***. New York: Dover Publications Inc (1991).

Joyner, W. B., and A. T. F. Chen. "Calculation of Nonlinear Ground Response in Earthquakes," *Bulletin of the Seismological Society of America*, ***65***(5), 1315-1336 (October 1975).

Kolsky, H. ***Stress Waves in Solids***. New York: Dover Publications (1963).

Kuhlemeyer, R. L., and J. Lysmer. "Finite Element Method Accuracy for Wave Propagation Problems," *J. Soil Mech. & Foundations Div., ASCE*, ***99***(SM5), 421-427 (May 1973).

Kunar, R. R., P. J. Beresford and P. A. Cundall. "A Tested Soil-Structure Model for Surface Structures," in ***Proceedings of the Symposium on Soil-Structure Interaction (Roorkee University, India, January 1977)***, Vol. 1, pp. 137-144. Meerut, India: Sarita Prakashan (1977).

Lemos, J. "A Distinct Element Model for Dynamic Analysis of Jointed Rock with Application to Dam Foundations and Fault Motion." Ph.D. Thesis, University of Minnesota (June 1987).

Lysmer, J., and R. Kuhlemeyer. "Finite Dynamic Model for Infinite Media," *J. Eng. Mech., Div. ASCE*, ***95:EM4***, pp. 859-877 (1969).

Lysmer, J., and G. Waas. "Shear Waves in Plane Infinite Structures," *J. Eng. Mech., Div. ASCE*, ***98***, 85-105 (1972).

Mejia, L. H., and E.M. Dawson. "Earthquake Deconvolution for FLAC," in ***Numerical Modeling in Geomechanics – 2006 (CD Proceedings of the 4th International Symposium, Madrid, Spain, May 2006)***, paper no. 04-10. R. Hart and P. Varona, eds. Minneapolis, Minnesota: Itasca Consulting Group Inc. (2006).

Miller, R. K. "The Effects of Boundary Friction on the Propagation of Elastic Waves," *Bull. Seismic. Assoc. America*, ***68***, 987-998 (1978).

Myer, L. R., L. J. Pyrak-Nolte and N. G. W. Cook. "Effects of Single Fractures on Seismic Wave Propagation," in ***Proceedings of the International Symposium on Rock Joints (Loen, Norway, June 1990)***, pp. 413-422. N. Barton and O. Stephansson, eds. Rotterdam: A. A. Balkema (1990).

Ohnishi, Y., et al. "Verification of Input Parameters for Distinct Element Analysis of Jointed Rock Mass," in ***Proceedings of the International Symposium on Fundamentals of Rock Joints (Bjorkliden, Sweden, September 1985)***, pp. 205-214. O. Stephansson, ed. Luleå: CENTEK Publishers (1985).

Otter, J. R. H., A. C. Cassell and R. E. Hobbs. "Dynamic Relaxation," *Proc. Inst. Civil Eng.*, ***35***, 633-665 (1966).

Roesset, J. M., and M. M. Ettouney. "Transmitting Boundaries: A Comparison," *Int. J. Num. & Analy. Methods Geomech.*, ***1***, 151-176, 1977.

Salvado, C., and J. B. Minster. "Slipping Interfaces: A Possible Source of S Radiation from Explosive Sources," *Bull. Seism. Soc. Amer.*, ***70***, 659-670 (1980).

Schnabel, P. B., J. Lysmer and H. Bolton Seed. "SHAKE: A Computer Program for Earthquake Response Analysis of Horizontally Layered Sites," University of California, Berkeley, Earthquake Engineering Research Center, Report No. UCB/EERC-71/12 (1972).

Seed, H. B., P. P. Martin and J. Lysmer. "The Generation and Dissipation of Pore Water Pressures During Soil Liquefaction," Earthquake Engineering Research Center, University of California, Berkeley, NSF Report PB-252 648 (August 1975).

Singh, B. "Continuum Characterization of Jointed Rock Masses: Part I – The Constitutive Equations," *Int. J. Rock Mech. Min. Sci. & Geomech. Abstr.*, ***10***, 311-335 (1973).

Wegel, R. L., and H. Walther. "Internal Dissipation in Solids for Small Cyclic Strains," *Physics*, ***6***, 141-157 (1935).

Westergaard, H. M. "Water Pressure on Dams During Earthquakes,"*Proceedings of ASCE*, Transactions number 98, Vol. 59, No. 8, Part 3 (1933).

White, W., S. Valliappan and I. K. Lee. "Unified Boundary for Finite Dynamic Models," *J. Eng. Mech., Div. ASCE*, ***103***, 949-964 (1977).

Wolf, J. P. ***Dynamic Soil-Structure Interaction***. New Jersey: Prentice-Hall (1985).